# Sorption and diffusion of caesium in some nuclear graphites.

Mehew, R. D.

*Award date:*
1974

*Awarding institution:*
University of Bath

# SORPTION AND DIFFUSION OF CAESIUM IN SOME NUCLEAR GRAPHITES

submitted by R.D.Mehew

for the degree of Ph.D.

of the University of Bath

1974



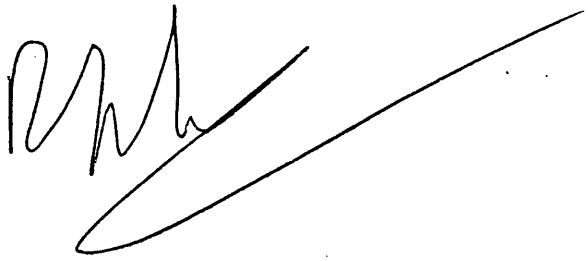



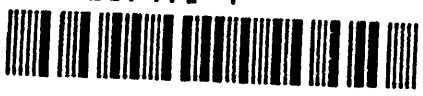

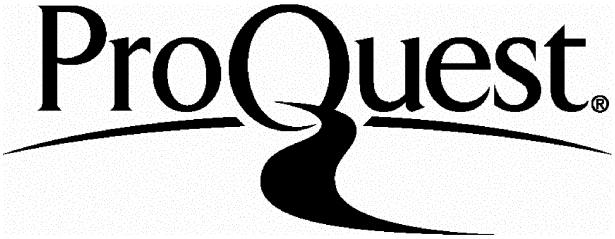

To the memory of my mother

Acknowledgements

Thanks are due to the OECD Dragon Project who supported this work financially and in particular to Dr L.W.Graham and Dr H.Hick for continued interest and helpful discussions. The aid of Dr S.L.F.Richards in programing the numerical solution method of Chapter V.4 is gratefully acknowledged. I would also like to thank my supervisor, Dr B.McEnaney for his continued support and help, especially during the times when progress seemed so small and success so distant. Finally I wish to thank my father for his unfailing support, which made all this possible.

The firm determination to submit to experiment is not enough; there are still dangerous hypotheses; first, and above all, those which are tacit and unconscious. Since we make them without knowing it, we are powerless to abandon them.

Henri Poincaré

## SUMMARY

The sorption and diffusion of caesium in two nuclear graphites at a concentration range of $5 \times 10^{-2}$ to $10^{-3}$ atom % and at temperatures in the range 500 to 1400 K has been studied using a microgravimetric desorption technique. Concentration profiles have been obtained at various stages in an adsorption, heat treatment, desorption programme by electron probe micro-analysis. The desorption curves consisted of an initial fast period controlled by evaporation of caesium from the surface, followed by a slow rate, controlled by diffusion from the bulk of the graphite. The desorption curves were analysed to obtain diffusion coefficients by several techniques and the validity of each method is considered. The effects of a non-uniform concentration of caesium and a surface evaporation step on the transport of caesium in the graphite were also considered. The concentration profiles for caesium in graphite, found by electron probe microanalysis, showed evidence of a complex mechanism for transport of caesium in graphite with apparent violations of Fick's Law. This behaviour was qualitatively explained in terms of a two part diffusion mechanism combined with surface evaporation. Slow diffusion in gilsonite graphite was described by $\log(D) = -5.1 - 137000/2.303\ RT$. Desorption from the fine grain graphite was controlled by mixed diffusion. Evidence for sensitivity of diffusion coefficients to graphite structure and thermal history was found, although no evidence for the dependence of diffusion coefficients upon the concentration of caesium was found. The construction of a Knudsen double cell-mass spectrometer apparatus designed to measure caesium-graphite equilibrium vapour pressures is also described.

CONTENTS

# CHAPTER I

## INTRODUCTION

The OECD Dragon high temperature gas cooled nuclear reactor represents one possible design of the next generation of nuclear reactors. The basic philosophy of the design is the provision of increased fuel and primary circuit coolant temperatures leading to more efficient power generation than is possible in carbon dioxide cooled nuclear reactors such as the Magnox and Advanced Gas Cooled reactors (AGR). Problems of materials stability and corrosion resulting from high temperatures are considerably reduced by the use of helium as the primary circuit coolant, graphite as the principal structural element within the reactor core and a ceramic fuel. The fuel is in the form of microspheres which are coated with pyrocarbon-silicon carbide layers, which retain fission products. The microspheres are dispersed in an annular graphite matrix, the fuel element, which is loaded in a graphite fuel rod. The helium coolant is divided into two streams; one, the purge stream, flows within the fuel rod and is in intimate contact with the fuel elements; the other, the primary circuit coolant, flows around the fuel rods and transfers heat to the heat exchangers. The purge stream leads directly to a helium clean-up plant where fission product trapping occurs.

One of the major problems of nuclear reactors is the release of fission products from the fuel elements. Release of fission products to the primary circuit coolant may cause 'plate out' of condensable fission products on heat exchangers and coolant circulators, which must be maintained at a low level of activity to remain accessible for servicing. The possibility of accidental loss

of primary coolant by leakage may cause fission products to escape into the atmosphere. Also, the problems associated with the final shut down of the reactor are reduced if a low level of fission product contamination of the primary circuit has been maintained throughout the reactor's life time.

The attainment of a low level of fission product release from the fuel elements and a subsequent low concentration level throughout the coolant circuit has been achieved in the Dragon reactor primarily by the development of a very low permeability pyrocarbon-silicon carbide coating for the particle fuel. Analysis of irradiated fuel elements has shown that the dominating factor controlling the release of fission products from the coated fuel particles is the proportion of defective coatings resulting from manufacture and from failure of coatings under operating conditions, Nabielek et al.(1973). Indeed no release of fission products from an intact pyrocarbon-silicon carbide coated fuel particle has been observed, Graham (1970). The contribution due to other factors is very much smaller. For instance, contamination of the coated fuel particles by free uranium is equivalent to one broken particle in one million, as against a level of one broken particle in ten thousand for defective coatings, Graham (1970). Although the fuel particle coating provides a very efficient barrier for retention of fission products, the various graphites within the fuel tube afford an important secondary barrier for retention of fission products released from the small but finite fraction of defective particles.

Although much data on fission product release has been obtained from operating experience of the Dragon reactor, and information on diffusion and sorption of fission products is provided by post

irradiation examination of fuel rods, many factors combine to make the interpretation of the data difficult. It is thus necessary to perform experiments outside the reactor in order to obtain basic data on the transport of fission products through nuclear graphites, in order to provide a basis for confident interpretation of information provided by reactor experience. It is for this reason that the present work was undertaken.

## I.1 The Aims of the present work

Of the many fission products that are produced, post irradiation examination and other work have shown that caesium, strontium and silver are the most important of non-gaseous fission products, Flowers et al. (1972). Of these three elements, caesium 137 has a life time of 30 years and also, being a gamma ray emitter presents a serious long-term radiological problem. The work reported in this thesis was therefore commissioned to investigate sorption and diffusion of caesium in various nuclear graphites at temperatures relevant to the operation of the Dragon reactor.

In consultation with members of the Dragon project, it was proposed to study sorption and diffusion of caesium in graphites in the temperature range 970 to 1370 K, and at concentrations of caesium in graphite of the order of milligrams per gram, using microgravimetric techniques and electron probe microanalysis. Initially, it was proposed to make preliminary measurements of caesium-graphite equilibria using a glass-silica microgravimetric apparatus and to follow up this work with a high purity study using an ultra high vacuum (UHV) microgravimetric apparatus. However, serious problems were encountered in attempting to measure caesium-graphite equilibria with the glass-silica microgravimetric apparatus and methods were

therefore devised to measure diffusion of caesium in graphite from rates of desorption. It was subsequently decided to develop a Knudsen cell-mass spectrometer technique using the UHV apparatus to attempt to measure caesium-graphite equilibria. In addition the movement of caesium through graphites before and after desorption was monitored by electron probe microanalysis of caesium concentration profiles in the graphites. Hence it was hoped that analysis of dynamic and equilibrium caesium-graphite systems would lead to an understanding of sorption and diffusion mechanisms. Comparison of data from various nuclear graphites used in the Dragon reactor would allow assessment of various possible diffusion modes to be made, and hence provide useful data for extrapolation of sorption and diffusion characteristics to other nuclear graphites.

## I.2 The structure of the thesis

The structure of the thesis is based upon traditional lines. The following chapter contains a review of the literature on the identification and structure of caesium-graphite intercalation compounds, leading to the postulation of a reaction boundary below which crystal compounds are not formed. The chapter also reviews the literature on sorption and diffusion of caesium in graphites, most of which results from investigations sponsored by nuclear technology. Chapter III is concerned with the initial phase of the sorption experiments, which results in the development of a preliminary analysis for extracting diffusion coefficients for caesium in graphite from rates of desorption of caesium. Chapter IV deals with the extension of the microgravimetric experiments to include electron probe microanalysis of caesium in the graphite

samples. The results of this combination of techniques are presented and analysed. Chapter V reports more gravimetric experiments on a second form of nuclear graphite. The analysis of desorption rates is rigorously investigated and two, more accurate analytical methods are applied. A critical analysis of the various analytical methods is also presented. Chapter VI contains a discussion of the effect of non-uniform concentrations of caesium in the graphite and a finite surface resistance upon the analysis of desorption data. A two part diffusion model for caesium in graphite is also considered and the desorption curves obtained from the microgravimetric experiments are explained in terms of these various effects. Chapter VII deals with the development of the Knudsen cell-mass spectrometer technique. In Chapter VIII the results obtained and conclusions made are summarised and suggestions made of areas for further work. Two appendices dealing with the character of the nuclear graphites and the effect of diffuse and specular reflection on desorption rates are presented at the end of the thesis. Figures and tables are included at the end of their relevant chapters.

# CHAPTER II

## A REVIEW OF THE LITERATURE

This review of the literature is in three parts. The first part deals with graphite-alkali metal systems formed in the presence of high vapour pressures of the metal. It is, therefore, concerned mainly with the history of the identification and determination of the structure of alkali metal-graphite intercalation compounds. Reference to other alkali-metals in addition to caesium is made, in order to give a more comprehensive account. In the second part of the review the caesium-graphite equilibria at low pressures will be considered, i.e. at pressures below the dissociation pressure of known caesium-graphite intercalation compounds. The work in this section has largely been carried out in connection with the release of caesium as a fission product in nuclear reactors.

The third part of this review deals with the diffusion of caesium in graphite. Since all the work carried out in this section has been sponsored by nuclear technology, a considerable portion of the data obtained has been found under various unspecified conditions. Diffusion of caesium in graphite is considered, together with diffusion of other fission products which help elucidate the transport of caesium.

### II.1 The Identification and Structure of Alkali metal-Graphite Intercalation compounds

Fredenhagen and Cadenback (1926) were the first to report the interaction of graphite with potassium, rubidium and caesium. They

reported the existence of three phases corresponding to $C_4M$, $C_8M$ and $C_{16}M$ where M is the metal. Further work by Fredenhagen and Suck (1929) confirmed the existence of these three compounds.

They reported the formation at 573 K of a bronze-coloured product of approximate composition $C_8M$ which decomposed on heating in the range 633 to 673 K to give a stable, bluish-coloured product corresponding to the approximate composition $C_{16}M$.

Schleede and Wellmann (1932) showed by X-ray diffraction that both the reaction products $C_8M$ and $C_{16}M$ were formed by intercalation of alkali metal atoms between the carbon layer planes of graphite. They reported that the interplanar spacing of the graphite is increased from 334 to 595 pm by intercalation of caesium. The structure of $C_8M$ is a regular array of metal atoms arranged in a triangular pattern so that they lie over the centres of the alternate carbon hexagons, the carbon layer planes being orientated relative to each other as in hexagonal graphite, i.e. in the packing sequence ABAB. This structure confirmed the formula $C_8M$, when each layer plane of the graphite is separated from its neighbours by a plane of metal atoms. They also assigned the same structure to the compound $C_{16}M$ except that each layer of metal atoms was separated by two graphite layer planes.

However, when Rüdorff and Schulze (1954) and Hérold (1951, 1955) re-examined this work, they both found that the postulated $C_{16}M$ compound was not present. Rüdorff and Schulze reported that the blue compound formed by the intercalation of graphite by potassium, rubidium and caesium had a structure corresponding to the formula $C_{24}M$. They also confirmed the structure assigned to $C_8M$ except that the sequence of the graphite planes was AAAA and not ABAB as Schleede

and Wellmann had suggested. The AAAA arrangement is energetically more favourable since every metal atom has twelve equidistant, nearest-neighbour carbon atoms, whereas in the ABAB arrangement there is one nearest-neighbour carbon atom, nine next-nearest and two at a further distance. In addition, Rüdorff and Schulze also showed the presence of the distinct phases $C_{36}M$, $C_{48}M$ and $C_{60}M$. They proposed that the structure of the five phases were similar, differing only in the layer plane sequence.

Hérold (1955) investigated the potassium-graphite system using an isobaric technique. Samples of either purified Ceylon flake graphite or Acheson graphite heated to varying temperatures for vaying periods of time were equilibrated with a constant pressure of potassium vapour, the latter being maintained by holding liquid potassium at a constant temperature (523 K). The system was cooled and the graphite analysed for potassium. By this means an isobaric graph was compiled which shows two distinct phases corresponding to the composition $C_8K$ and $C_{24}K$ and an uncertain phase corresponding to $C_{40}K$. X-ray analysis on the samples confirmed the structure of $C_{24}K$ reported by Rüdorff and Schulz.

Recent work by Parry (1971) on the structure of $C_8Cs$ has cast some doubt on the structure proposed by Schleede and Wellmann. Tentative analysis of X-ray data points to a completely different structure, where the caesium atom is associated with a carbon-carbon bond, rather than the centre of the carbon hexagon.

It is of interest to note that whilst the compounds of potassium, rubidium and caesium were made by simple mixing of the metals with graphite, sodium and lithium do not appear to undergo a similar

reaction when mixed with graphite. Fredenhagen and Suck (1929) reported a sodium compound formed by reaction with soot, but not with graphite. Asher and Wilson (1958) were the first to report such a compound of sodium and graphite having a composition of approximately $C_{60}Na$ to $C_{68}Na$. Hérold (1955) has also reported compounds of lithium and graphite. He found compounds with various carbon/lithium ratios and with a limiting ratio corresponding to the compound $Li_2C_2$.

Ternary systems involving the alkali metals and graphite have been well reported, especially the ammonium-graphite-alkali metal system, Rüdorff (1959). A wide range of physical and chemical properties of the alkali metal-graphite compounds have also been reported and the reviews by Rüdorff (1959), Croft (1960), Hennig(1959), Hérold et al. (1967) and Novikov and Vol'pin (1971) give good summaries. Only those properties which are relevant to the present work will be considered further in this review.

Since 1960, interest in the caesium-graphite system has increased because of the importance of caesium as a fission product in nuclear reactors. Bromley (1963) records that a disc of nuclear grade graphite 10 mm diameter x 0.1 mm thick which was exposed to a vapour pressure of caesium of 133 mN $m^{-2}$ had turned golden-brown after 20 hours and had cracked; after a further 2 hours at a vapour pressure of 67 N $m^{-2}$ the disc had completely disintegrated.

Salzano and Aronson (1964) investigated the equilibria between a pyrolytic graphite annealed at 3473 K and caesium. The uptake of caesium by the graphite was monitored using a radioactive tracer technique and the caesium vapour pressure was varied by altering the

temperature of the caesium vapour source. By following the variation of equilibrium concentration of caesium in the graphite with caesium vapour pressure, evidence for a new phase of approximate composition $C_{10}Cs$ was found. A change in the rate of decomposition of $C_8Cs$ was also observed at a concentration equivalent to $C_{10}Cs$. They suggested that the sensitivity of the techniques used by Hérold (1951, 1955) and Rüdorff and Schulze (1954) was not sufficient to detect this phase. Salzano and Aronson have since reported the presence of a similar phase in the potassium-graphite (1967(a)) and rubidium-graphite (1966(a)) systems. However, such a phase has not yet been reported in either the lithium-graphite or the sodium-graphite systems.

Salzano and Aronson (1965(a)) followed this work with a detailed analysis of the kinetics of the decomposition of the caesium-graphite system over the composition range of $C_8Cs$ to below $C_{60}Cs$, using the same radioactive tracer technique. Samples of annealed pyrolytic graphite of different sizes, and doped with caesium, were subjected to various temperatures in the range 673 to 923 K and the decomposition of the compounds was followed (figure II.1).

The existence of the new phase of composition $C_{10}Cs$ was verified and also changes in the rate of decomposition at caesium concentrations equivalent to $C_{24}Cs$, $C_{36}Cs$, $C_{48}Cs$ and $C_{60}Cs$ were observed. They also noted that below $C_{60}Cs$ the rate of decomposition continued to diminish. Although they postulated the following hypothetical reaction for the decomposition of $C_{60}Cs$ :

$$6C_{60}Cs\ (s) \rightarrow 5C_{72}Cs\ (s) + Cs(g)$$

they could not resolve any phases below $C_{60}Cs$. For each stage of

the decomposition they derived the constants of the rate equation

$$W = U \exp(-\Delta H/RT) \qquad \text{II.1}$$

where W is the rate of decomposition and $\Delta H$ and U the activation energy and pre-exponential constant respectively. It was found that the activation energy (153 kJ $mol^{-1}$) of the initial decomposition stage :

$$5\ C_8Cs\ (s) \rightarrow 4\ C_{10}Cs\ (s) + Cs(g)$$

was greater than those for the further stages of decomposition, which were similar to each other ($135 \pm 4$ kJ $mol^{-1}$). It was also found that the rate of decomposition was independent of the sample size, except for the largest sample used.

Salzano and Aronson concluded that the decomposition of the caesium-graphite system proceeds by a mechanism which allows the structure to pass through the various equilibrium compounds. Each linear portion of the decomposition curve corresponds to a transition from one phase to another, the rate of removal of caesium in each two-phase region being constant. In order for the caesium-graphite system to decompose at a linear rate, the phase decomposing and that forming must be in equilibrium and the rate of decomposition must be controlled by the rate of removal of caesium from the surface layer. Further work on the same type of graphite by Salzano and Aronson (1965(b)) investigated the thermodynamics of the various phases using radioactive caesium and a Knudsen effusion cell method. The results substantiated their analysis of the kinetics of decomposition. Later work by these authors (1966(b)) on Madagascar natural graphite crystals gave results in very good agreement with those for annealed pyrolytic graphite.

On the basis of these results, Salzano and Aronson proposed a model for the bonding (1966(c)) in caesium-graphite compounds based on an electrostatic interaction of caesium ions and the metal-like graphite layer planes. On the basis of their model, they calculated the bonding energy, using an image force theory which was in close agreement with the value obtained from their experimental results.

Using the general formula $C_{(n-1)12}\ C_{12}\ Cs \quad n>1$ , Salzano and Aronson (1966(b)) put forward the general equation:

$$n_2C_{(n_1-1)12}C_{12}Cs\ (s) + Cs\ (g) \rightleftharpoons (n_2+1)C_{(n_2-1)12}C_{12}Cs\ (s)$$

to describe the equilibrium between two successive compounds, where $n_1 = n_2 + 1$. Using their value for the bonding energy, Salzano and Aronson (1967(b)) deduced that the initial case of compound formation resulting from the first layer of caesium to penetrate into the graphite is bounded by the equation

$$\ln (P\ m^2\ N^{-1}) = 9.1 - 8300/T \qquad \text{II.2}$$

This boundary and the corresponding boundaries of the postulated equilibrium:

$$6C_{60}Cs\ (s) \rightleftharpoons 5\ C_{72}Cs\ (s) + Cs\ (g)$$

and of the final equilibrium:

$$5\ C_8Cs\ (s) \rightleftharpoons 4C_{10}Cs\ (s) + Cs\ (g)$$

are shown in figure II.2.

Thus for vapour pressures of caesium and temperatures of the graphite below the postulated boundary, the interaction of caesium

and graphite should be one of adsorption and bulk diffusion with no stoichiometric compound formation. Although many reports of the violent reaction of caesium on graphite and graphite cokes have been recorded, the disintegration of graphite samples at temperatures above 1173 K subjected to caesium vapour pressures below 1.3 kN $m^{-2}$ has not yet been recorded.

Merz and Scharf (1971) using radioactively tagged caesium, followed the decomposition of various caesium-graphite compounds at temperatures between 970 and 1373 K, using several types of nuclear graphite. The decomposition curves obtained were in agreement with earlier work of Merz (1968) and showed a definite reaction boundary near to that postulated by Salzano and Aronson (figure II.2). It is interesting to note, however, that two distinct boundaries were observed for the pyrolytic and reactor grade graphites, suggesting that the reactor grade graphite is more susceptible to compound formation. The works of Yates and Fitzpatrick (1968) and De Beni et al. (1970) show a definite reaction boundary at a concentration level equivalent to the compound $C_{24}Cs$. This may be attributed to the use of an insensitive technique to monitor caesium concentration levels and hence the isotherms found at lower concentrations do not show compound formation. Neither was any difference found between the various graphites used.

## II.2 Caesium-Graphite interactions at low Pressures and high Temperatures

The previous section has been confined to work involving high concentrations of caesium where compound formation has definitely occurred. This section deals mainly with the work done at lower concentration levels, but will include some work where compound

formation has occurred.

Anderson et al. (1962) studied the adsorption of caesium on two activated charcoals at a caesium vapour pressure of $10^{-2}$ to $10^{2}$ N $m^{-2}$ over a temperature range of 470 to 870 K and found that adsorption varied with pressure according to the Freundlich isotherm equation

$$P = K_2 C^u \qquad \text{II.3}$$

where C is the concentration adsorbed at a pressure P and $K_2$ and u are constants. However, they noted a break in the curve for one of the charcoals at the highest loading, equivalent to $C_8Cs$, and reported that the technique may have been too insensitive to measure the break for the other charcoal. More recently, Trofinov et al. (1973) have observed a deviation from the Freundlich isotherm at 573 K and caesium vapour pressures greater than 1 N $m^{-2}$ for adsorption of caesium on three activated charcoals.

Bromley and Moul (1964) conducted some experiments on the adsorption of caesium on HX 10 graphite using a radioactive tracer technique. They obtained adsorption isotherms over a caesium pressure range of 15.4 kN $m^{-2}$ to 1.33 N $m^{-2}$ at temperatures of 1273, 1472 and 1773 K. They found that monolayer formation occurred at a caesium vapour pressure of around 13 N $m^{-2}$ and at a concentration of 1 mg $g^{-1}$. Using the B.E.T. surface area for the graphite they calculated that monolayer coverage should occur at 0.93 mg $g^{-1}$. Their plot of the isosteric heat of adsorption against the caesium concentration showed a rapid decrease from 418 kJ $mol^{-1}$ to 104 kJ $mol^{-1}$ at the point of monolayer coverage. They postulated that the initial high value indicates chemical rather than physical bonding

of the adsorbed monolayer. They noted that the heat of reaction of a caesium atom undergoing ionisation on the surface of graphite is of the order of 264 kJ $mol^{-1}$ which would indicate that a high proportion of the monolayer of caesium is held by an ionic type of bond. Further results of this work were later published by Bromley (1964).

Milstead et al. (1966) using a similar technique to that used by Bromley and Moul reported that the adsorption of caesium on various graphite samples in the sub-monolayer region could be described by the Freundlich isotherm equation in the caesium pressure range of 1 mN $m^{-2}$ to 705 N $m^{-2}$ and at temperatures in the range 1073 to 1373 K. However, in the region of monolayer coverage and above, the isotherms became more complex. They found that the amount of adsorption depended upon the degree of graphitisation of the material, from which they concluded that the energy distribution of adsorption sites was also dependent upon the degree of graphitisation. By use of powdered samples of different particle size, they found that sorption measurements could be reduced to a common isotherm by expressing the caesium concentration as a function of the B.E.T. surface area. Their values of monolayer coverage and isosteric heats of adsorption were in reasonable agreement with those of Bromley and Moul.

Further work by Milstead (1969) on a TS688 (EGGR) Union Carbide graphite at lower pressures, in the range 1.3 N $m^{-2}$ to 1.3 $\mu$N $m^{-2}$ and at temperatures between 1073 and 1373 K gave isotherms which deviated from the Freundlich equation. At adsorption values greater than 40 $\mu$g $g^{-1}$, the isotherm could be represented by the Freundlich equation but below 30 $\mu$g $g^{-1}$ the isotherms were better

represented by the Langmuir equation

$$P = K\theta/(1 - \theta) \qquad \text{II.4}$$

where $\theta$ is the fraction of monolayer covered at pressure P and K is a constant. Milstead found that in the region represented by the Langmuir equation the isosteric heat of adsorption approached a constant value of 500 kJ $mol^{-1}$, which is consistent with the ionic type of bonding.

More recent work by Haire and Zumwalt (1973) on the mixed sorption of caesium and rubidium on TS 688 (EGGR) Union Carbide graphite at concentration levels where Freundlich behaviour is observed has shown a moderate difference in results, although an identical technique was used. The Freundlich behaviour observed by Milstead (1969) may be expressed as

$$\log(P) = (-13.2 + 22.5(10^3/T)) \log(C) + (0.05 + 4.11(10^3/T)) \qquad \text{II.5}$$

where P has the units of N $m^{-2}$, C mg $g^{-1}$ and T K; against that observed by Haire and Zumwalt (1973)

$$\log(P) = (-7.32 + 15.26(10^3/T)) \log(C) + (16.13 - 36.02(10^3/T)) \qquad \text{II.6}$$

This difference may be attributed to variations in structure and properties within one type of graphite and serves as an indication of the lack of reproducibility when working with nuclear graphites.

Similar transitions from Freundlich to Langmuir behaviour have been observed in the adsorption of hydrogen and nitrogen on tungsten powder, Frankenburg (1944), and also for the strontium-graphite system at low pressures, Faircloth and Flowers (1970). Milstead (1969) suggested that the transition represented a transition from

adsorption on sites with different energy values (Freundlich behaviour) to sites of essentially constant energy value (Langmuir behaviour). However, the Langmuir equation also transforms to the Henry's Law relation

$$P = K\theta \qquad \text{II.7}$$

at low surface coverage. This equation has also been derived by considering adsorption of a two-dimensional ideal gas on an energetically homogeneous surface under conditions where the surface concentration ($\theta$) tends to zero, Everett (1957). Thus, whether adsorption is localised or delocalised, the adsorption isotherm equation has the same form as the surface concentration tends to zero. Therefore at the lowest levels of caesium adsorption a Henrian type of behaviour would be expected, though this has not been reported.

As a possible alternative interpretation, it has been proposed by Faircloth and Flowers (1970) that, as the caesium concentration approaches the level of metallic and other impurities of the graphite, interactions between caesium and other metals may occur and these may account for the transition from Freundlich to Langmuir behaviour observed by Milstead. It is however interesting to note that Haire and Zumwalt (1973) in their work on the mixed adsorption of caesium and rubidium, observed little change in the Freundlich behaviour of caesium on graphite, even at the low concentration level of 4% caesium, 96% rubidium.

## II.3 Diffusion of Caesium in Graphite

Smith and Young (1953, 1957) were the first to report diffusion of caesium from AUF graphite discs. They impregnated graphite with

molten uranium nitrate which was then converted to the carbide by heat treatment and subsequently the uranium graphite was irradiated. Post-irradiation annealing at various temperatures for different times allowed the measurement of release rates for a variety of fission products. They found the release rates obeyed an equation of the form

$$t \exp(-\Delta H/RT) = K_5 \qquad \text{II.8}$$

where t is the time, $\Delta H$ the activation energy and $K_5$ a constant. Doyle (1953) using a similar technique, observed for a variety of fission products including caesium an initial fast release rate which subsequently decreased to a slow rate of release. Young (1953) confirmed this result and also observed that diffusion of caesium 134 and 137 was not affected by the diffusion of the isotopes' precursors. Cowan and Orth (1958) using a similar technique to Doyle and Young observed a large number of fission product release rates, but added little to the knowledge of caesium diffusion in nuclear graphites.

Bromley and Large (1962) reported the diffusion of caesium in Pile Grade A, HX 10, Morgans EY 9 and HX 12 graphites in the temperature range 773 to 1373 K, using in pile and out of pile experiments. The in pile experiments were designed to measure the concentration profiles resulting from irradiation over varying time periods of various fission products in an EY 9 graphite can surrounding fissile material. It was found that caesium, amongst others, exhibited a high diffusivity in the EY 9 graphite. Out of pile measurements were made by annealing, in a stream of helium at various temperatures for up to 200 hours, a sandwich structure

consisting of a thin graphite disc impregnated with caesium 137 nitrate between two rods of the particular graphite. Radioactive analysis was made of samples of the core and outer regions at varying distances from the disc for both the up-stream and down-stream samples. The diffusion coefficients found, for the four graphites, showed remarkable similarity, giving an activation energy of approximately 73 kJ $mol^{-1}$. Abnormal surface concentrations which were not consistent with a simple diffusion model were also observed. This effect was ascribed to an evaporation phenomenon, but the possibility of oxide formation was also admitted. Bromley and Large concluded that the migration of caesium through the graphites took place mainly by an activated surface process. Riedinger et al. (1962) measured the rate of permeation and diffusion of caesium through a plug of HC-27 graphite using metallic caesium tagged with caesium 137. The diffusion coefficients obtained at two temperatures gave an activation energy of 21 kJ $mol^{-1}$ for steady state flow.

Findlay and Laing (1962) used a uranium impregnation/irradiation technique on a Pile Grade A graphite followed by removal of the uranium by leaching with nitric acid, to obtain fission products located within the graphite grains. The fraction of fission products emitted at 1073 K was followed and from this data they obtained reduced diffusion coefficients (i.e. units of $s^{-1}$) for a variety of fission products including caesium. In extended work on Xenon 133 release, they found that the apparent grain size was controlled by the recoil length of the fission products (approximately 12.5 $\mu$m). Bryant et al. (1963) using a similar technique to Findlay and Laing, reported on release rates of a wide range of fission

products over the temperature range of interest. They observed a linear relationship between the log of the fraction of caesium remaining and time, and obtained an activation energy for the diffusion of caesium of 167 kJ $mol^{-1}$. They did, however, note a relationship between the diameter of the sample and the fraction retained. They also investigated the effect of surface emissivity and obtained a value of 17.1 D, where D is the diffusion coefficient, for the surface emissivity of barium. It is therefore possible that the surface evaporation step causes the relation between specimen size and diffusivity, whereas Salzano and Eshaya (1960) have shown that xenon cannot reside on the surfaces of graphite and hence precludes a surface evaporation step, at temperatures of interest.

Bromley et al. (1963) followed the diffusion of caesium through HX 10 graphite, using a radioactively tagged caesium metal source to generate a set vapour pressure in the interior of a hollow graphite tube. The uptake of caesium by the graphite, and the amount diffusing through, were monitored and concentration profiles found at the end of the experiment. Experiments were carried out for various temperatures (between 1273 and 1773 K), vapour pressures and lengths of time (up to 26 hours). The results were analysed in terms of an adsorption, diffusion and evaporation process, and values for diffusion coefficients and evaporation surface emissivities were found. The diffusion coefficients had an activation energy of 72 kJ $mol^{-1}$, although the error is relatively large, with diffusion coefficients varying by up to a factor of ten. It should however be noted that such variations were observed in the unsteady state diffusion coefficients, which were obtained from the time lag for caesium to pass through the graphite. The diffusion

coefficients calculated from the steady state flow of caesium through the graphite were, however, in very good agreement. The surface emissivities found did not vary consistently with temperature or time. They concluded that the results of the earlier work by Bromley and Large (1962) were consistent with these results, and that the existence of an evaporation step was confirmed. It is interesting to note that Salzano and Aronson (1964) postulated that the linear rates of decomposition (of caesium-graphite compounds) represent processes controlled by the rate of removal of caesium from the external surface of the solid. Bromley also produced two useful reviews on the transport of fission products through graphite, Bromley (1962, 1964).

Gethard and Zumwalt (1966) reported some work on the diffusion of caesium in discs of pyrolytic carbon at temperatures between 1273 and 1973 K. Caesium was initially allowed to diffuse into pyrolytic carbon discs (of 100 $\mu$m thickness) from a radioactively tagged caesium nitrate/chloride-graphite powder to achieve an approximately even concentration. The discs so prepared were then annealed for varying times at various temperatures and the caesium remaining in the discs was monitored. They reported no concentration effect over a range of $10^{-7}$ to $10^{-3}$ g $g^{-1}$, and that the activation energy of diffusion in the pyrolytic carbon was 176 kJ $mol^{-1}$. Comparing this with the value of Bryant et al. (1963) and Bromley and Large (1962) they suggested that the high value for the activation energy was indicative of diffusion through the grains.

Iwamoto and Oishi (1969) studied the release of some non-gaseous fission products including caesium 137, from graphites prepared in a similar manner to Findlay and Laing (1962). They measured the

fraction of fission product leached by nitric acid from the sample after the anneal, and the fraction remaining after wet oxidation of the sample. The fraction desorbed into an argon stream during the anneal was calculated by comparison with an untreated specimen. They postulated that the fission products were initially recoiled into the grains and were trapped at defects. Upon annealing, loss of fission products from the defects or 'trapping sites' occurred, followed by diffusion through the grain to the surface. At the surface, loss of fission product occurred by evaporation.

Iwamoto and Oishi then argued that the nitric acid leach only removed the surface-bound fission products. They found that this fraction was constant throughout the range of annealing times for a set temperature. They also observed that the fraction not leached initially dropped relatively quickly and then achieved a constant rate of loss. The fraction desorbed was not found to achieve a steady state, except for the longer periods of annealing time at the highest temperatures. They thus concluded that rate control occurred within the grain, and was in fact due to the rate of release of fission products from the trapping sites. Each trapping site was associated with a particular activation energy for the release of the fission product, and the population of fission products in discrete trapping sites of a range of activation energies was calculated. These calculations showed that for caesium 137 there was a peak in the population level for a trapping site with an activation energy of 193 kJ $mol^{-1}$ and another possible peak at 280 kJ $mol^{-1}$. They also observed, for other fission products, a peak at 125 kJ $mol^{-1}$. They claimed that this initial activation energy spectrum was capable of accounting for the loss

of any fission product, and that it governed the rate-controlling step; the further steps of diffusion and evaporation did not control the rate of loss.

It is considered, however, that such an interpretation of trapping sites ignores the possibility of slower diffusion along the layer planes, and does not satisfactorily account for the initial period of fission product escape during annealing. It is felt that an interpretation based upon a variety of diffusion paths arising from the initial homogeneous distribution of fission products, achieved by the random process of recoil would give an equally plausible account of the complex movement of fission products through nuclear graphites. Furthermore, such an interpretation can be used for systems of fission products in nuclear graphites, which arise from processes other than recoil from fissile uranium atoms.

Zumwalt (1970) comments on the non-linear Freundlich isotherm displayed by caesium adsorption on nuclear graphites over a wide range of concentration, and the sharp decrease in diffusion coefficients of caesium diffusing in nuclear graphites over an unspecified concentration range. He uses a model proposed by Glueckauf (1953) to account for the adsorption/diffusion/ concentration variations of barium in nuclear graphites, and obtains moderate agreement of the theory over a wide range of barium concentrations.

Flowers et al. (1972) in presenting a paper on the present state of data in the safety analysis of the high temperature reactor gave a brief review of the diffusion coefficients of caesium in

gilsonite, natural and fine grain graphites, obtained from both post irradiation examination and laboratory experiments. Diffusion coefficients were obtained from fitting postulated mathematical models of fission product movement to the post irradiation concentration profiles observed in fuel tube assemblies. Such models rely upon other data, such as gaseous transport across the purge stream and a knowledge of the fuel particle failure rate. A general agreement between laboratory and post irradiation examination diffusion coefficients for caesium in gilsonite and natural graphite was found. However, the fine grain graphite exhibited a wide range of diffusion coefficients, covering up to four orders of magnitude.

There is a considerable dearth of information on the concentrations of caesium at which the diffusion coefficients have been obtained. Only Riedinger et al. (1962), Bromley et al. (1963) and Gethard and Zumwalt (1966) give concentrations of caesium in graphite in terms of gram per gram, rather than the widely used disintegrations per gram. The data of Gethard and Zumwalt are based upon two concentration levels of $10^{-7}$ and $10^{-3}$ g $g^{-1}$ using tagged caesium nitrate and at $10^{-3}$ g $g^{-1}$ using tagged caesium chloride. There did appear, however, a small difference in the diffusion coefficients obtained from the two different caesium compounds. The work of Riedinger et al. (1962) was done over a concentration range of 0.1 to 1 mg $g^{-1}$ and that of Bromley et al. (1963) over a range of 6 to 38 mg $g^{-1}$, both using caesium metal sources. It is interesting to note that recent work, Hick (1973) using a Knudsen effusion cell technique on a caesium-gilsonite graphite system at concentration levels of 1 to 6 $\mu$g $g^{-1}$, has indicated a mixed diffusion evaporation control of the caesium

vapour pressure within the cell. This tentative observation is in agreement with that observed at a concentration level over one thousand times greater, Bromley et al.(1963).

From the considerable variation of diffusion coefficients obtained from a wide range of nuclear graphites, it would appear necessary to characterise the graphite used. However, even a particular nuclear graphite exhibits variation in properties, cf. Haire and Zumwalt (1973). It would seem necessary to use statistical methods, on a large number of determinations of diffusion coefficients in one type of nuclear graphite, in order to provide an accurate description of caesium transport in graphite. Such a program would however require very large resources.

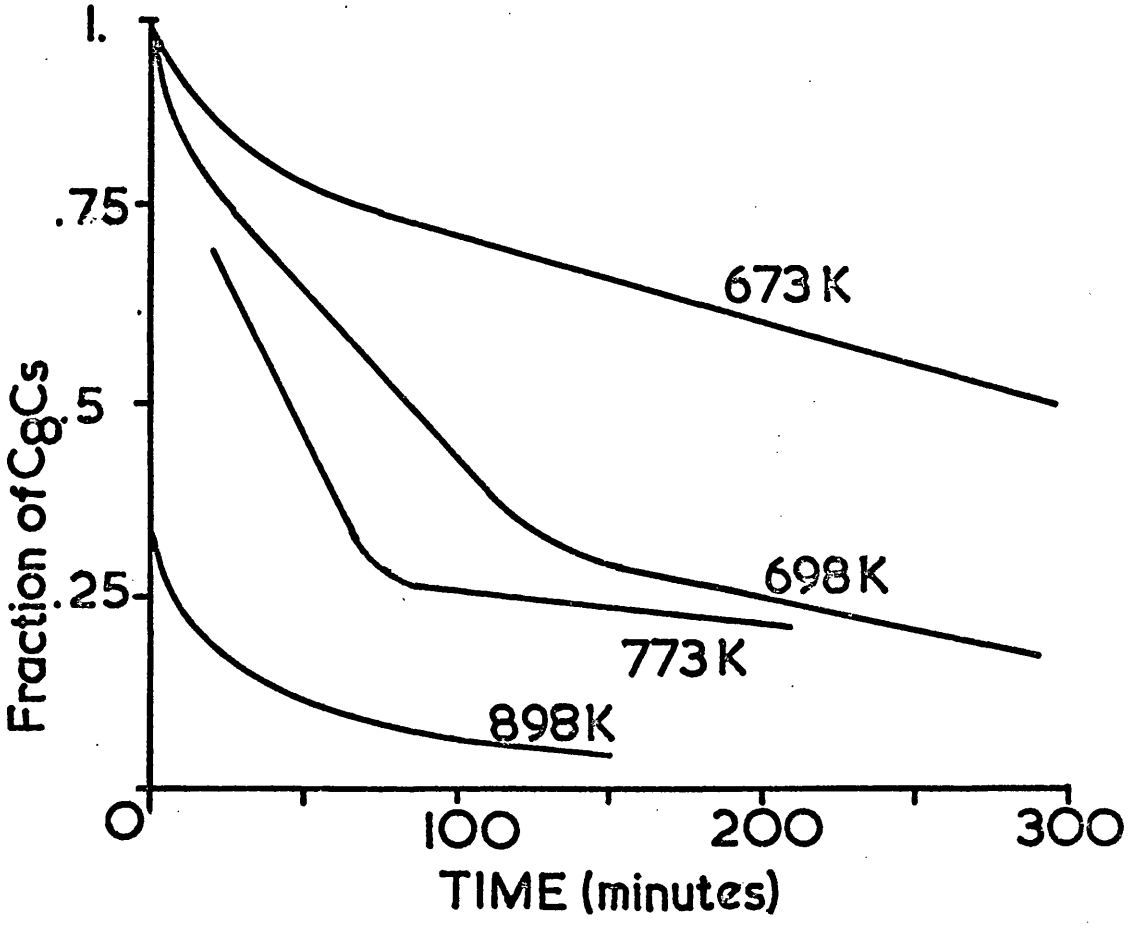


Figure II.1 Rates of Decomposition of Caesium Graphite Compounds ( Salzano and Aronson (1965(a)) )

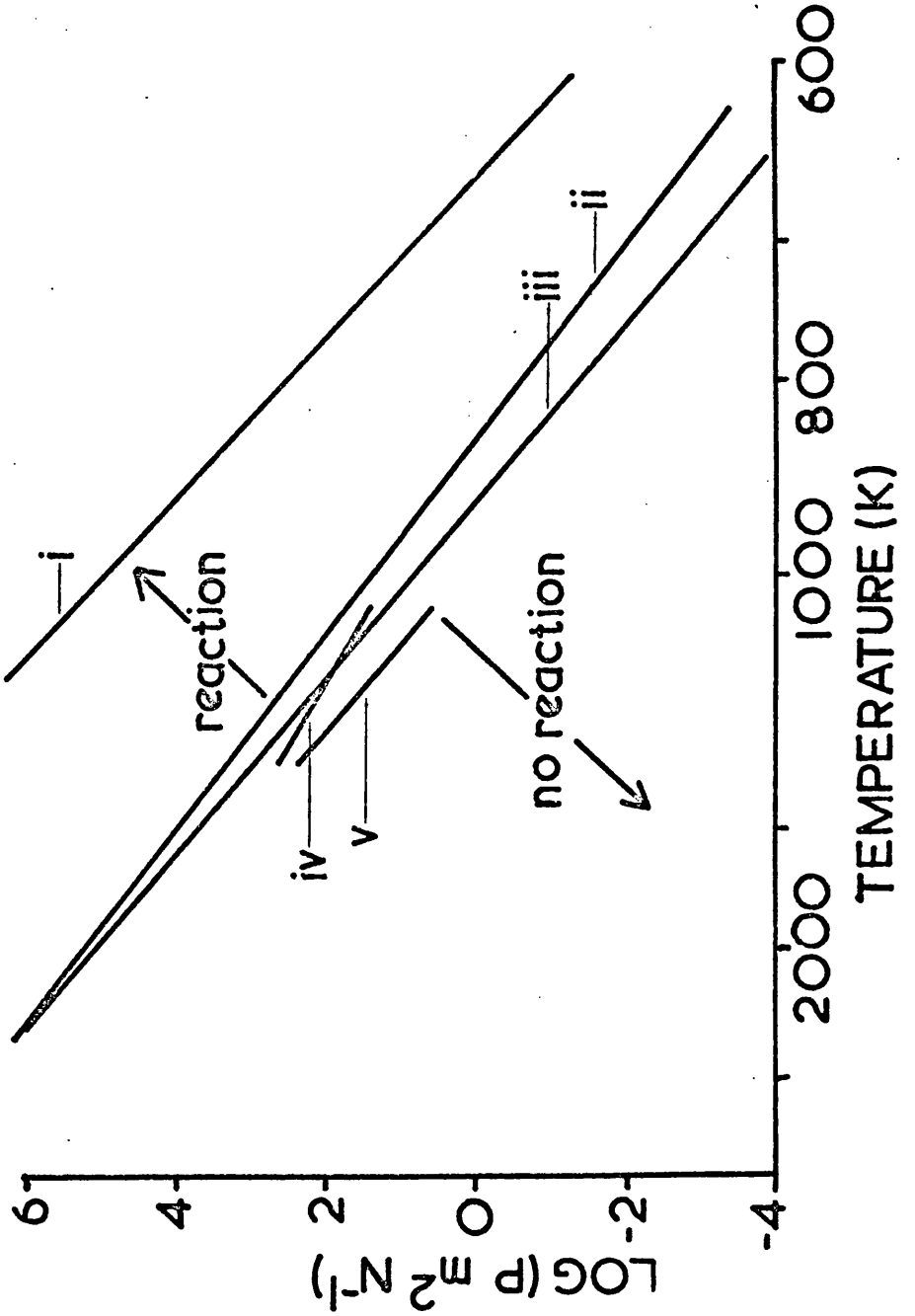


Figure II.2 Experimental and Theoretical Boundaries of Caesium Graphite Compounds

i $C_{10}Cs \rightleftharpoons C_8Cs$ Salzano and Aronson ( 1967(b))

ii $C_{72}Cs \rightleftharpoons C_{60}Cs$ ibid

iii Theoretical Boundary ibid

iv Pyrolytic Graphite Boundary Merz and Scharf ( 1971)

v Reactor Grade Graphite ibid

# CHAPTER III

## INITIAL MICROGRAVIMETRIC STUDIES OF SORPTION OF CAESIUM BY NUCLEAR GRAPHITES

This chapter deals with the initial phase of sorption experiments on the caesium-gilsonite graphite system. It includes an account of the preliminary work on, and modifications made to the microgravimetric apparatus, the production and analysis of adsorption/desorption data and an initial experiment with the electron probe microanalyser. The chapter concludes with a summary of the information obtained from this phase of work together with suggestions for future work.

### III.1 Preliminary Work

A glass silica apparatus (figure III.1) was constructed to make preliminary measurements of adsorption of caesium on two nuclear graphites of interest to this study (see Appendix I). The principal components of the apparatus are a vacuum microbalance (C.I. Electronics, Mark 2 Model B), a fused silica furnace tube containing the graphite sample, heated by a nichrome wound furnace controlled by an Ether potentiometric programme controller, and a caesium vapour source. The apparatus is evacuated by a 2-inch oil diffusion pump backed by a rotary pump, pressures being measured on Penning and Pirani gauges located near to the caesium vapour source. The vacuum microbalance is enclosed in a water-cooled aluminium cabinet in order to eliminate effects of variation in room lighting on the photocells incorporated into the microbalance head and to maintain

constant the temperature of the microbalance head. A chromel-alumel thermocouple located near to the balance head inside the system and another outside the system but within the cabinet showed only minor temperature changes (less than 10 K) on operating the system throughout the full temperature range, i.e., sample temperatures up to 1470 K. The temperature of the sample was initially measured by an optical pyrometer using an optical flat window and mirror at the bottom of the furnace tube; the pyrometer was calibrated against a calibrated chromel-alumel thermocouple located in the sample position. Another chromel-alumel thermocouple located outside the furnace tube at the same level as the sample was initially used to measure the furnace temperature but it was found to indicate a temperature which agreed with the sample temperature measured by the optical pyrometer to within $\pm$ 5 K, and thus in later runs this thermocouple was used to measure the sample temperature. The sample is suspended from the balance by articulated lengths of molybdenum and tungsten wire. The caesium in the vapour source is contained in a break-seal glass ampoule which is opened by a magnetic slug enclosed in glass. The caesium (99.98% min., 0.01% other alkali metals) is supplied by Kawecki Chemical Company (U.S.A.) distributed by Koch Light Laboratories Ltd. in 5 g break-seal ampoules. The caesium was sub-divided into approximate 1 g quantities by vacuum distillation into small ampoules which were then attached to the apparatus. The temperature of the vapour source during the initial runs was controlled to $\pm$ 3 K by an oil-filled thermostat bath.

It became apparent during initial experiments with the apparatus that there were a number of undesirable features of the design which prevented the establishment of equilibrium between the graphite and the caesium vapour source. (i) There was slow attainment of a desirable preliminary vacuum (1.3 N $m^{-2}$) and a desirable initial steady weight condition at high temperature (i.e. a weight change of less than 15 $\mu g\ h^{-1}$ at or above 1370 K), due principally to slow out-gassing of the gilsonite graphite sample. Typical outgassing times to 1.3 mN $m^{-2}$ were in the order of a few days; this time was significantly reduced (to less than 12 hours) by prior heat treatment of the gilsonite graphite in flowing argon at 1870 K in a graphite-resistance furnace and also by heat treatment at 1870 K in vacuum. However, it was considered desirable to modify the apparatus to improve pumping speeds at the sample when at low pressures. (ii) It proved difficult to prevent cold spots occurring between the caesium vapour source and the graphite sample, prticularly at high caesium vapour pressures (greater than 133 mN $m^{-2}$) when the lines between the vapour source and the graphite needed to be maintained at ca. 420 K with heater tapes. In addition, the tortuosity of the lines between the vapour source and the sample did not facilitate vapour transfer. The mean free path of the caesium atom at 13 mN $m^{-2}$ and 1270 K is 40 mm while the minimum diameter of the connecting lines between the vapour source and the sample was 8 mm so that vapour transfer down the tube is by a process of Knudsen flow, that is, via collisions with the surfaces of the connecting lines. The presence of cold spots

will effectively prevent vapour transfer by condensation and in fact visual evidence of caesium condensation at such sites was observed in prolonged experiments. It was also found necessary to maintain a very high standard of cleanliness in order to prevent interaction of caesium vapour with impurities on the surfaces of the system. In some experiments yellow-coloured deposits were observed on cold spots indicating a reaction product of caesium. It was also noted that the silica surfaces which had been at high temperatures (up to 1370 K) developed a grey colouration which could not be removed by normal cleaning processes nor by flaming. The grey colouration is thought to be the product of reaction between caesium and silica at high temperatures. Remarkably short working life times above 970 K (ca. 20 days) were found for the vitreous silica tubes used in these experiments, and a white powder, which was shown to be $\alpha$-cristobalite by X-ray analysis was also observed at the bottom of the hang-down tube at the end of each run. Thus it is possible that caesium promotes devitrification of fused silica by catalysis of the rate of crystallisation to $\beta$-cristobalite at high temperatures which then undergoes the phase transformation to $\alpha$-cristobalite on cooling down. Rowland (1972) has reported that for low caesium concentrations in a helium carrier gas, silica containers adsorb caesium quantitatively.

Despite extensive experiments, no detectable increases in weight were found for gilsonite graphite exposed to pressures of caesium (133 $\mu$N $m^{-2}$ to 133 mN $m^{-2}$) and temperatures (970 to 1370 K) in the range of interest of this study. No weight

increases were observed when a gilsonite graphite sample at 470 K was exposed to a caesium pressure of 133 mN $m^{-2}$ at the source, although the intercalation compound $C_8Cs$ is reported to be stable under these conditions, Salzano and Aronson (1967(b)). Electron microprobe analysis also failed to reveal the presence of caesium in any of the samples of graphite used in this phase of the work.

In view of these results the apparatus was modified as shown in figure III.2. Modifications were aimed to (i) improve pumping speeds (ii) eliminate cold spots between the graphite sample and the caesium vapour source and (iii) locate the caesium vapour source in direct line of sight with the graphite sample.

In an attempt to reduce the long equilibration times reported by Milstead et al. (1966) for caesium-graphite sorption it was decided to adopt an isobaric desorption technique in the micrograviметric experiments. The results of the initial experiment are shown in figure III.3. A cylindrical gilsonite graphite sample at 470 K was exposed to the caesium vapour source held at a constant temperature equivalent to a vapour pressure of 80 mN $m^{-2}$. Adsorption of caesium was recorded at at a steady rate of 1.1 mg Cs per g of graphite per hour (1.1 mg $g^{-1}$ $h^{-1}$) until a loading of 20.8 mg $g^{-1}$ was obtained. By reference to previously published work, Milstead et al. (1966), this was considered to be in excess of the equilibrium amount of Caesium which would be adsorbed at this pressure in the range 970 - 1370 K. The temperature was therefore raised to 970 K,

the caesium vapour pressure being maintained constant. An initial rapid desorption of 7.8 mg $g^{-1}$ occurred, followed by a slower weight loss at a steady rate of 76 $\mu g\ g^{-1}\ h^{-1}$; no evidence of an approach to equilibrium was found after 10 hours desorption. A further increase in temperature to 1070 K produced an initial rapid desorption of 0.4 mg $g^{-1}$ followed by a similar steady rate of weight loss of 75 $\mu g\ g^{-1}\ h^{-1}$ which continued for 9 hours.

The relatively rapid rate of adsorption at 470 K indicates that there is effective transfer of caesium from the source to the sample at this temperature. However, the long desorption times at higher temperatures suggest that the desorption rate is controlled by slow diffusion of caesium from the graphite sample.

## III.2 Initial Experiments

Following the preliminary work, further experiments were carried out to attempt to determine the rate-controlling mechanism for desorption of caesium from the graphite.
A cylindrical sample of a gilsonite graphite was machined from a block to a size of 10.54 mm length by 5.66 mm diameter and a 0.5 mm hole was drilled along the length of the cylindrical axis to take the hang-down wire. The specimen was subjected to a preliminary heat treatment at approximately 1870 K under vacuum (less than 0.13 mN $m^{-2}$) for 22 hours in order to remove volatile impurities. The specimen was then weighed on an analytical balance before being transferred to the microbalance

in the modified apparatus (figure III.2). The specimen was maintained at atmospheric pressure and room temperature for a period of 2 hours, to allow the microbalance to stabilise, after which the apparatus was slowly evacuated and the furnace raised to 1270 K over a period of 6 hours. A steady weight condition (as defined in Chapter III.1) was achieved within 6 hours, with a background pressure of 0.7 mN $m^{-2}$; the caesium ampoule was opened and its temperature raised to 370 K (equivalent to a pressure of 0.13 N $m^{-2}$). A sequence of three runs was then carried out, each run comprising an initial adsorption (or readsorption) of caesium at 470 K, followed by desorption at 970, 1070, 1170 and 1270 K. The runs are designated IA, IB and IC and are also subdivided by i, ii, iii and iv to indicate temperature in ascending order. The rates of adsorption and desorption were extracted for analysis. A summary of part of the experiment is presented in figure III.4. The experiment was concluded by an investigation of the influence of caesium pressure at the source on desorption rate at 970 K, the results being presented in figure III.5 (Run ID). These results show that there is little effect of caesium pressure on the desorption rate, since the rate decreases from 14.5 to 8.8 mg $g^{-1}$ $h^{-1}$ for an increase in caesium source pressure of four orders of magnitude.

## III.3 Analysis of desorption data

If it is assumed that during the desorption stage the rate of readsorption of caesium is negligible compared to the rate of desorption, i.e. the Langmuir free evaporation condition applies,

then in principle the rate of desorption of caesium from the graphite is controlled by two limiting processes :-

(i) evaporation of caesium from the surface, or

(ii) diffusion of caesium from the bulk of the graphite.

The intermediate condition of mixed control of the desorption rate will be considered in Chapter VI.

The assumption of Langmuir free evaporation conditions may be justified from the following considerations. The mean free path of the caesium atom at a pressure equivalent to a flux rate of 200 $\mu$g of caesium per minute desorbing from a specimen of surface area of 200 $mm^2$ (a sphere of 8 mm diameter) at a temperature of 900 K is 50 mm. This, the classical mean free path, in comparison to the furnace tube radius of 15 mm, suggests that there are negligible gas phase collisions occurring before the caesium atoms strike the fused silica walls of the furnace tube. Atoms striking the wall may suffer three fates, (i) surface adsorption, (ii) specular reflection, or (iii) diffuse reflection.

Evidence that surface adsorption occurs is provided by Rowland (1972) who found that fused silica acts as an efficient getter of trace quantities of caesium at high temperatures. This may be linked with the observation in the present work that caesium adsorbed on fused silica at high temperatures promotes devitrification. Similar reactivity has been observed with sodium and lithium at temperatures above 500 K. An experiment was carried out using a fused silica disc (10 mm diameter by 1 mm thick) suspended from the hang-down wire with the plane of

the disc in the horizontal plane, in an attempt to measure adsorption of caesium on fused silica. No observable weight gain was found (i.e., the weight change was less than 100 $\mu g\ g^{-1}\ h^{-1}$) for a caesium source pressure of 0.13 $N\ m^{-2}$ over a temperature range for the silica disc of 470 to 1270 K. However, caesium transport through the hot zone occurred, since a silvery deposit was found at the end of the equipment near the water-cooled joint above the furnace (figure III.2). Under similar conditions, a sample of gilsonite graphite adsorbed caesium at a rate of 1.1 $mg\ g^{-1}\ h^{-1}$ at 470 K (figure III.3) thus indicating that the sticking coefficient on fused silica at 470 K is low in comparison to that for gilsonite graphite. In contrast, run ID shows that the rate of desorption of caesium from gilsonite graphite at 970 K is insensitive to large variations in caesium pressure at the source (figure III.5). Thus, either the rate of transport of caesium to the sample decreases on increasing temperature, by the emergence and domination of adsorption of caesium by fused silica, or else the sticking coefficient of caesium on gilsonite graphite dramatically reduces on increasing temperature. If adsorption is the cause, then caesium atoms desorbing from the graphite sample will be effectively adsorbed on the fused silica walls and, hence, reduce the flux returning to the graphite sample to an insignificant amount, i.e., a Langmuir free evaporation condition.

If, however, the sticking coefficient of caesium on gilsonite graphite is the cause, then the Langmuir free evaporation condition can still hold. Consider the caesium flux desorbing from the specimen. On collision with the fused silica walls, the

atoms may be specularly or diffusely reflected. If specular reflection occurs, then it can easily be shown (Appendix 2) that the flux returning to the graphite sample is less than 3% of that emitted. Hence in conjunction with a low sticking coefficient, specular reflection leads to a very low readsorption ratio. However, if only diffuse reflection occurs, then calculations (Appendix 2) show that 0.3% of the flux returns to the graphite sample after one wall collision. The number returning after two or more wall collisions was not calculated, but it must cause an increase in the percentage return. Again, in conjunction with a low sticking coefficient, the readsorption ratio becomes very low.

The three cases expounded represent extremes of the experimental situation, and since it is most probable that all three play a role in the transport mechanism, then the conclusion of a Langmuir free evaporation condition is justifiable. Furthermore, in view of the complexity of the mechanism of caesium transport, the use of the thermal transpiration equation

$$P_1/P_2 = (T_1/T_2)^{\frac{1}{2}} \qquad \text{III.1}$$

where P and T are the pressure and temperature of two regions subscript 1 and 2, cannot be justified. Also, equation III.1 is only applicable to an equilibrium system, whereas in the present case a dynamic system of caesium transport from the source to the water cooled joint (figure III.2) occurs. Thus the control of the caesium vapour source temperature was discontinued since no assessment of the gaseous concentration around the specimen could be made.

The shape of the desorption curves (figure III.4) suggests qualitatively that desorption is controlled in the early stages by evaporation of caesium from the surface and that after the surface layer of caesium has been depleted, the rate of desorption becomes controlled by diffusion of caesium from the bulk. Assuming this interpretation to be correct, an analysis of the later portion of the desorption curve at each temperature was attempted using the following equation, Jost (1960)

$$\bar{C}_t/\bar{C}_o = \frac{4}{(2.405)^2} \exp\left(\frac{-Dt^2 2.405^2}{a^2}\right) \qquad \text{III.2}$$

where $\bar{C}_t$ is the mean concentration at a time t, $\bar{C}_o$ the initial mean concentration, D the diffusion coefficient and a, the radius of the cylinder. Equation III.2 is based upon the solution of Fick's laws of diffusion for an isotropic cylindrical specimen considering radial flow only, i.e. neglecting end effects, with the boundary conditions of an initial uniform concentration profile except at the surface where the concentration is zero and time-independent and that no barrier to evaporation exists. It is also assumed that the diffusion coefficient is independent of other variables e.g. concentration, time or position. Equation III.2 is an approximation of the solution, but a discussion on the limitations of this approximation will be considered in Chapter V.2. Thus a plot of log $(\bar{C}_t / \bar{C}_o)$ versus t over the later portion of the desorption curve enables a value of D to be calculated.

The values of diffusion coefficient obtained by use of equation III.2 are presented in Table III.1 together with the desorption temperatures and the mean concentration range.

Figure III.6 shows the resultant Arrhenius plot which includes the data of Flowers et al. (1972) for diffusion of caesium in similar types of graphite, the latter results being obtained from steady flow measurements and post irradiation experiments. Thus the present results can be seen to be in reasonable agreement with published data obtained from other techniques.

## III.4 Preliminary Electron Probe Microanalysis

It is recognised that the assumption made in the derivation of equation III.2 that desorption of caesium occurs from an initial uniform concentration profile is not likely to apply in practice. It was therefore considered desirable to investigate the penetration of caesium into the graphite sample. A further run was carried out using a cylindrical specimen (Run 2). After the initial preparation, the graphite sample was exposed to a caesium atmosphere at 470 K until 54 mg $g^{-1}$ had been adsorbed (within 2 hours) and then subjected to heat treatment at 570 K for a further 57.5 hours to allow some penetration of the caesium into the graphite; during this time no appreciable weight change occurred. The specimen was then removed and sectioned along the cylindrical axis and subjected to electron probe microanalysis to obtain the radial and cylindrical axis concentration profiles for caesium; details of the procedure will be given in Chapter IV. The cylindrical axis profile was remarkably even, increasing only at a small distance from the end. The radial profile, figure III.7, shows an even concentration of caesium in the inner portion, with a dramatic increase in the outer layers. The presence of caesium in the central regions of the cylinder clearly indicates that rapid diffusion of caesium to the centre has

occurred. Extrapolation of the diffusion coefficients obtained between 970 and 1270 K (figure III.6) to 570 K gives a diffusion coefficient of the order of $10^{-20}$ $m^2$ $s^{-1}$; reference to Carslaw and Jaeger (1973) indicates that with such a low diffusion coefficient, negligible penetration of the graphite by caesium should occur. Clearly therefore the mechanism of diffusion undergoes a change between 570 K and 970 K.

## III.5 Conclusions

Preliminary experiments on the microgravimetric apparatus showed that it was not possible to obtain equilibrium data on adsorption of caesium by gilsonite graphite using a classical gravimetric method. This was attributed to a strong interaction at high temperatures between caesium and the fused silica walls of the furnace tube and a temperature sensitivity of the sticking coefficient of caesium on gilsonite graphite. This process did not allow an assessment of the vapour pressures of caesium around the specimen at high temperatures with any degree of confidence. However, because of this problem, it enabled desorption of caesium from the caesium graphite sample to be treated as a Langmuir free evaporation process. An application of a simple diffusion equation to the later portion of desorption curves gave diffusion coefficients for transport of caesium through graphite which were in reasonable agreement with results obtained by other techniques. The initial stages of desorption were considered to be controlled by diffusion of caesium to and evaporation from the surface of the graphite. Electron probe microanalysis of a caesium graphite specimen prepared at a low temperature showed that considerable penetration of caesium into the graphite had occurred. Comparison with a diffusion coefficient

obtained from extrapolation of high temperature data suggests that a change in the diffusion mechanism occurs between 570 and 970 K.

These results suggest the need for further work to obtain more detailed information on sorption and diffusion of caesium in gilsonite graphite; this work is discussed in Chapter IV. It is also desirable to extend the method of analysis to cover the initial period of desorption in which evaporation of caesium from the surface is important; this work is discussed in Chapter VI.

Table III.1

Diffusion Coefficients calculated for caesium in cylindrical specimens of gilsonite graphite using Equation III.2.

| Run No. | D ($m^2\ s^{-1}$) x $10^{12}$ | Temperature ( K ) | Initial Concentration ( mg $g^{-1}$ ) | Final Concentration ( mg $g^{-1}$ ) |
|---|---|---|---|---|
| IA i | 2.0 | 970 | 1.70 | 1.43 |
| IA ii | 2.6 | 1070 | 1.43 | 1.35 |
| IA iii | 4.8 | 1170 | 1.35 | 1.20 |
| IA iv | 9.4 | 1270 | 1.20 | 0.85 |
| IB i | - | 970 | 2.25 | 2.05 |
| IB ii | 2.0 | 1070 | 2.05 | 1.96 |
| IB iii | 4.6 | 1170 | 1.96 | 1.72 |
| IB iv | 5.4 | 1270 | 1.72 | 1.20 |
| IC i | 0.8 | 970 | 8.45 | 5.80 |
| IC ii | 0.6 | 1070 | 5.80 | 5.50 |
| IC iii | 3.0 | 1170 | 5.50 | 4.92 |
| IC iv | 11.0 | 1270 | 4.92 | 3.52 |

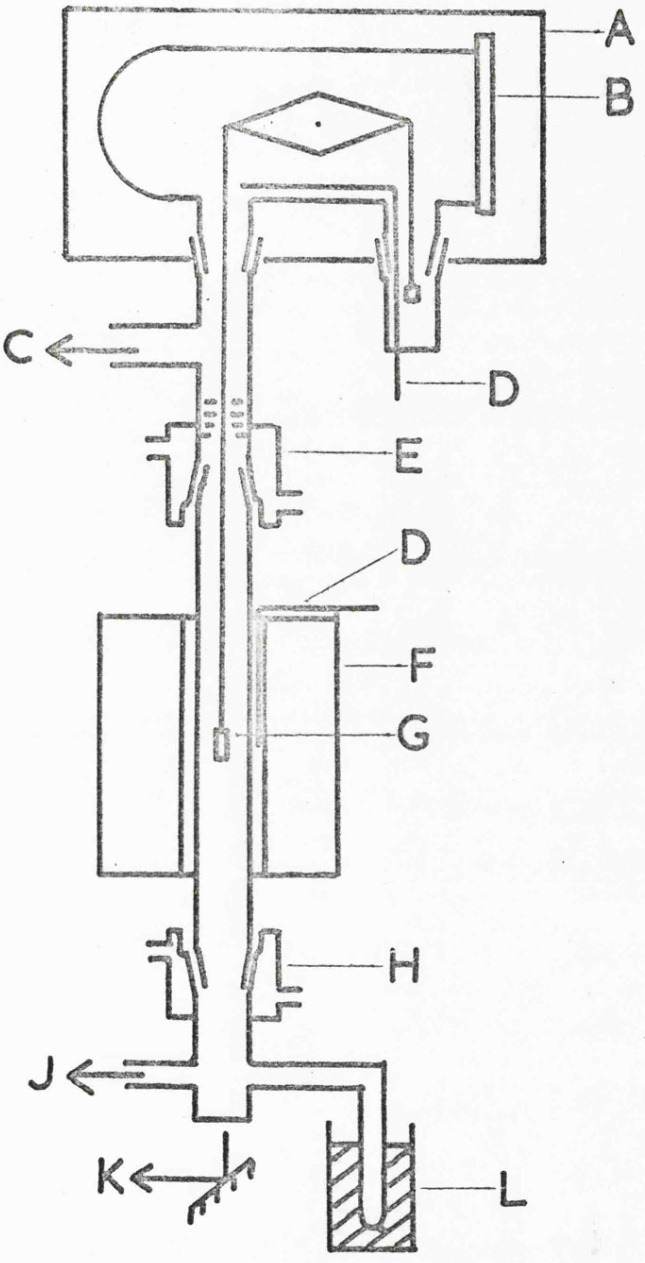


Figure III.1 Schematic Diagram of the Original Micro-gravimetric apparatus

A Water Cooled Cabinet
B Microbalance
C To Pumps
D Thermocouple
E Water Cooled Joint and Baffle
F Furnace
G Specimen and Hang down wire
H Water Cooled Joint
J To Vacuum Gauges
K Optical Pyrometer Viewing System
L Caesium Ampoule and Oil Bath

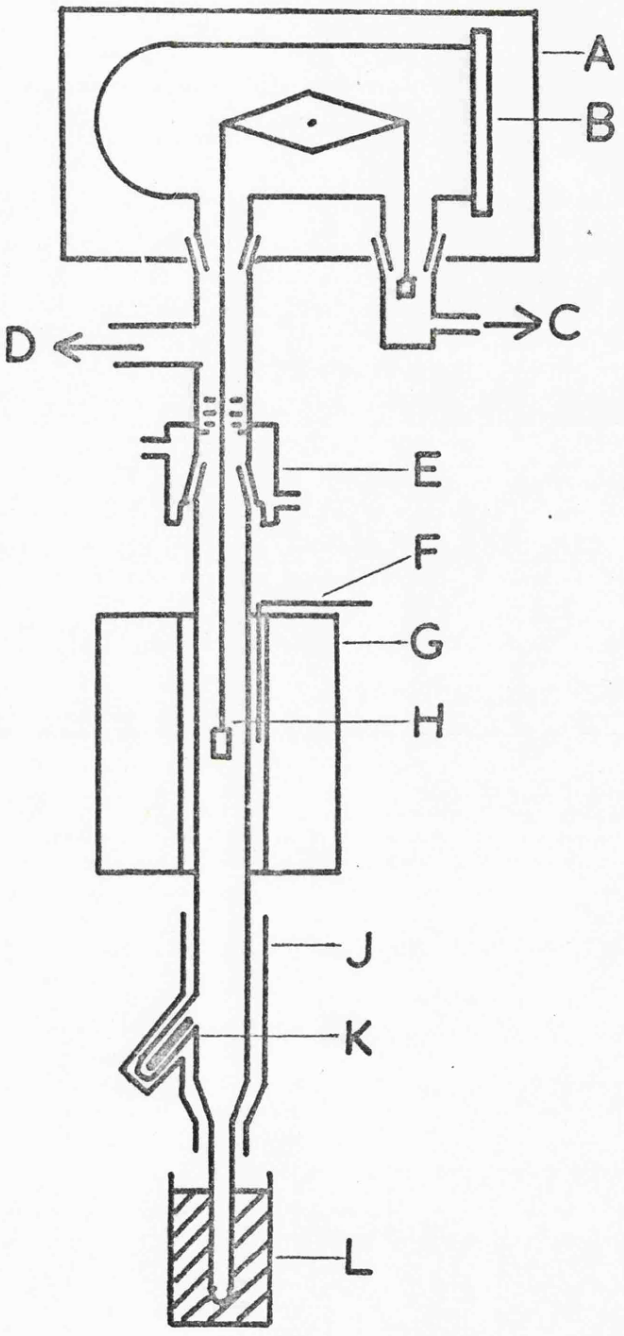


Figure III.2 Schematic Diagram of the Modified Microgravimetric apparatus

A Water Cooled Cabinet
B Microbalance
C To Vacuum Gauges
D To Pumps
E Water Cooled Joint and Baffle
F Thermocouple
G Furnace
H Specimen and Hang down wire
J Heating Tape
K Magnetic slug
L Caesium Ampoule and Oil Bath

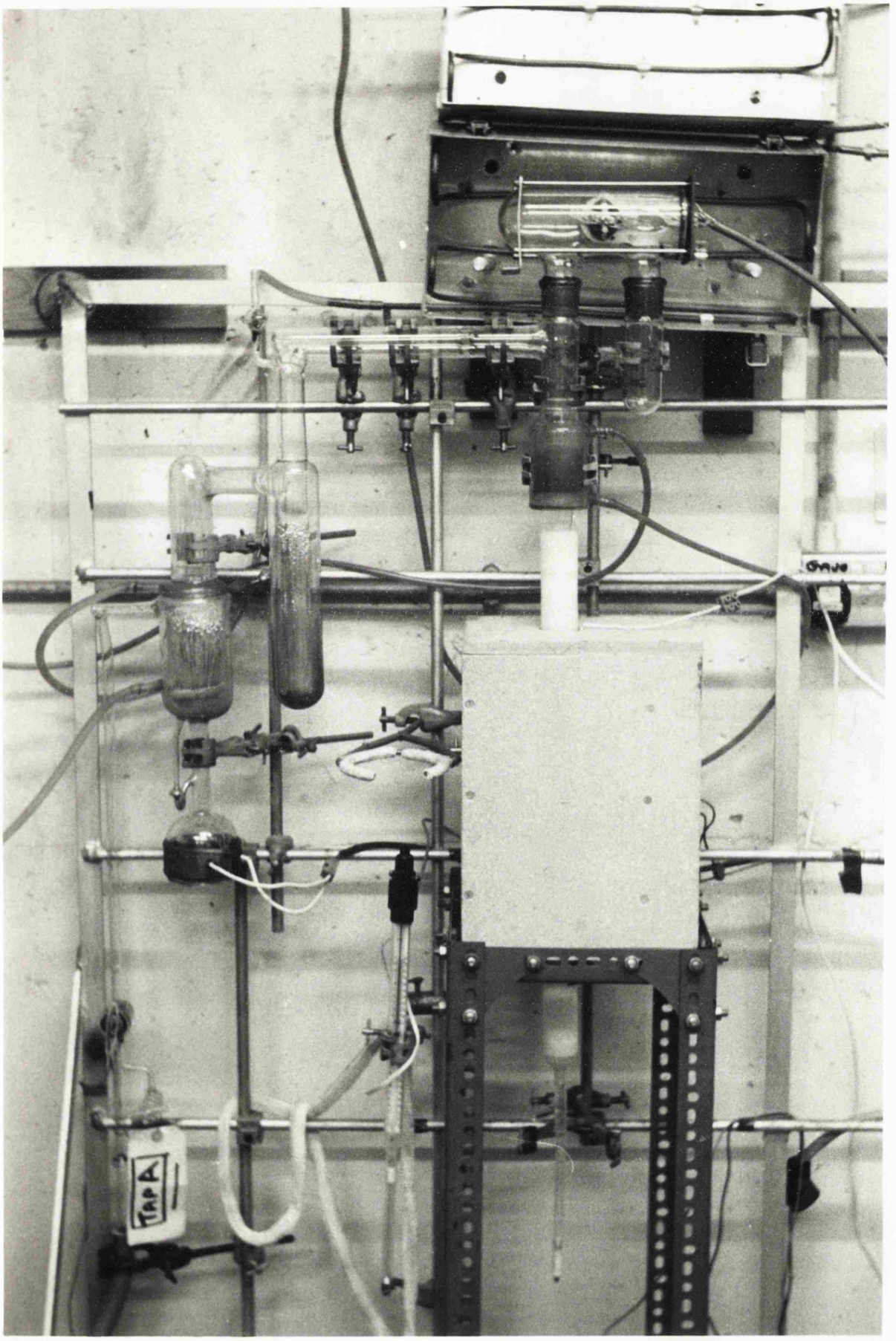


Figure III.2 The Microgravimetric Apparatus

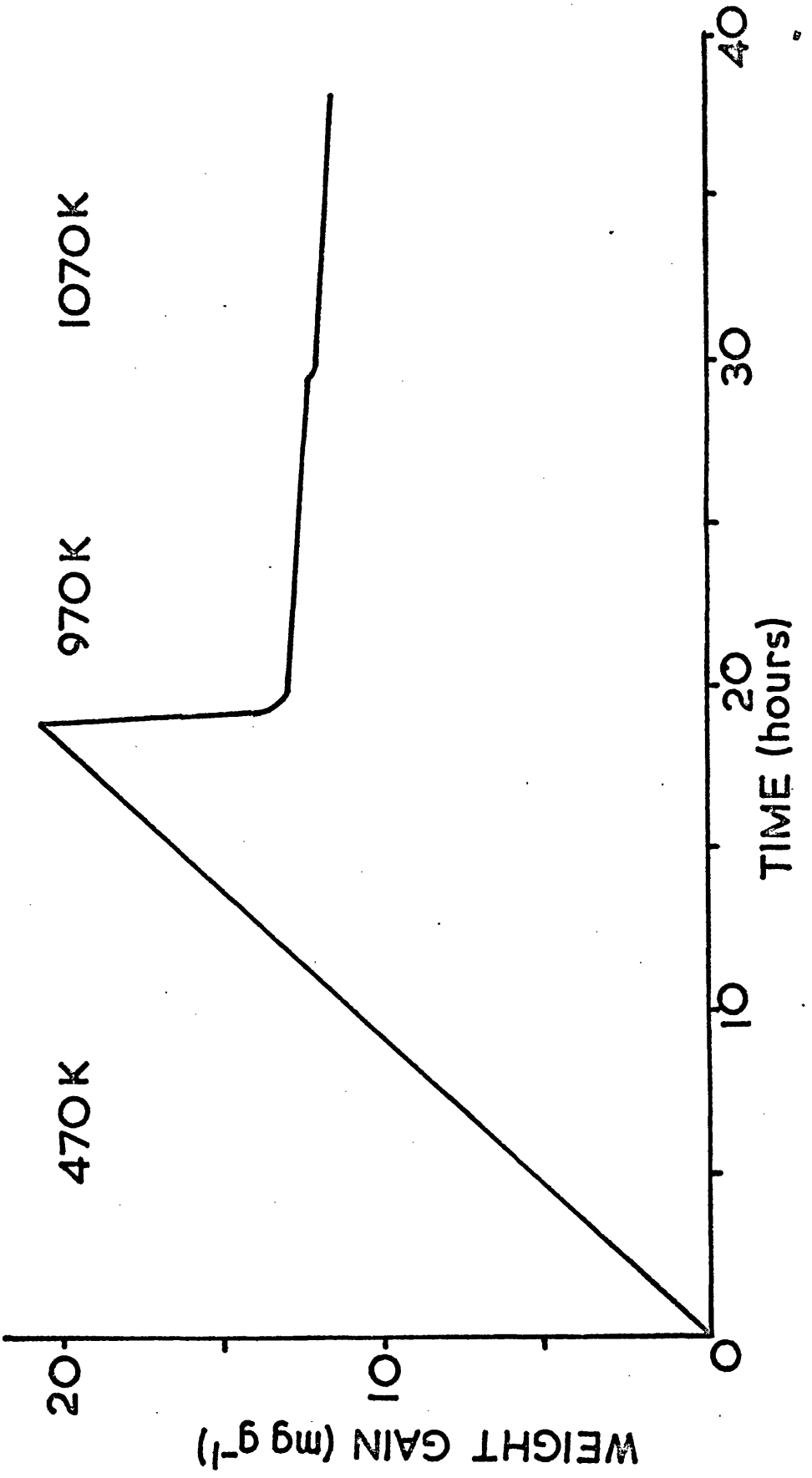


Figure III.3 Isobaric Sorption of Caesium on Gilsonite Graphite at various Temperatures

$P_{Cs} = 80\ mN\ m^{-2}$

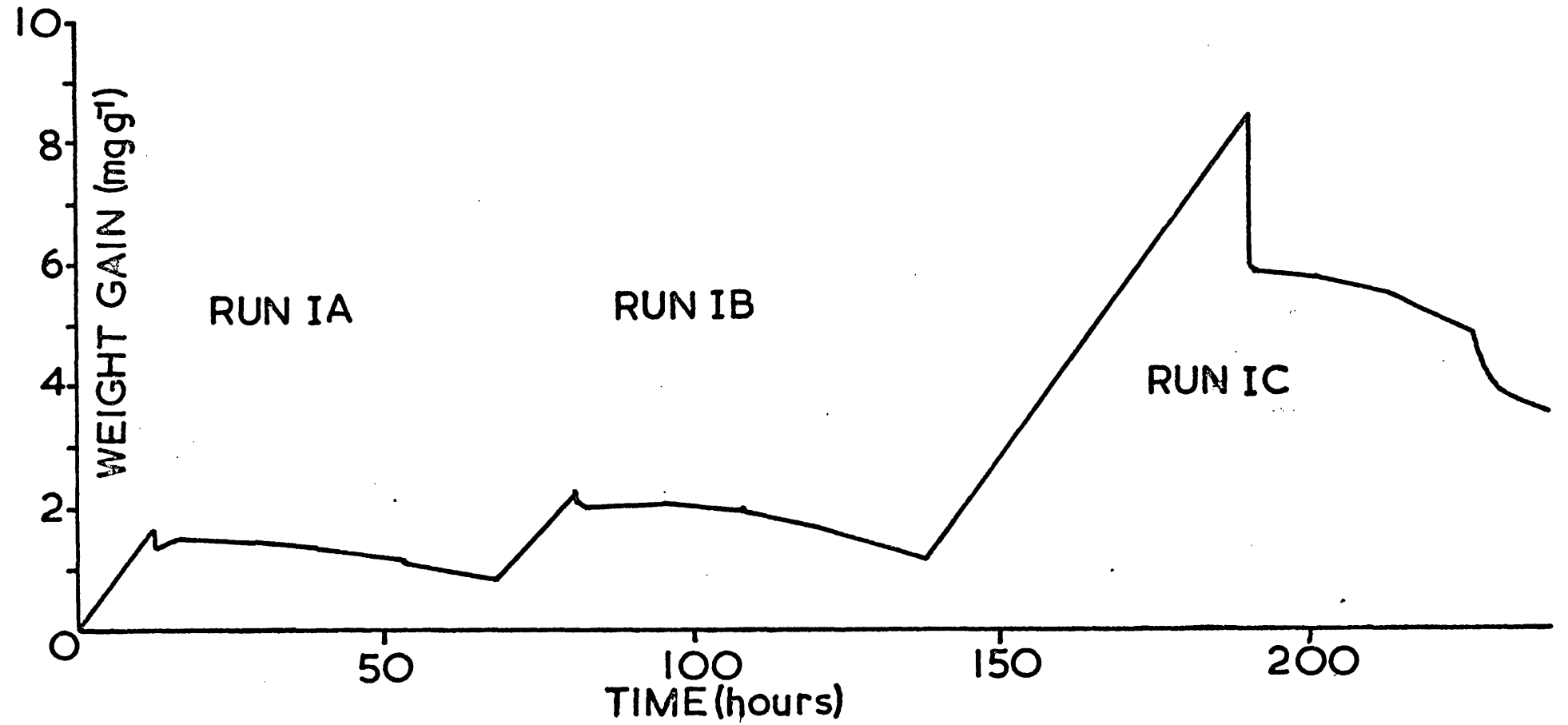


Figure III.4 Results of Adsorption/Desorption Cycles on Gilsonite Graphite ( Run I)

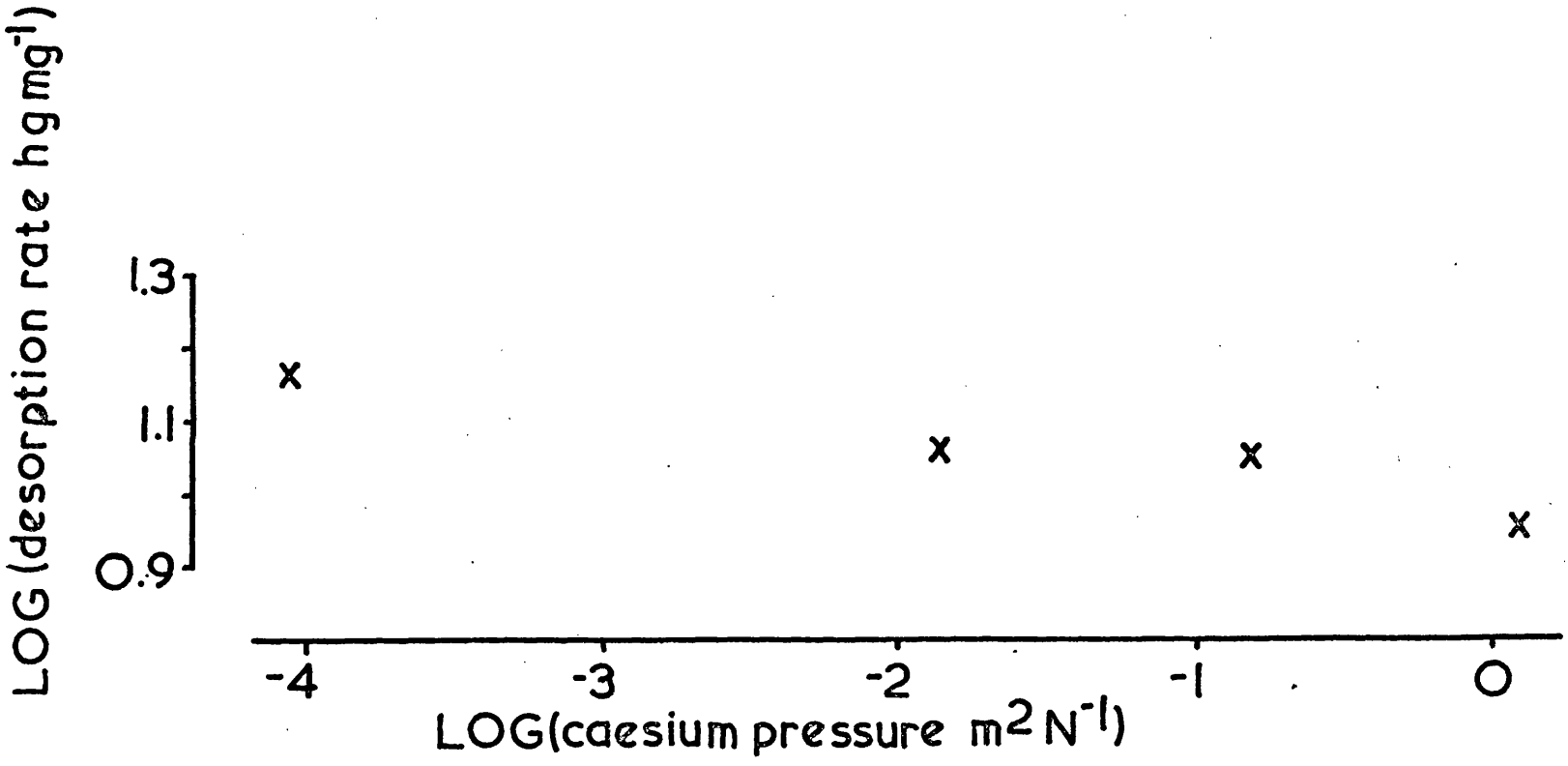


Figure III.5 Variation of Rate of Desorption of Caesium from Gilsonite Graphite at 970 K with Caesium vapour Pressure at source

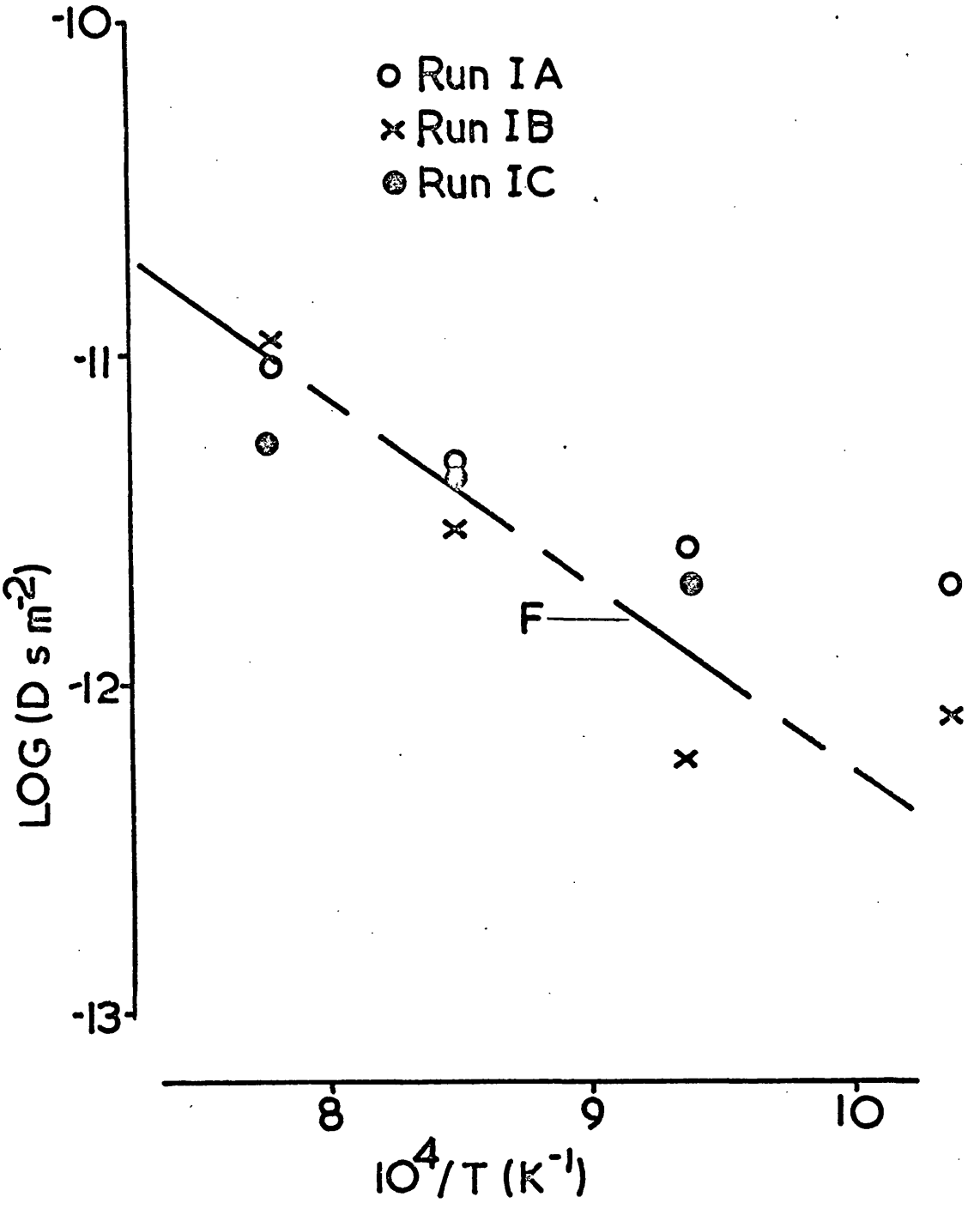


Figure III.6 Arrhenius plot of Diffusion Coefficients for Caesium in a Cylindrical specimen of Gilsonite Graphite ( Run 1)

F data of Flowers et al. (1972)

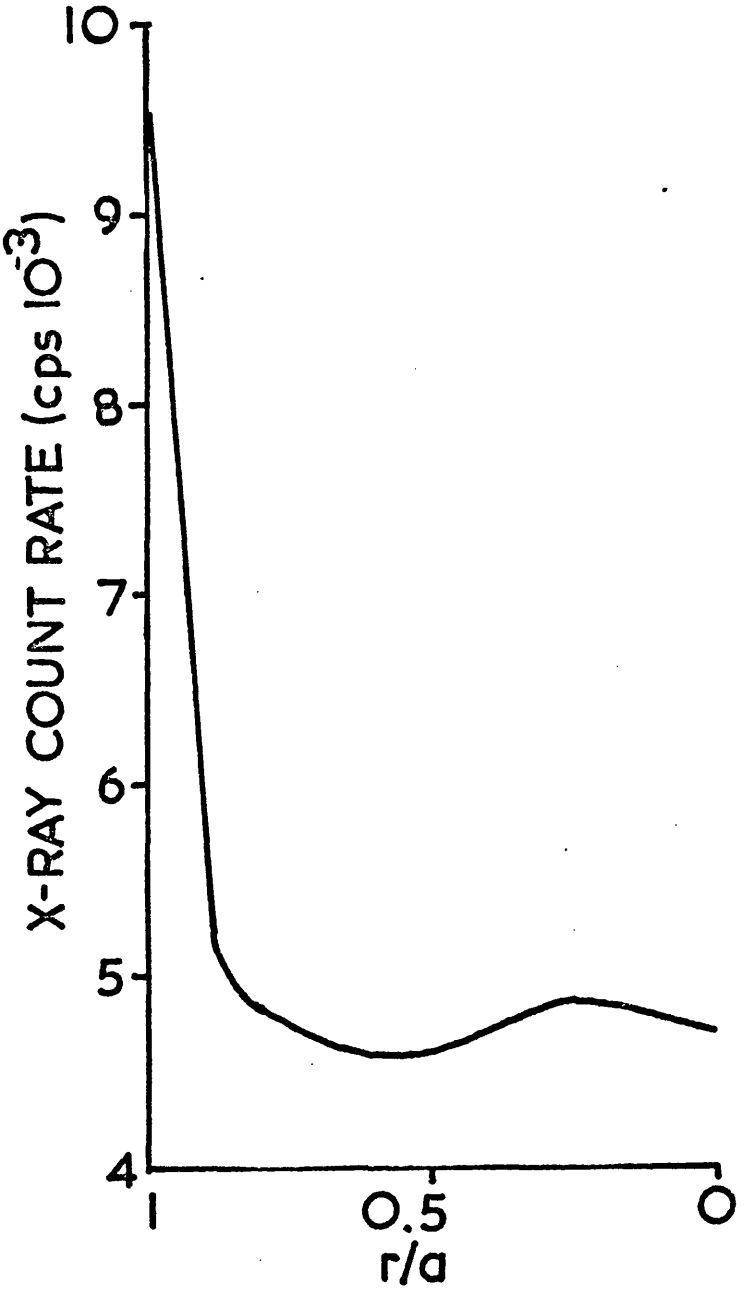


Figure III.7 The Smoothed Radial Concentration Profile for Caesium in a Cylindrical specimen of Gilsonite Graphite ( Run 2 )

# CHAPTER IV

## ELECTRON PROBE MICROANALYSIS OF THE CAESIUM-GILSONITE GRAPHITE SYSTEM

In the previous chapter it has been shown that diffusion coefficients for caesium in gilsonite graphite can be obtained from measurements of the rate of desorption of caesium which are in reasonable agreement with other workers' results. Since the analysis used to obtain the diffusion coefficients is based upon an assumption of an initial uniform caesium concentration profile, a series of experiments was carried out to obtain both caesium desorption curves and caesium concentration profiles at stages in the adsorption/desorption programme, the work being described in this chapter. The chapter starts with a brief outline of the theory of electron probe microanalysis and its application to the present study, and concludes with a summary of the results and conclusions obtained and some further questions that the results give rise to.

### IV.1 Electron Probe Microanalysis

Electron probe microanalysis is a flexible technique for elementary analysis of solid materials which is based upon the excitation of X-rays from a small portion of the sample by a beam of electrons, the emitted X-rays being analysed and counted by an X-ray spectrometer and detector. An electron beam produced by a conventional hot filament source is focused onto the specimen causing some of the atoms to be ionised via a mechanism involving the loss of an inner electron. The resultant transition of an outer electron involves the emission of an X-ray photon which is

characteristic of the excited atom, and thus the emitted X-ray spectrum is characteristic of the elements present within the excited portion of the sample.

Quantitative analysis of the sample is performed by obtaining the ratio of the sample count rate to the count rate of a standard, being either the element or a pure compound containing the element of interest. However, various effects combine to obscure quantitative analysis, notably absorption by surrounding atoms, fluorescence, electron back-scatter, secondary electron emission and the efficiency of the process of X-ray emission.

The principal advantages of electron probe microanalysis are : (i) the technique can be applied to all elements of atomic number higher than 3 (ii) it is non-destructive and (iii) analysis of small areas of interest may be performed with relative ease compared to other techniques, typical excitation volumes being approximately 5 $\mu$m cube. The limiting sensitivity of the technique is normally quoted in absolute terms, as approximately $10^{-15}$ g, Marton (1969), but in relative terms the limiting sensitivity is about 10 $\mu g\ g^{-1}$ of sample. This figure, however, can only be achieved using the maximum possible care and specially modified apparatus of high sensitivity; a more realistic limiting sensitivity for normal operation is a factor of a hundred lower, i.e. about 1 mg $g^{-1}$. Indeed, experiments on the caesium-gilsonite graphite system indicated that concentrations of less than 2 mg $g^{-1}$ were not detectable. Hence in the present studies relatively high total concentrations of caesium in gilsonite graphite were used (approximately 40 mg $g^{-1}$) in order to obtain reasonable X-ray count rates.

To a first approximation, the concentration is linearly dependent upon the ratio of the specimen X-ray count rate to the standard X-ray count rate. In order to improve upon this approximation various corrections must be applied to the data, which can be conveniently subdivided into two, namely a correction due to matrix effects and a correction due to self effects, i.e., the element of interest. These corrections are applied to both specimen and standard. However, in the present work, because the total concentration is known from the microgravimetric experiments, the use of a standard is not necessary, if the corrected X-ray count rate is integrated over the whole specimen. It was for this reason and also that the analysis of desorption data from cylindrical specimens neglects end effects, that the specimen shape was changed to a sphere. Diffusion equations are accurately known for spherical specimens and the integration over a sphere only requires a radial profile to be known, whereas a cylindrical specimen requires both the radial and the cylindrical axis profiles to be known. It was also considered that because of the low concentrations of caesium, approaching the limit of detection, the corrections due to the matrix, i.e. graphite, would be constant and the corrections due to self-effects would be negligible. Thus the conversion factor of X-ray count rate to concentration was found by integrating the X-ray count rate radial profile over the whole of the sphere and dividing the total concentration by the integral sum of the X-ray count rate.

The instrument used in this work is a J.E.O.L. JXA 50A analyser, which is designed with a "low take off angle" for X-ray emission. A low angle of take off enables the final objective lens of the electron optical system to be placed close to the specimen without

obscuring the X-ray spectrometer view of the specimen. However, the X-ray spectrometer system is sensitive to surface topography because of this feature and therefore care must be taken in the surface preparation in order to minimise this effect. It is desirable to obtain a surface finish of metallographic quality, e.g. by polishing with 1 $\mu$m diamond dust, which for a sample of gilsonite graphite is a long and complex task. The gilsonite graphite used in the present work suffers from 'pluck out' during polishing since it comprises of hard graphitic particles in a soft matrix (see Appendix I). The reactivity of the caesium-graphite compounds, Croft (1970), also gives rise to the question of stability of the specimens during polishing. For instance Iwamoto and Oishi (1969) found that treatment with dilute nitric acid effectively leached all fission products from the surfaces of the crystallites within a bulk sample of a nuclear graphite. In polishing to metallographic standards the removal of the polishing compound and debris requires a 'wet' technique, e.g., water or alcohol, and thus leaching of the caesium from the graphite will occur, hence affecting the concentration profile. In view of the problems that would arise from polishing to such a standard it was decided to prepare the surface using carborundum paper only and then subject the resultant profile to an averaging process in order to reduce the effect of surface asperities.

IV.2 Microgravimetric experiments and results

Spherical specimens of gilsonite graphite (8 mm nominal diameter) were machined from bulk samples to within 5% tolerance in the diameter. A 0.5 mm hole was also drilled through the specimen to take the hang-down wire. Each specimen was subjected to a preliminary heat treatment in a separate apparatus in order to remove

volatile impurities from the sample by subjecting the specimen to a temperature of approximately 1970 K for 24 hours under a vacuum (0.1 mN $m^{-2}$ approximately).

The specimen was then removed from the apparatus, weighed in air and then placed in the microgravimetric apparatus (figure III.2) and evacuated. This operation was completed as quickly as possible (less than half an hour) in order to minimise recontamination on exposure to air. A fresh break-seal ampoule of caesium was used for each run and prior to each run the hang-down tube was cleaned with a hydrofluoric/nitric acid mixture, rinsed with distilled water followed by acetone and finally allowed to dry.

The microgravimetric experiments can be conveniently divided into four stages: (i) the initial stabilisation program outlined in Chapter III (ii) adsorption of caesium at approximately 470 K (iii) heat treatment at 570 K and (iv) desorption of caesium in the range 973 to 1373 K. The adsorption stage was carried out by distilling caesium from the ampoule and allowing the specimen to adsorb caesium to a concentration of approximately 40 mg $g^{-1}$; this loading was achieved within 1 hour. It was not considered necessary to closely control the temperature of the ampoule (see Chapter III.3).

The temperature of the specimen was then increased to 573 K for a 60 hour period of heat treatment to allow caesium to diffuse into the specimen. It was found necessary to subject the specimen to an initial short temperature excursion to approximately 670 K before heat treatment at 573 K in order to achieve a near steady weight condition (less than $\pm$ 40 $\mu$g $h^{-1}$) over the 60 hour period. The caesium ampoule was maintained at room temperature during heat treatment.

The specimen was then raised to the desired temperature for desorption and the weight loss monitored for a period of time. At the end of desorption the specimen was allowed to cool to room temperature and removed from the apparatus and reweighed on an analytical balance. The weight gains so measured usually exceeded the weight gains recorded on the microbalance by approximately 2% (5% for Run 3). This discrepancy was considered acceptable since relatively rapid adsorption of water-vapour and other gases will occur on exposing the caesium-graphite to air.

Details of each run are tabulated in Table IV.1. Runs 3 and 4 were made in order to obtain caesium concentration profiles after adsorption and after adsorption and heat treatment respectively. Runs 5 to 9 were made to obtain both desorption data (figure IV.1) and caesium concentration profiles at temperatures between 973 and 1373 K on separate samples of graphite.

It was considered desirable to perform a preliminary analysis of the desorption data in a similar manner to that used in Chapter III.3. Jost (1960) gives the following equation for diffusion in spherical specimens for those conditions assumed in Chapter III.3 for cylindrical specimens (equation III.2)

$$\bar{C}_t/\bar{C}_o = 6 \exp(-Dt\pi^2/a^2)/\pi^2 \qquad \text{IV.1}$$

where a is the radius of the sphere and the other terms are as defined in Chapter III. The later portions of the desorption curves were plotted as $\log(\bar{C}_t/\bar{C}_o)$ vs. t and the values of the diffusion coefficients and their standard deviations were calculated from the gradients using the method of least mean squares, and tabulated in Table III.1. The resultant diffusion coefficients are

shown in the form of an Arrhenius plot in figure IV.2 together with the data of Flowers et al. (1972). The diffusion coefficients obtained show marked deviation at low desorption temperatures from those found from the cylindrical specimen (Run I, figure III.6). This increase cannot be ascribed to the neglect of end effects on cylindrical specimens, since neglect of end effects causes the diffusion coefficients so calculated to be increased. Thus diffusion coefficients for cylindrical specimens would be expected to be larger than the spherical specimen diffusion coefficients. It is possible that the deviation found reflects the different adsorption and heat treatment programs used in each case. This point will be discussed in more detail in Chapter VI.

## IV.3 Electron Probe Microanalysis experiments and results

The specimens obtained from Runs 3 to 9 were cut into hemispheres along the vertical axis, i.e. the axis of support in the microbalance, so that the possibility of a non-uniform concentration of caesium resulting from the position of the specimen relative to the caesium ampoule could be investigated. The surface was polished with P 500 grade paper, lightly drawn across soft tissues in order to remove any debris and then mounted on the specimen holder. The surface of the specimen was checked for being in the plane of the top of the specimen holder by the use of an optical microscope with a narrow depth of focus, and rechecked within the electron probe microanalyser. After setting up the electron probe microanalyser, the electron beam was checked for focus and a beam intensity corresponding to a specimen current of 0.2 $\mu$A at an accelerating voltage of 20 keV was obtained. The high current was used in order

to obtain reasonable X-ray count rates (of the order of $10^3$ cps) and the beam area was estimated at 10 $\mu$m square. The X-ray detector was focused on the L$\alpha$, X-ray emission of caesium using a P.E.T. crystal to resolve the X-ray emission. The background count rate was also measured at approximately one degree either side of the L$\alpha$ peak and the subsequent count rates were corrected using the average value for background so obtained.

The specimen was then scanned at a rate of 2 $\mu$m $s^{-1}$ along (i) a diagonal parallel to the axis of support and (ii) a diagonal perpendicular to (i); the time for one scan being of the order of 45 minutes. The resultant traces, an example of which is shown in figure IV.3, were considered to be adequate for analysis and no extension to the polishing process was required. Each profile obtained was then averaged at 100 $\mu$m intervals by a graphical method and the gross average of all the various scans for each run was computed in the form of count rate vs. radius at 100 $\mu$m intervals. These values of mean count rate (cps) vs. the normalised radius (r/a) were then summed at 100 $\mu$m intervals according to the formula

$$S_m = \sum_{r/a = 0}^{r/a = 1} (cps)(r/a)^2 \, \Delta r/a \qquad \text{IV.2}$$

where $\Delta$ r/a is the interval length, i.e. 100 $\mu$m. The proportionality constant, k, between (cps) and total concentration of caesium was then obtained from

$$k = \bar{C}_F/3 \, S_m \qquad \text{IV.3}$$

where $\bar{C}_F$ is the total concentration at the end of the sorption

experiment. The resultant concentration profiles are shown in figure IV.4 and some specific data in Table IV.1. Figure IV.5 is a summary graph in which the concentration profiles have been normalised to $\bar{C}_o$.

IV.4 Discussion of Electron Probe Microanalysis results

Figure IV.4(a) shows that after adsorption at 523 K for half an hour (Run 3) caesium is confined to the outer part of the sample ($r/a > 0.65$). However, heat treatment at 573 K for approximately 60 hours results in significant penetration of caesium to the centre of the graphite (Run 4, figure IV.4(a)). The flat concentration profile in the inner part of the graphite ( $0 < r/a < 0.6$) also shows that the penetration is relatively rapid, cf. Run 2, figure III.7. A comparison of runs 3 and 4 from the normalised concentration profiles (figure IV.5) suggests a two part inward diffusion process is occurring at 573 K :- (i) a rapid penetration to the centre (as above) and (ii) a slower inward movement of the bulk of the caesium, indicated by the shift of the peak r/a value from 0.95 to 0.84 (Table IV.1).

The normalised concentration at the centre rises again during the desorption stage at 973, 1053 and 1177 K (Runs 5 to 7) and then drops slightly for desorption at 1270 K (Run 8) and back to zero for desorption at 1373 K (Run 9, Table IV.1). The normalised surface concentration (figure IV.5) is highest after adsorption (Run 3) and drops to a relatively constant level after heat treatment (Run 4) and during desorption at the lower temperatures, i.e., up to 1177 K (Runs 5 to 7). However, desorption at higher temperatures results in a lower normalised surface concentration. These effects are

almost certainly obscured by the varying times of desorption, especially in the case of desorption at 1373 K (Run 9) where the time for desorption was almost twice that for desorption at the lower temperatures (Runs 5 to 7).

A general feature of the concentration profiles is the apparent contradiction of Fick's Law which can be expressed in the form "diffusion tends to reduce the concentration gradient". This is most clearly seen for desorption at 1373 K (Run 9, figure IV.5) where the diffusion of caesium has occurred against the total caesium concentration gradient. Diffusion against a concentration gradient can be explained in terms of a two part diffusion model which will be discussed in detail in Chapter VI.

Some evidence for non-uniform concentrations of caesium was found, particularly at low temperatures. The largest difference was found after adsorption at 523 K (Run 3) where the caesium concentrations at the edge nearest to the caesium ampoule was twice that found on the edge diametrically opposite. This effect diminished with increase in temperature and was not observed after desorption at 1270 K (Run 8). The maximum caesium concentrations at spikes is noted in Table IV.1 as well as the mean peak concentrations obtained by the summation procedure. The former figures are considered to be unreliably high due to the sensitivity of the electron probe microanalyser to surface roughness, i.e., enhanced X-ray emission will occur from surface asperities. Related effects at the edge of the specimens are confined to less than 50 $\mu$m from the edge and will, therefore, make only a minor contribution to the shape of the profile.

## IV.5 Interlamellar Compound Formation

It has been suggested, Bromley (1973), that caesium-graphite interlamellar compound formation is a possibility during adsorption at 473 K and heat treatment at 573 K. However, mean peak concentrations of caesium during Runs 3 and 4 (Table IV.1) are much lower than the value required to form the most dilute compound definitely identified ( $C_{60}Cs$), Salzano and Aronson (1965(a)). Spike concentrations approach this value, but are thought to be unreliably high (see Chapter IV.1). The levels of caesium found at higher temperatures (Runs 5 to 9) appear to rule out any possibility of compound formation in these cases.

In order to confirm this view, X-ray diffraction measurements were obtained from two samples of gilsonite graphite before and after adsorption of 41.5 mg $g^{-1}$ and 17.3 mg $g^{-1}$ respectively of caesium at 473 K. In both cases no significant shift of the 002 reflection (the c axis spacing) was observed (figure IV.6).

However, a diminution of the peak intensity of the caesium-gilsonite graphite compared to gilsonite graphite was observed. This diminution was shown to correlate with the concentration levels assuming absorption of the X-rays by caesium according to the Beer law. Thus it was concluded that caesium-graphite interlamellar compound formation does not occur to a significant extent in the concentration range used in these experiments.

## IV.6 A summary of the Microgravimetric and Electron Probe Micro-analysis studies

The diffusion coefficients obtained from desorption curves on

spherical specimens are reasonably self-consistent but do not, however, agree very well with those found for cylindrical specimens, particularly at low temperatures (figure IV.2). Reference to figure IV.5 shows that the normalised concentration of caesium at the centre remains within $0.25 \pm 0.05$ for desorption at temperatures between 973 and 1270 K, but falls to zero after desorption at 1373 K.; this may reflect the longer duration of the experiment at 1373 K (figure IV.1) in addition to the high temperature. This may also be regarded as additional evidence of a two part diffusion process, the faster process causing caesium at the centre of the specimen to be completely removed. Furthermore, the perceptibly lower diffusion coefficient at 1373 K with respect to that at 1270 K, suggests the domination of the slower process after due time at 1373 K. Thus the slower diffusion process may be investigated by an initial heat treatment and desorption at 1373 K prior to desorption at lower temperatures. The significant surface concentration would imply that a surface condition exists. This effect will be referred to in Chapter VI.

TABLE IV.1

Sorption/Electron Probe Microanalysis
Results on Caesium Gilsonite-Graphite System

| Run No. | GRAVIMETRIC PROGRAM | | | GRAVIMETRIC RESULTS | | | ELECTRON PROBE MICROANALYSIS RESULTS | | | | |
|---|---|---|---|---|---|---|---|---|---|---|---|
| | Adsorb Temp.(K) Time(h) | Heat Treat Temp.(K) Time(h) | Desorb Temp.(K) | Initial Conc. ($mg\ g^{-1}$) | Final Conc. ($mg\ g^{-1}$) | D ($m^2\ s^{-1}$) x $10^{12}$ | Mean Peak Cs Conc. ($mg\ g^{-1}$) | r/a at Mean Peak Cs Conc. | Mean Cs Conc. at Centre ($mg\ g^{-1}$) | Mean Cs Conc. at Surface ($mg\ g^{-1}$) | Maximum Spike Cs Conc. ($mg\ g^{-1}$) |
| 3 | 523 0.5 | - | - | 42.8 | - | - | 84.0 $C_{134}Cs$ | 0.95 | Nil | 52 | 146 $C_{78}Cs$ |
| 4 | 473 1.0 | 573 59.5 | - | 43.5 | - | - | 79.3 $C_{143}Cs$ | 0.84 | 9.2 | 27.25 | 127 $C_{89}Cs$ |
| 5 | 523 1.0 | 573 60.0 | 973 | 32.2 | 25.4 | 8.8 $\pm$0.9 | 29.1 $C_{389}Cs$ | 0.90 | 7.3 | 22.5 | 92 $C_{124}Cs$ |
| 6 | 498 2.0 | 573 58.0 | 1053 | 40.5 | 23.6 | 11.7 $\pm$0.9 | 26.8 $C_{440}Cs$ | 0.95 | 10.9 | 26.25 | 39 $C_{291}Cs$ |
| 7 | 473 3.0 | 588 58.5 | 1177 | 40.5 | 21.9 | 40.9 $\pm$5.2 | 31.6 $C_{359}Cs$ | 0.98 | 13.6 | 25.0 | 45 $C_{252}Cs$ |
| 8 | 473 1.0 | 573 59.75 | 1270 | 41.9 | 16.6 | 50.2 $\pm$4.8 | 20.1 $C_{564}Cs$ | 0.90 | 13.5 | 15.75 | 29 $C_{391}Cs$ |
| 9 | 473 1.25 | 583 59.75 | 1373 | 45.4 | 15.2 | 36.9 $\pm$3.9 | 17.8 $C_{637}Cs$ | 1.0 | Nil | 17.5 | 32 $C_{354}Cs$ |

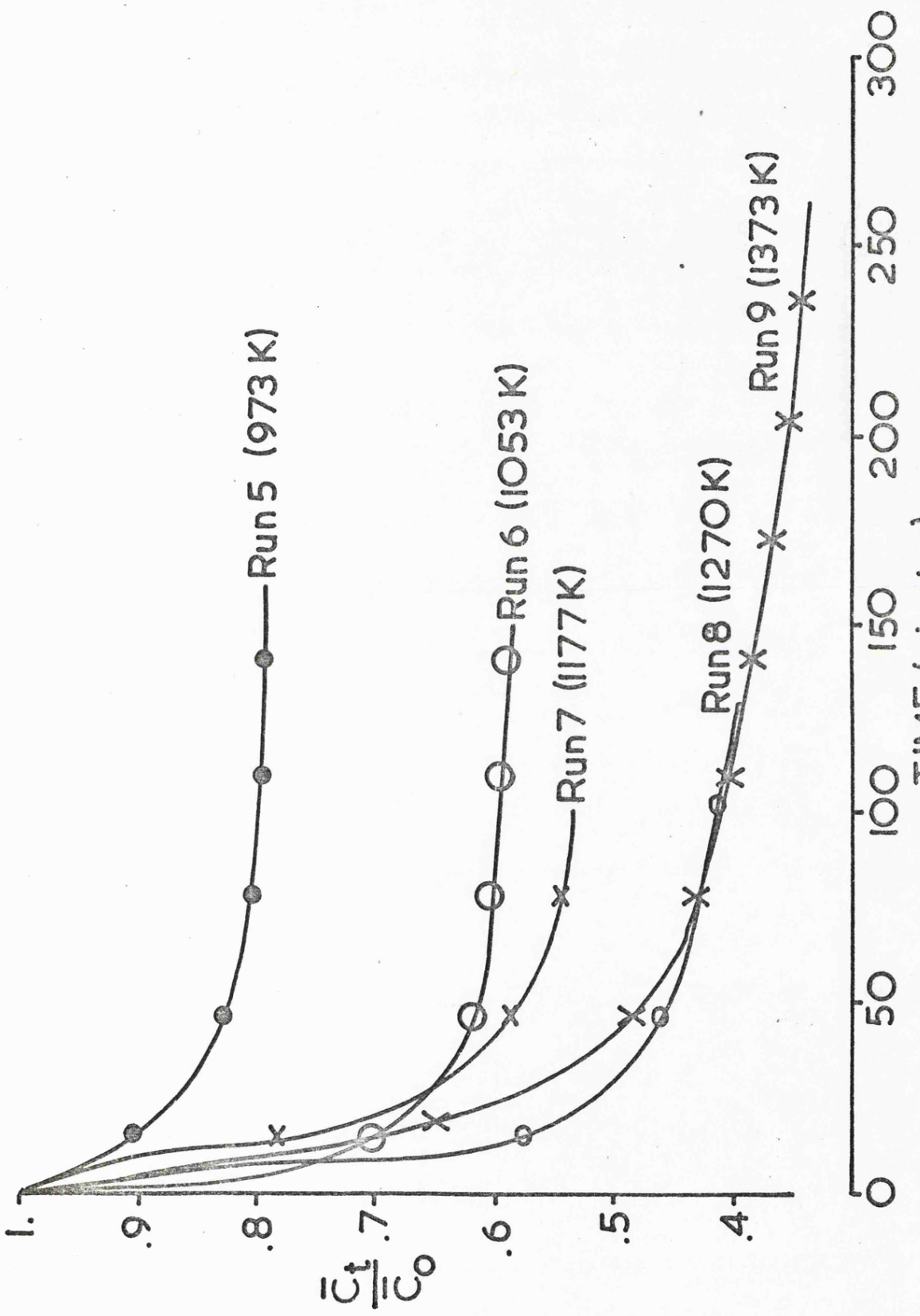


Figure IV.1 Desorption of Caesium from Gilsonite Graphite at various Temperatures

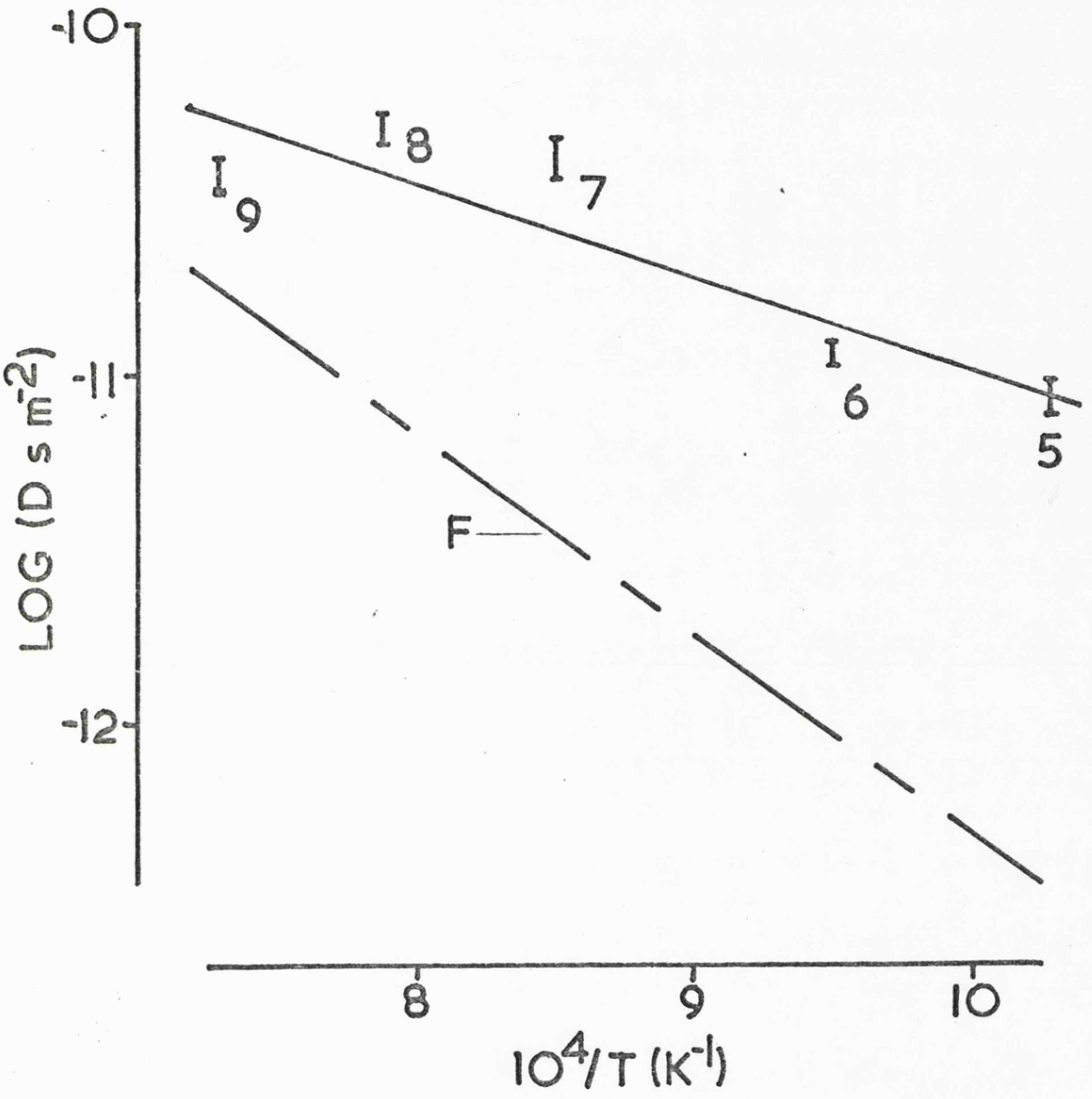


Figure IV.2 Arrhenius plot of Diffusion Coefficients for Caesium in Spherical specimens of Gilsonite Graphite

Run No. by datum point
F data of Flowers et al. (1972)

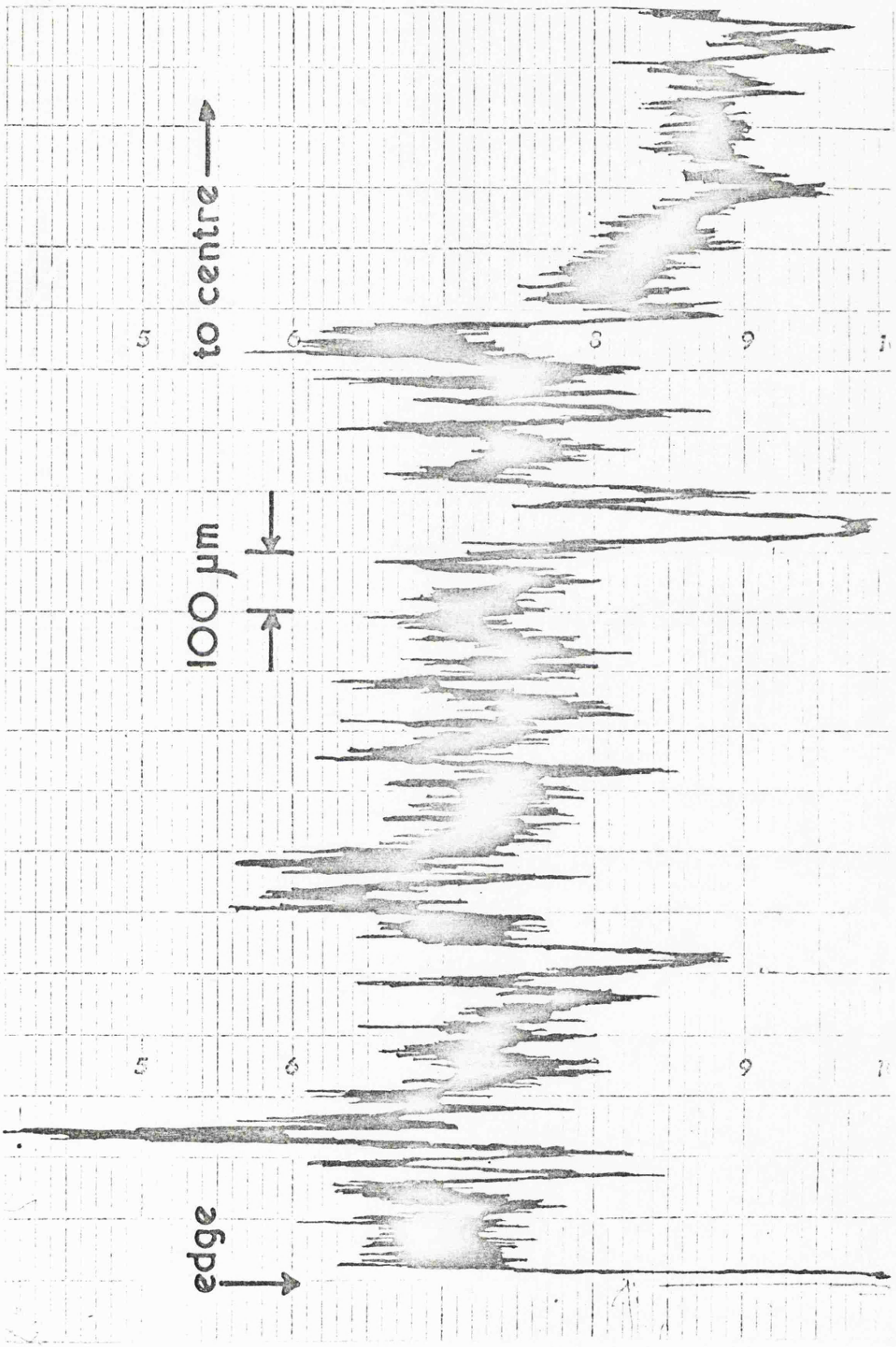


Figure IV.3 Part of Typical Electron Probe Microanalysis Trace ( Run 6)

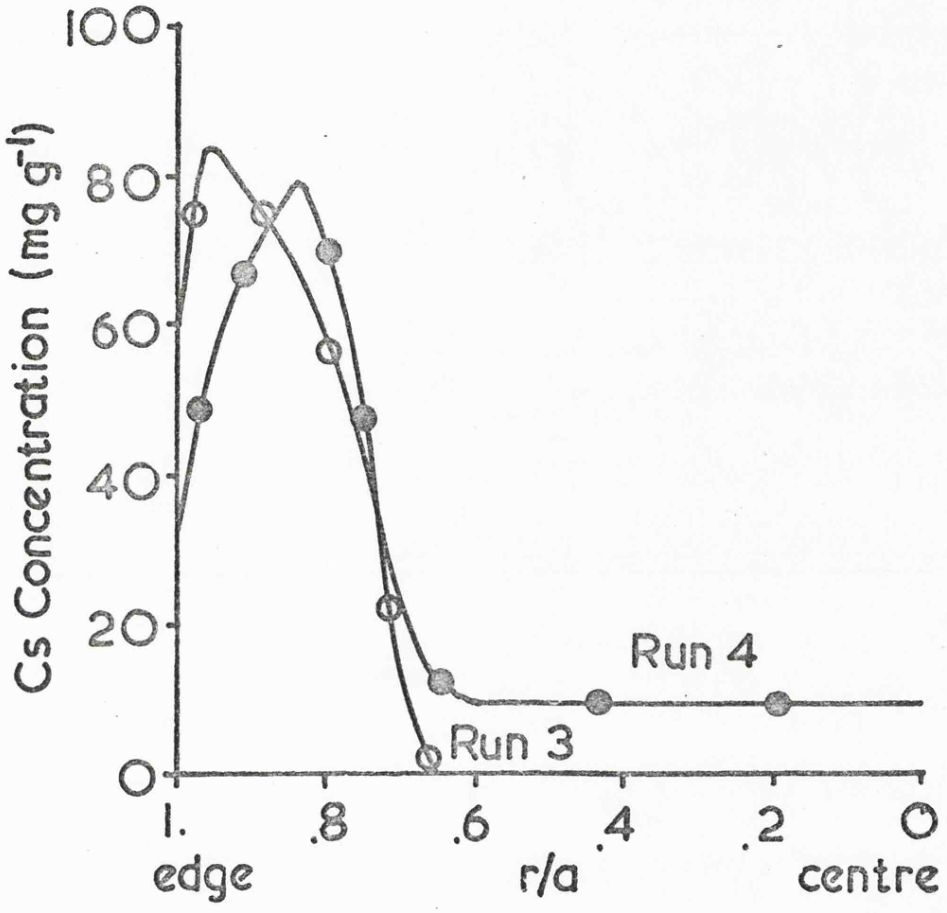


Figure IV.4 (a) Caesium Concentration Profiles through Spherical specimens of Gilsonite Graphite

after
Adsorption ( Run 3)
Adsorption and heat
treatment ( Run 4)

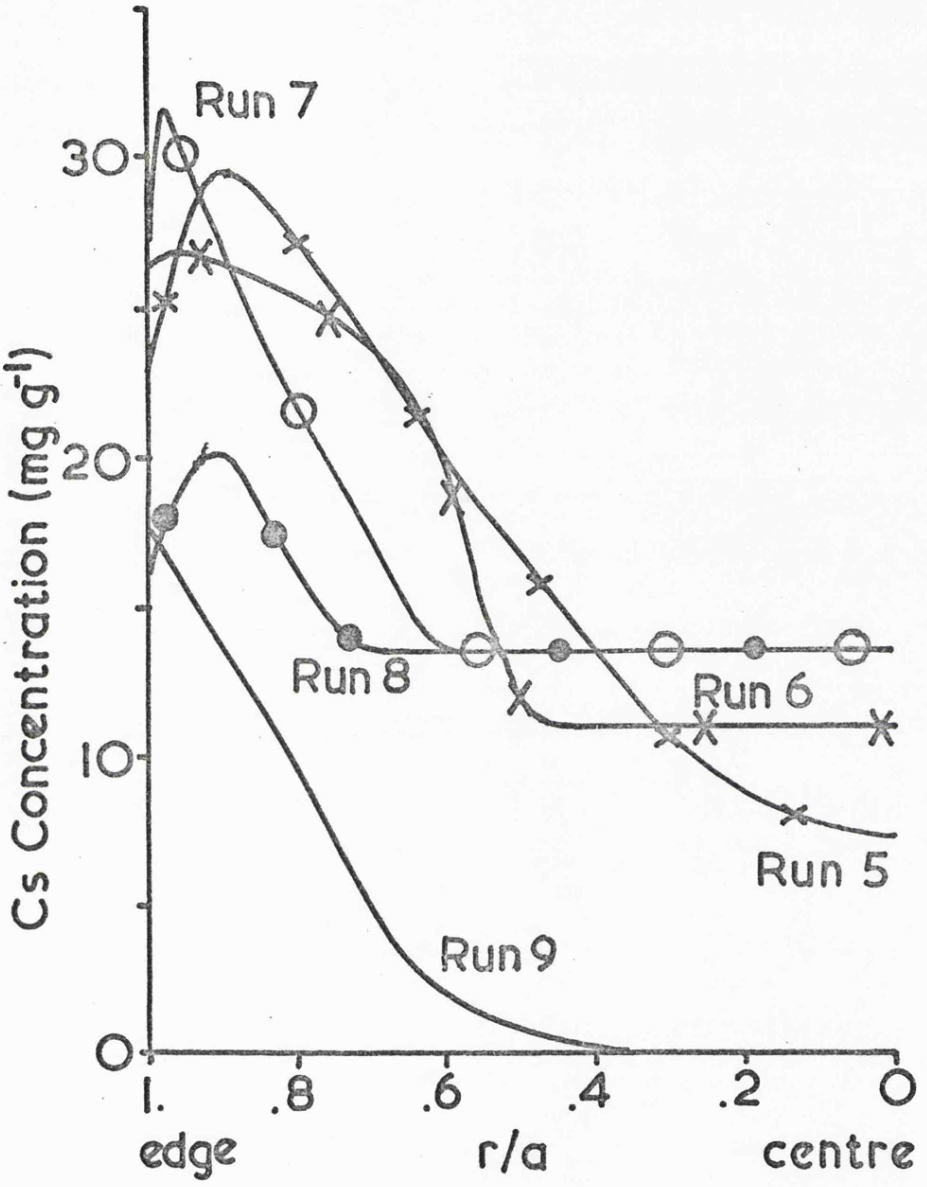


Figure IV.4 (b) Caesium Concentration Profiles through Spherical specimens of Gilsonite Graphite after
desorption at 973 K ( Run 5)
desorption at 1053 K ( Run 6)
desorption at 1177 K ( Run 7)
desorption at 1270 K ( Run 8)
desorption at 1373 K ( Run 9)

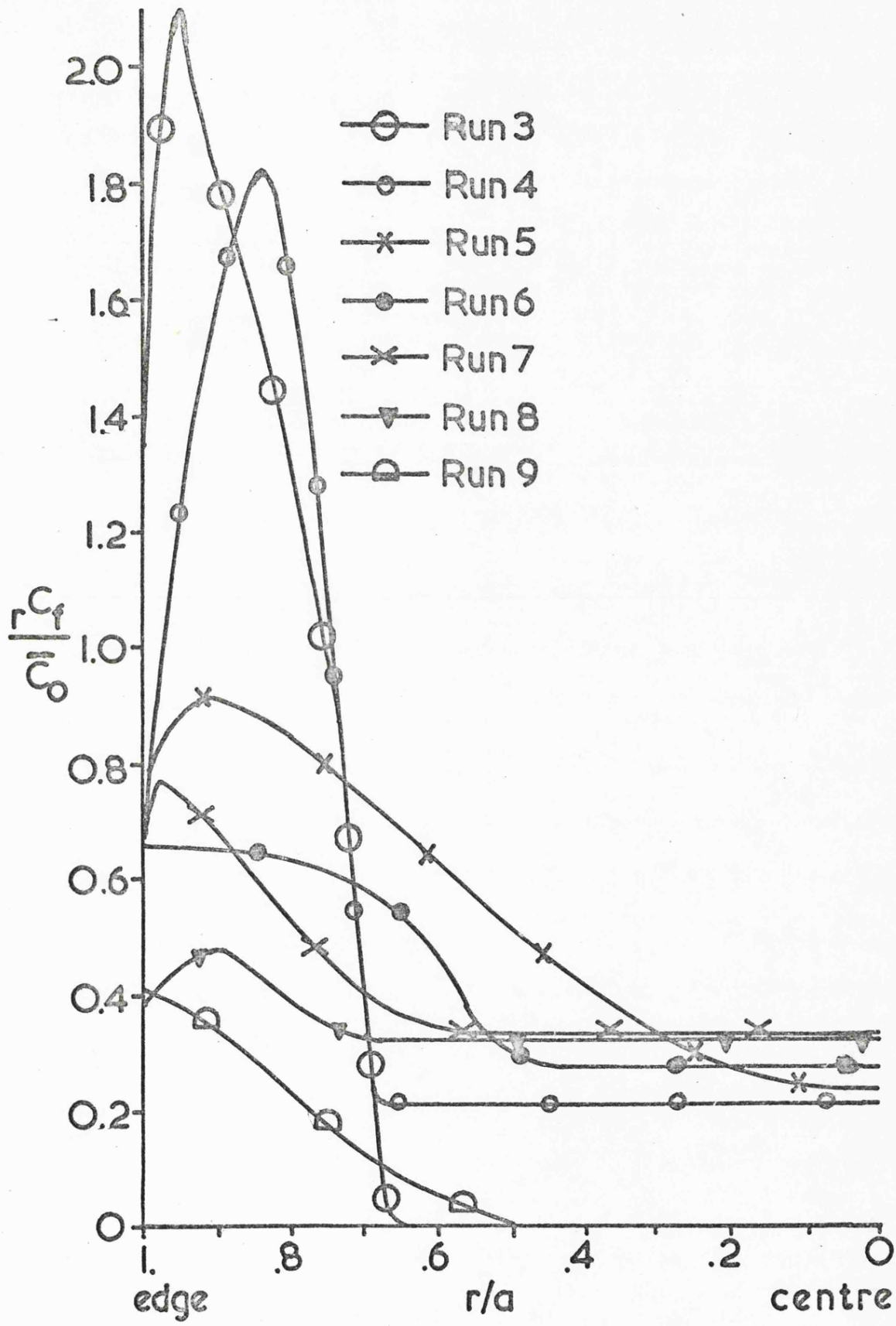


Figure IV.5 Normalised Concentration Profiles of Caesium in Gilsonite Graphite ( Runs 3 to 9)

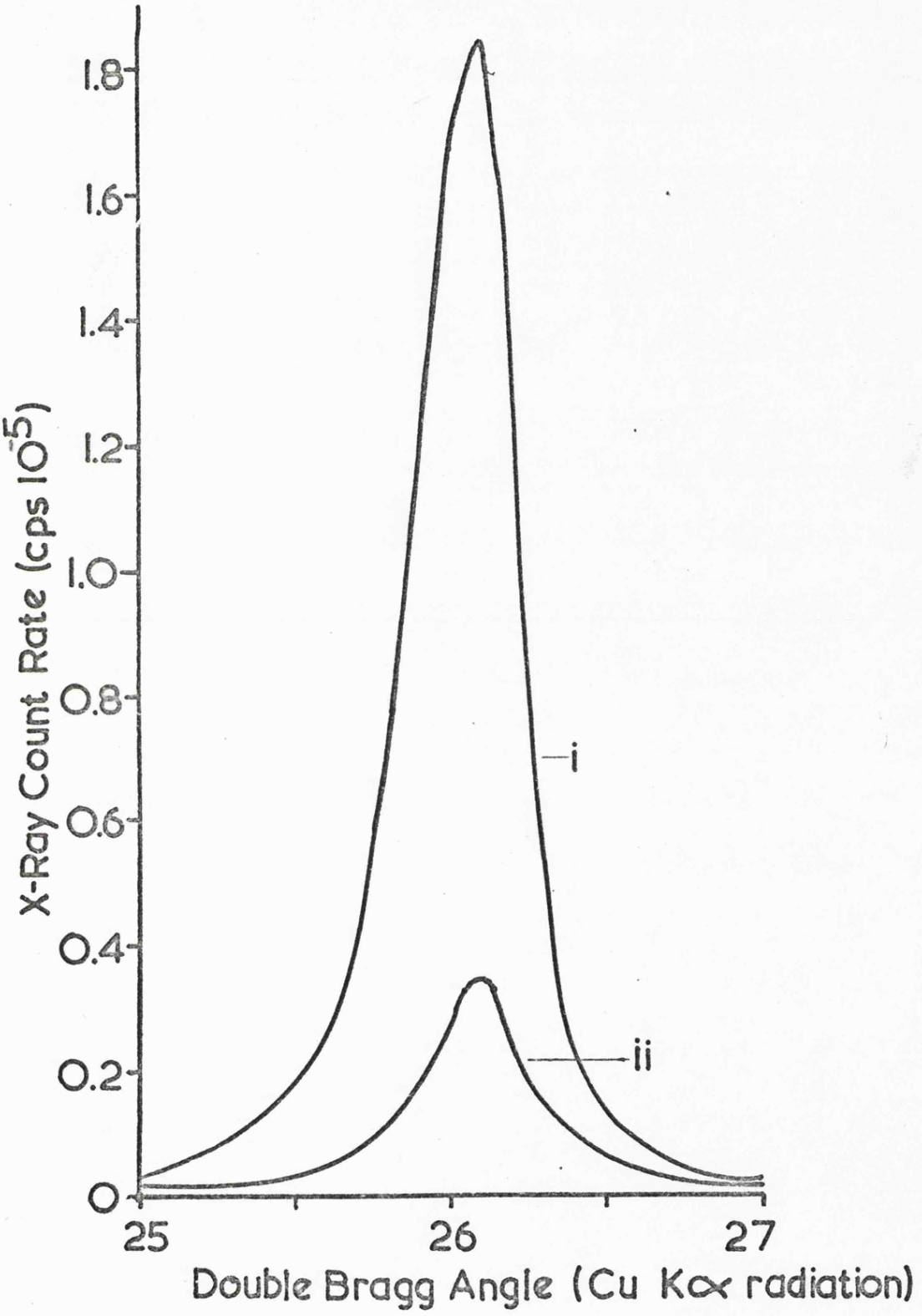


Figure IV.6 The 002 peak profiles of Gilsonite Graphite samples
i Gilsonite Graphite
ii Caesium-Gilsonite Graphite ( 17.3 mg $g^{-1}$)

# CHAPTER V

## FURTHER MICROGRAVIMETRIC STUDIES ON THE CAESIUM-GILSONITE GRAPHITE AND THE CAESIUM-FINE GRAIN GRAPHITE SYSTEMS

This chapter describes the final set of microgravimetric experiments on the caesium-gilsonite graphite system prompted by the information gained from the work of the previous chapter. Microgravimetric experiments on the sorption and diffusion of caesium in a fine grain graphite are also described, the fine grain graphite being similar to that used as the fuel matrix in the Dragon Reactor. This is followed by a detailed analysis of the equations used to obtain the diffusion coefficients which is divided into three sections :- (i) the approximate solution used in Chapters III and IV; (ii) an alternative approximation to the diffusion equation, and (iii) a numerical solution of the full diffusion equation. The chapter is concluded with a brief discussion of the various analyses used.

### V.1 Microgravimetric experiments and results

The electron probe microanalysis results in Chapter IV suggested that a second, slower diffusion mechanism was present and that this was most apparent during desorption at high temperatures, circa 1370 K. In order to investigate this mechanism a modified sorption experiment (Run 10) was performed which comprised (i) adsorption at 470 K; (ii) heat treatment at 570 K; (iii) an initial desorption period at 1370 K followed by (iv) desorption at temperatures between 1273 K and 973 K. Desorption curves were obtained from a series of decreasing temperature intervals (Runs 10i to 10v) followed by a

series of increasing temperature intervals (Runs 10vi to 10viii). Figure V.1 shows the initial portion of the desorption curve obtained, for desorption at 1373 K, the remainder comprised linear desorption curves varying with temperature only. The diffusion coefficients were found using equation IV.1 and are presented in Table V.1 together with other relevant data of Run 10. The resultant Arrhenius plot of the diffusion coefficients is shown in figure V.2, together with the data of Flowers et al. (1972). After the desorption experiments were completed, the specimen was subjected to electron probe microanalysis following the procedure described in Chapter IV.3; the resultant caesium concentration profile is shown in figure V.3.

The diffusion coefficients obtained from Run 10 show a higher temperature dependence than those from Runs 5 to 9. It is of interest to note the reproducibility that is obtained in the diffusion coefficients of Runs 9 and 10i, both undergoing desorption at 1373 K. The diffusion coefficients obtained in Run 10 at lower temperatures appear to confirm the theory of a two phase diffusion mechanism. The concentration profile (figure V.3) however does not follow that expected from the previous profiles (figure IV.5) in that caesium is still present at the centre, contrary to the trend shown in figure IV.5. Further discussion on these results will be left to Chapter VI where a comprehensive analysis will be made.

The experimental program was extended to include measurements of sorption and diffusion of caesium in a fine grain graphite. The choice of this graphite was made for two reasons, (i) its technological importance within the Dragon Reactor and (ii) its different structural characteristics to gilsonite graphite (see

Appendix I). Due to the lack of time, a comprehensive program similar to that carried out on the gilsonite graphite was not possible, and a shorter experimental program was designed with reference to the information obtained from electron probe microanalysis and desorption experiments on gilsonite graphite.

A spherical specimen (nominal diameter 6 mm) of the fine grain graphite was subjected to prior heat treatment at approximately 2300 K for 48 hours under a vacuum (approximately 0.1 mN $m^{-2}$) in order to remove volatile impurities. The increase in time and temperature of this heat treatment compared to gilsonite graphite (1970 K for 24 hours) was made as a result of advice (Hick, 1973) that the graphite had not been subjected to temperatures in excess of 1900 K during its manufacture and hence was considerably less pure than the gilsonite graphite. A sorption experiment (Run 11) was performed on a sample of fine grain graphite; this experiment consisted of (i) adsorption at 473 K, (ii) heat treatment at 573 K and (iii) desorption at 1373 K; details are given in Table V.2. The desorption curve is shown in figure V.4; a diffusion coefficient was calculated from the later part using equation IV.1 and is tabulated in Table V.2. After the conclusion of the sorption experiment, the specimen was subjected to electron probe microanalysis but owing to the low levels of caesium present (total weight of caesium within the specimen 840 $\mu$g) no X-ray emission from caesium was detected.

A further experiment was performed on the fine grain graphite (Run 12), the adsorption and heat treatment program being detailed in Table V.2, and desorption was followed over a range of increasing temperatures, the details of which are given in Table V.2.

Diffusion coefficients were calculated from the desorption curves (figure V.5) and are tabulated in Table V.2. The resultant Arrhenius plot of the diffusion coefficients obtained from work on the fine grain graphite is shown in figure V.6. The plot highlights the discrepancy between the diffusion coefficients obtained from desorption at 1373 K (Runs 11 and 12v) and the reproducibility obtained in Runs 9 and 10i. Figure V.6 also shows the 'turn over' of the diffusion coefficients of Run 12 more dramatically than was observed in the gilsonite graphite (see figure IV.2). However, further discussion will be left to Chapter VI, when the observations made upon the fine grain graphite can be interpreted in the light of observations made upon the gilsonite graphite.

## V.2 The First Approximate Solution of the Diffusion Equation

In Chapters III.3 and IV.2, equations III.2 and IV.1 respectively were introduced as equations suitable for preliminary analysis of the desorption curves. It is the purpose of this and the two following sections to investigate the basis of these equations and to consider alternative analyses.

According to Fick, Jost (1960), the diffusion of a species in a medium can be described by the following equations

$$F = -D\frac{\partial C}{\partial x} \qquad V.1$$

where F is the flux per unit area and

$$\frac{\partial C}{\partial t} = D\frac{\partial^2 C}{\partial x^2} \qquad V.2$$

the other terms taking their previously defined meaning.

Equations V.1 and V.2 represent a one dimensional system with a diffusion constant independent of time, concentration and position. Equation V.2 can be transformed to cylindrical co-ordinates

$$\frac{\partial C}{\partial t} = \frac{1}{r}\frac{\partial}{\partial r}\left( r D \frac{\partial c}{\partial r} \right) \qquad \text{V.3}$$

and to spherical co-ordinates

$$\frac{\partial C}{\partial t} = D\left(\frac{\partial^2 C}{\partial r^2} + \frac{2}{r}\frac{\partial C}{\partial r}\right) \qquad \text{V.4}$$

Equation V.3 is restricted to radial diffusion only and hence end effects are neglected. If it is further assumed that there exists at zero time a uniform concentration of the species throughout the cylinder or sphere, of radius a, except at the surface (r = a) where the concentration is zero and independent of time, and that there exists no surface exit resistance for the species, i.e., no barrier to evaporation, then equations V.3 and V.4 can be solved, Crank (1967), to give the radial diffusion out of a cylinder

$$\bar{C}_t / \bar{C}_0 = \sum_{n=1}^{\infty} 4 \exp( -D\gamma_n^2 t)/a^2\gamma_n^2 \qquad \text{V.5}$$

where $\gamma_n$ is the $n^{th}$ root of the zero order Bessel function

$$J_0(a\gamma_n) = 0 \qquad \text{V.6}$$

and for diffusion out of a sphere

$$\bar{C}_t / \bar{C}_0 = 6 \sum_{n=1}^{\infty} \exp( -Dt\pi^2 n^2/a^2) / n^2\pi^2 \qquad \text{V.7}$$

Equations V.5 and V.7 may be approximated by taking the first term of the summation and neglecting the second and subsequent terms in which case equations III.2 and IV.1 are obtained. It is reasonable to propose that this approximation is valid when the second term

is less than or equal to 1% of the first term, therefore the third and subsequent terms are also negligible, in which case the condition for the cylindrical case is given by

$$4 \exp(-Dt\gamma_2^2) / a^2\gamma_2^2 \leqslant 4 \exp(-Dt\gamma_1^2) / 100a^2\gamma_1^2 \qquad V.8$$

and substituting for the first two non-zero roots of equation V.6 it can easily be shown that this condition is met when

$$Dt / a^2 \geqslant 0.102 \qquad V.9$$

For the spherical case the condition is

$$\exp(-Dt\pi^2 4 / a^2) / 4 \leqslant \exp(-Dt\pi^2 / a^2) / 100 \qquad V.10$$

whence the condition

$$Dt / a^2 \geqslant 0.108 \qquad V.11$$

can easily be obtained. Thus, use of equations III.2 and IV.1 implies that $Dt/a^2$ takes a value larger than approximately 0.1. In the present work the range of values for $Dt/a^2$ varies from infinitely small (at $t = 0$) to a maximum value of approximately 0.05 (Run 11) and hence the use of equations III.2 and IV.1 is not fully justified.

## V.3 The second approximation solution of the diffusion equation

The analyses which follow are confined to specimens of spherical geometry due to the errors which arise with cylindrical specimens from neglecting end effects. For spherical geometry equation V.4 can be solved, Crank (1967), using a Laplace Transformation to give

$$\bar{C}_t/\bar{C}_o = 1 - 6(Dt/\pi)^{\frac{1}{2}}/a + 3Dt/a^2 - (12(Dt)^{\frac{1}{2}}/a)\sum_{n=1}^{\infty} \text{ierf}(na/(Dt)^{\frac{1}{2}}) \qquad \text{V.12}$$

(equation V.7 is found using a Fourier Series transformation)
If the summation term in equation V.12 is negligible compared to the other terms of the right hand side, equation V.12 reduces to a quadratic equation in the term $(Dt)^{\frac{1}{2}}/a$. Assuming that the first term of the summation of equation V.12 is less than 1% of the other terms of the right hand side of equation V.12 and that therefore the second and subsequent terms of the summation are also negligible, the condition can be expressed in the form

$$\frac{1}{100}\left(1 - \frac{6}{a}\left(\frac{Dt}{\pi}\right)^{\frac{1}{2}} + \frac{3Dt}{a^2}\right) \geqslant \frac{12(Dt)^{\frac{1}{2}}}{a} \text{ierf}\left(\frac{a}{(Dt)^{\frac{1}{2}}}\right) \qquad \text{V.13}$$

The solution of equation V.13 is complicated by the presence of the ierf term. However, by the use of an iterative techique, the condition

$$\frac{Dt}{a^2} \leqslant 0.66 \qquad \text{V.14}$$

was found to satisfy equation V.13. Thus the approximation is better suited for application to the present work than the previous approximation leading to equations III.2 and IV.1. In such a case, equation V.12 approximates to

$$\bar{C}_t/\bar{C}_o = 1 - \frac{6}{a}\left(\frac{Dt}{\pi}\right)^{\frac{1}{2}} + 3Dt/a^2 \qquad \text{V.15}$$

As previously stated, equation V.15 is a quadratic equation whose roots are

$$(Dt/a^2)^{\frac{1}{2}} = \frac{1}{\sqrt{\pi}} \pm \left(\frac{1}{\pi} - \frac{1}{3}(1 - \bar{C}_t/\bar{C}_o)\right)^{\frac{1}{2}} \qquad \text{V.16}$$

The positive root of equation V.16 leads to a negative and therefore physically meaningless diffusion coefficient, whereas the negative root gives a positive diffusion coefficient. The data of Runs 5 to 12 were analysed using equation V.16 and the squares of the resultant negative roots and their corresponding time values were subjected to a least mean squares analysis to obtain the diffusion coefficients and their standard deviations which are presented in Table V.3

## V.4 A numerical solution of the diffusion equation

It was decided to attempt to analyse the data by means of an iterative technique to find a value of $Dt/a^2$ which satisfied equation V.7 for a given experimental value of $\bar{C}_t/\bar{C}_o$. In this way an exact value of $Dt/a^2$ would be obtained and the resultant plot against time should give the most accurate assessment of the diffusion coefficient based upon the hypothetical system. Briefly, a computer program was written which took the value of $\bar{C}_t/\bar{C}_o$, and using a function supplied, obtained an initial estimate of $Dt/a^2$. Using this estimated value, a value of $\bar{C}_t/\bar{C}_o$ was computed using equation V.7. This value of $\bar{C}_t/\bar{C}_o$ was used in a modification of Newton's method for estimating roots to obtain a better estimate of $Dt/a^2$. The process was repeated until a value of $Dt/a^2$ was found which gave a computed value of $\bar{C}_t/\bar{C}_o$ equal to the experimental value of $\bar{C}_t/\bar{C}_o$.

The supplied function for the initial estimate of $Dt/a^2$, denoted by $(Dt/a^2)_i$, was found by first computing values of $\bar{C}_t/\bar{C}_O$ for set values of $Dt/a^2$ using equation V.7 and the following criterion to

end the summation

$$\frac{1}{(m+1)^2} \exp\left(-(m+1)^2 \, Dt\,\pi^2/a^2\right) \leqslant 10^{-6} \sum_{n=1}^{m} \frac{1}{n^2} \exp\left(-n^2 Dt\pi^2/a^2\right) \qquad \text{V.17}$$

Equation V.7 was used, rather than equation V.12, since the time for evaluation of equation V.7 on the computer is faster than the evaluation of equation V.12 to a similar end condition of equation V.17. The data so obtained, of $\bar{C}_t/\bar{C}_o$ versus $Dt/a^2$, was subjected to a multiple regression routine (supplied by I.C.L. Statistical Package) to fit the equation

$$\log(w) = b + c \log\left(\frac{1}{v} - 1\right) + d\left(\log\left(\frac{1}{v} - 1\right)\right)^2 + e\left(\log\left(\frac{1}{v} - 1\right)\right)^3 + f\left(\log\left(\frac{1}{v} - 1\right)\right)^4 + g\left(\log\left(\frac{1}{v} - 1\right)\right)^5 \qquad \text{V.18}$$

where w and v are the variables, equivalent to $Dt/a^2$ and $\bar{C}_t/\bar{C}_o$ respectively; and b, c, d, e, f and g constants. Equation V.18 is derived from the equation

$$v = 1/(1 + \exp(hw + j)) \qquad \text{V.19}$$

where h and j are constants. Equation V.19 has the same shape as equation V.7, in that both v and $\bar{C}_t/\bar{C}_o$ tend to unity for low w and $Dt/a^2$ respectively and also tend to zero for large w and $Dt/a^2$ respectively. Rearrangement of equation V.19 leads to

$$w = \ln(1/v - 1)/h - j/h \qquad \text{V.20}$$

Since the values of $Dt/a^2$ ranged over five orders of magnitude in the present work, equation V.20 was transposed to take the form of equation V.18. The regression routine was allowed to reject terms on the right hand side of equation V.18 in order to obtain the best fit in terms of both the standard error of the curve and the

effective contribution of each term, and gave a fit of the form

$$\log (Dt/a^2) = b + c \log (\bar{C}_o/\bar{C}_t - 1) + e \left( \log (\bar{C}_o/\bar{C}_t - 1) \right)^3 \qquad V.21$$

Using equation V.21 the experimental value of $\bar{C}_t/\bar{C}_o$ denoted by $(\bar{C}_t/\bar{C}_o)_e$ was inserted to obtain the initial estimate of $(Dt/a^2)_i$. A function

$$w = (\bar{C}_t/\bar{C}_o)_e - \frac{6}{\pi^2} \sum_{n=1}^{\infty} \frac{1}{n^2} \exp (-n^2 Dt\pi^2/a^2) \qquad V.22$$

was defined, where w is a variable, different from that in equation V.18, so that for the root of equation V.22 a value of $Dt/a^2$ would be found for the value of $(\bar{C}_t/\bar{C}_o)_e$.

Because the first derivative of equation V.22, being

$$\frac{dw}{d(Dt/a^2)} = \frac{6}{\pi^2} \sum_{n=1}^{\infty} \exp (-n^2 Dt\pi^2/a^2) \qquad V.23$$

involves a summation which is slow to converge, the method of Newton's formula for approximation to the root of an equation i.e.

$$V_B = V - f(V)/f'(V) \qquad V.24$$

where V is a variable, different from that in equation V.18, and $V_B$ a better estimate, was modified to

$$V_B = V_1 - \frac{f(V_1)\,(V_1 - V_2)}{f(V_1) - f(V_2)} \qquad V.25$$

where the first derivative has been replaced by the gradient of the function near the estimate of the root. Thus a better estimate of $Dt/a^2$ can be found by the use of equation V.25 where

$$V_1 = (Dt/a^2)_i$$

$$V_2 = 1.1(Dt/a^2)_i$$

and $V_B = (Dt/a^2)_m$, the better estimate of $Dt/a^2$.

The process was iterated by using $(Dt/a^2)_m$ in place of $(Dt/a^2)_i$ and continued until the condition

$$w \leqslant 2(\bar{C}_t/\bar{C}_o)_e \, 10^{-6} \qquad \text{V.26}$$

was satisfied. The process was then repeated with a new value of $(\bar{C}_t/\bar{C}_o)_e$ to obtain the corresponding value of $Dt/a^2$. It was found that the condition of equation V.26 was satisfied within ten iterative steps, due mainly to the good fit of equation V.21.

The resultant $Dt/a^2$ values obtained and their corresponding time values were subjected to a least mean square analysis and the diffusion coefficients and their standard deviations are tabulated in Table V.3, together with the diffusion coefficients found by the first approximation (equation IV.1) and those found by the second approximation (equation V.16). Figure V.7 shows the Arrhenius plot of the diffusion coefficients of the gilsonite and fine grain graphites obtained from the numerical solution.

## V.5 A Discussion of the Methods of Analysis and Conclusions

The data used for both the quadratic equation method and the numerical solution method were restricted to that which was used for the first approximation, i.e. the later portions of the desorption curves, and hence the three diffusion coefficients are directly comparable, both in value and standard deviation. It is also of interest to note that in none of the methods used did the plot of the particular function against time have a zero intercept. This

is because the actual time origin used in every run did not coincide with the effective time origin. However, for each technique, the diffusion coefficients were calculated from the gradient of the appropriate plot and thus are independent of time origin.

The analysis by the first approximation is shown to be considerably in error since the condition of validity of equation V.11, i.e. $Dt/a^2$ greater than 0.1 is never held. The second approximate solution, the quadratic equation method, is, however, valid for the experimental conditions used in the present work and therefore more credence can be attached to the diffusion coefficients so calculated. The difference in diffusion coefficients between the first and the second approximation is shown most dramatically in Runs 5 to 9 and 12 (Table V.3). There is not a dramatic difference between the diffusion coefficients obtained by the quadratic equation method and the numerical solution method. No relation in the standard deviations can be found; in some cases the best fit is found by use of the first approximation, in others the best fit is found by the second or third method.

The Arrhenius plot of the numerical solution values of diffusion coefficients (figure V.7) shows two definite activation energies for the gilsonite graphite in Runs 5 to 9 and Run 10 (Table V.4). It is interesting to note that whilst the activation energy of Runs 5 to 9 is just over half that of Run 10 the diffusion coefficients of Run 9 and 10i agree within two standard deviations. The diffusion coefficient for Run 9 is lower than that which would be expected by extrapolation of the diffusion coefficients of Runs 5 to 8, leading to a 'turn over' in the Arrhenius plot (figure V.7). A smaller effect is found for the fine grain graphite (Run 12).

The definite change in activation energy of Runs 5 to 9 and Run 10 indicates that a different rate controlling mechanism occurs in Run 10 due possibly to the presence of the initial desorption stage at 1373 K (Run 10i) causing the concentration profile to change compared to that which occurs in Runs 5 to 8. This will be further discussed in Chapter VI.

The methods of analysis used are all based upon the model cited in Chapter V.2. However, it is concluded from electron probe microanalysis studies that a two phase diffusion mechanism is occuring in the system, which is contrary to the assumed model. The justification for the use of this model in analysing the desorption curves will be considered in Chapter VI, but it is appropriate to comment here that there appears to be little extra benefit in the use of the numerical solution method rather than the second approximation method, especially in view of the complexity of the calculations required for the former method. However, the numerical solution results will be quoted in view of their availability.

TABLE V.1

Diffusion Coefficients and Desorption Data[&] for Caesium-Gilsonite Graphite System (Run 10)

| Run No. | Temp. (K) | Initial Conc. at Time (mg $g^{-1}$) (min) | Final Conc. at Time (mg $g^{-1}$) (min) | D ($m^2$ $s^{-1}$) x $10^{12}$ |
|---|---|---|---|---|
| 10i | 1373 | 29.91 40 | 25.34 330 | 37.4 ± 2.5 |
| 10ii | 1273 | 25.2 360 | 24.92 470 | 13.8 ± 0.4 |
| 10iii | 1194 | 24.88 500 | 24.74 590 | 8.9 ± 0.2 |
| 10iv | 1073 | 24.7 660 | 24.49 910 | 5.0 ± 0.3 |
| 10v | 980 | 24.49 940 | 24.47 1480 | 0.17 ± 0.13 |
| 10vi | 1073 | 24.47 1490 | 24.42 1630 | 2.0 ± 0.4 |
| 10vii | 1165 | 24.41 1640 | 24.24 1740 | 10.1 ± 0.4 |
| 10viii | 1272 | 24.22 1750 | 23.9 1860 | 18.7 ± 0.3 |

[&] Adsorption of 39.64 mg $g^{-1}$ in 1 hour at 473 K followed by Heat Treatment at 573 K for 60.25 hours.

TABLE V.2

Diffusion Coefficients and Adsorption /Desorption Data for Caesium-Fine Grain Graphite ( Runs 11 and 12)

| Run No. | Adsorb. Temp (K) Time (h) | Heat Treat. Temp (K) Time (h) | Desorp. Temp (K) | Initial Conc. (mg $g^{-1}$) | Final Conc. (mg $g^{-1}$) | D ($m^2$ $s^{-1}$) x $10^{12}$ |
|---|---|---|---|---|---|---|
| 11 | 473 0.75 | 573 59.75 | 1373 | 36.6 | 4.5 | 68.9 ± 1.2 |
| 12i | 473 1.0 | 573 59.5 | 979 | 52.9 | 36.2 | 5.0 ± 0.5 |
| 12ii | - | - | 1076 | 35.4 | 31.8 | 10.2 ± 1.3 |
| 12iii | - | - | 1177 | 30.9 | 25.7 | 19.7 ± 2.2 |
| 12iv | - | - | 1272 | 23.6 | 17.7 | 14.3 ± 0.8 |
| 12v | - | - | 1381 | 15.3 | 11.2 | 10.5 ± 0.7 |

TABLE V.3

Diffusion Coefficients calculated by the various methods of analysis

| Run No. | Diffusion Coefficient ($m^2\ s^{-1}$) x $10^{12}$ | | | Temp. (K) |
|---|---|---|---|---|
| | First Approx. | Second Approx. | Numerical Solution | |
| Gilsonite Graphite | | | | |
| 5 | 8.80 ± 0.90 | 3.23 ± 0.31 | 2.84 ± 0.26 | 973 |
| 6 | 11.7 ± 0.90 | 7.80 ± 0.59 | 7.24 ± 0.54 | 1053 |
| 7 | 40.9 ± 5.2 | 28.8 ± 3.4 | 26.9 ± 3.1 | 1177 |
| 8 | 50.2 ± 4.8 | 44.3 ± 3.9 | 41.4 ± 0.4 | 1270 |
| 9 | 36.9 ± 3.9 | 34.4 ± 3.2 | 32.3 ± 3.5 | 1373 |
| 10i | 37.4 ± 2.5 | 37.4 ± 2.5 | 37.9 ± 1.4 | 1373 |
| 10ii | 13.9 ± 0.4 | 14.2 ± 0.4 | 11.9 ± 1.3 | 1273 |
| 10iii | 8.88 ± 0.18 | 9.15 ± 0.22 | 8.42 ± 0.21 | 1194 |
| 10iv | 5.02 - 0.31 | 5.19 - 0.32 | 4.78 - 0.29 | 1073 |
| 10v | 0.17 ± 0.13 | 0.18 ± 0.14 | 0.17 ± 0.13 | 980 |
| 10vi | 1.99 ± 0.40 | 2.12 ± 0.45 | 1.91 ± 0.40 | 1073 |
| 10vii | 10.1 ± 0.4 | 10.7 ± 0.8 | 9.68 ± 0.40 | 1165 |
| 10viii | 18.7 ± 0.3 | 22.8 ± 3.1 | 19.8 ± 1.6 | 1272 |
| Fine Grain Graphite | | | | |
| 11 | 68.9 ± 1.2 | 79.9 ± 1.1 | 68.9 ± 2.3 | 1373 |
| 12i | 4.99 ± 0.48 | 2.55 ± 0.22 | 2.29 ± 0.22 | 979 |
| 12ii | 10.2 ± 1.3 | 6.33 ± 0.76 | 5.75 ± 0.69 | 1076 |
| 12iii | 19.7 ± 2.2 | 14.8 ± 1.5 | 13.9 ± 1.4 | 1177 |
| 12iv | 14.3 ± 0.8 | 13.5 ± 0.7 | 12.8 ± 0.7 | 1272 |
| 12v | 10.5 ± 0.7 | 11.1 ± 0.7 | 10.1 ± 0.4 | 1381 |

TABLE V.4

Log ($D_0$) and Activation Energy of the various Runs derived by least mean squares analysis using the Numerical Solution Diffusion Coefficients

| Run No's. | Log ($D_0$ s $m^{-2}$) | $\Delta H$ (kJ $mol^{-1}$) |
|---|---|---|
| 5 - 9 | -7.44 ± 0.70 | 75 ± 18 |
| 10 | -5.12 ± 0.28 | 137 ± 31 |
| 11 - 12 | -8.12 ± 1.0 | 65 ± 33 |

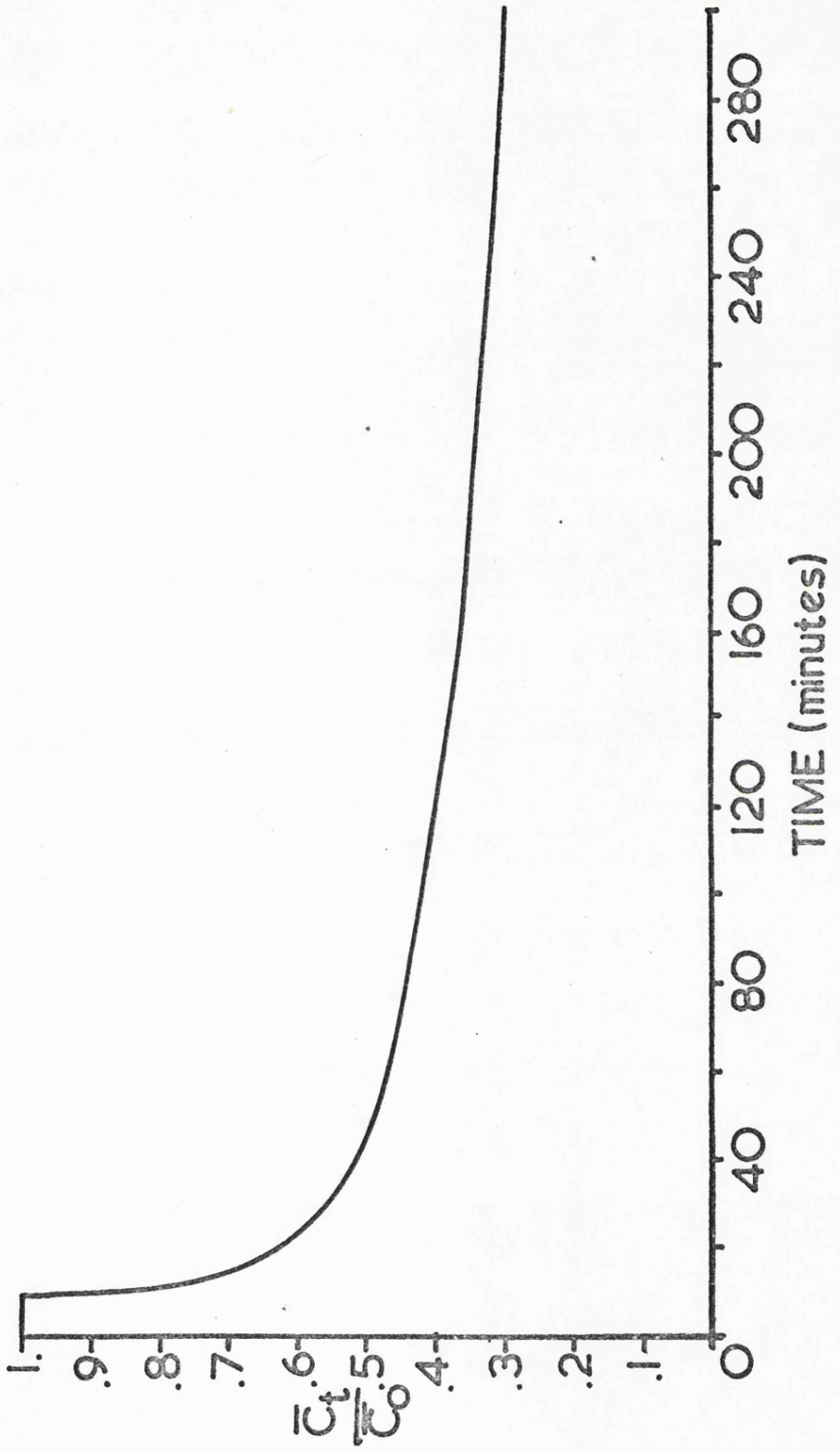


Figure V.1 Initial portion of the Desorption Curve of the Caesium-Gilsonite Graphite system at 1373 K ( Run 10)

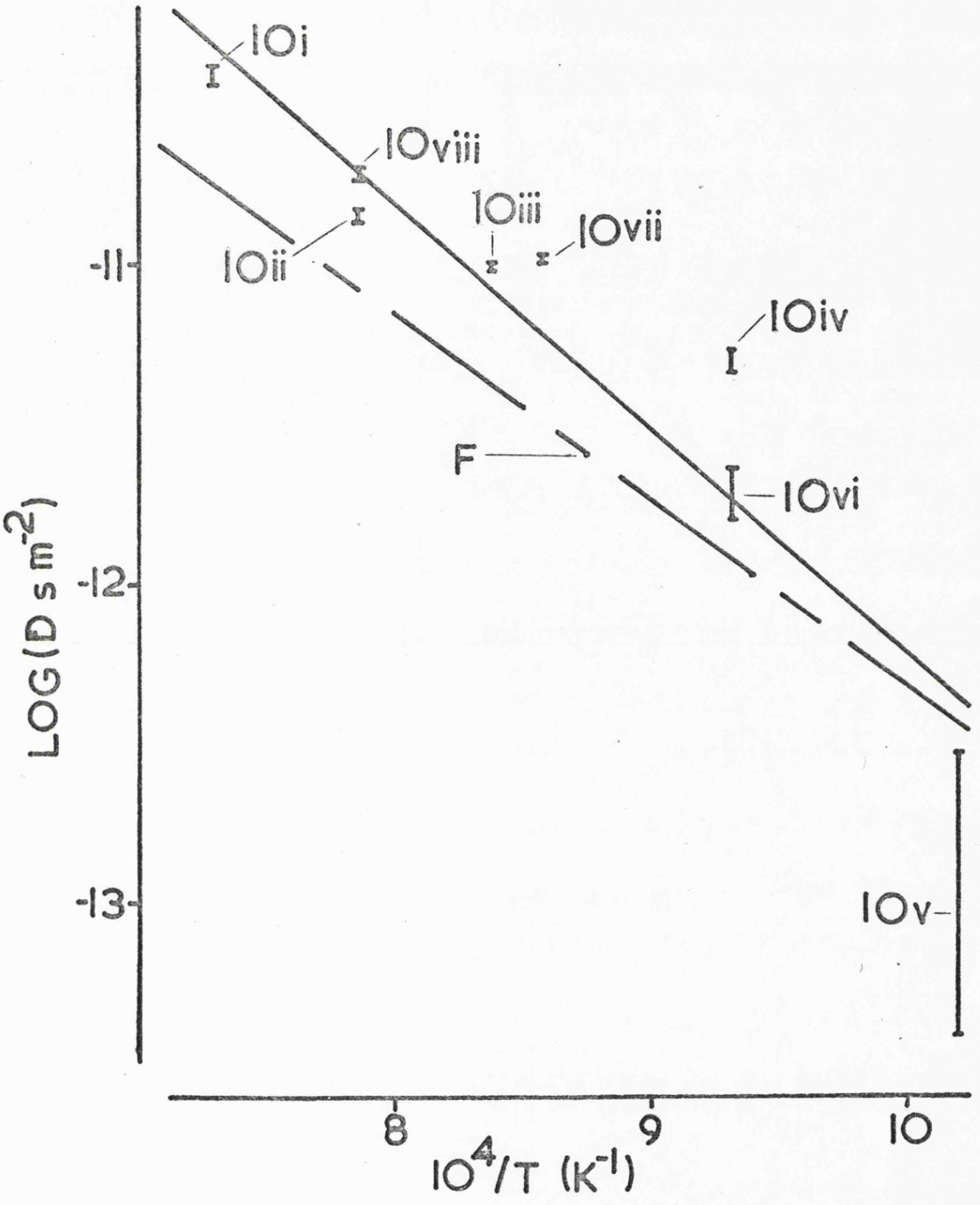


Figure V.2 An Arrhenius plot of Diffusion Coefficients of Caesium in Gilsonite Graphite ( Run 10)

Run No. by datum point

F data of Flowers et al. (1972)

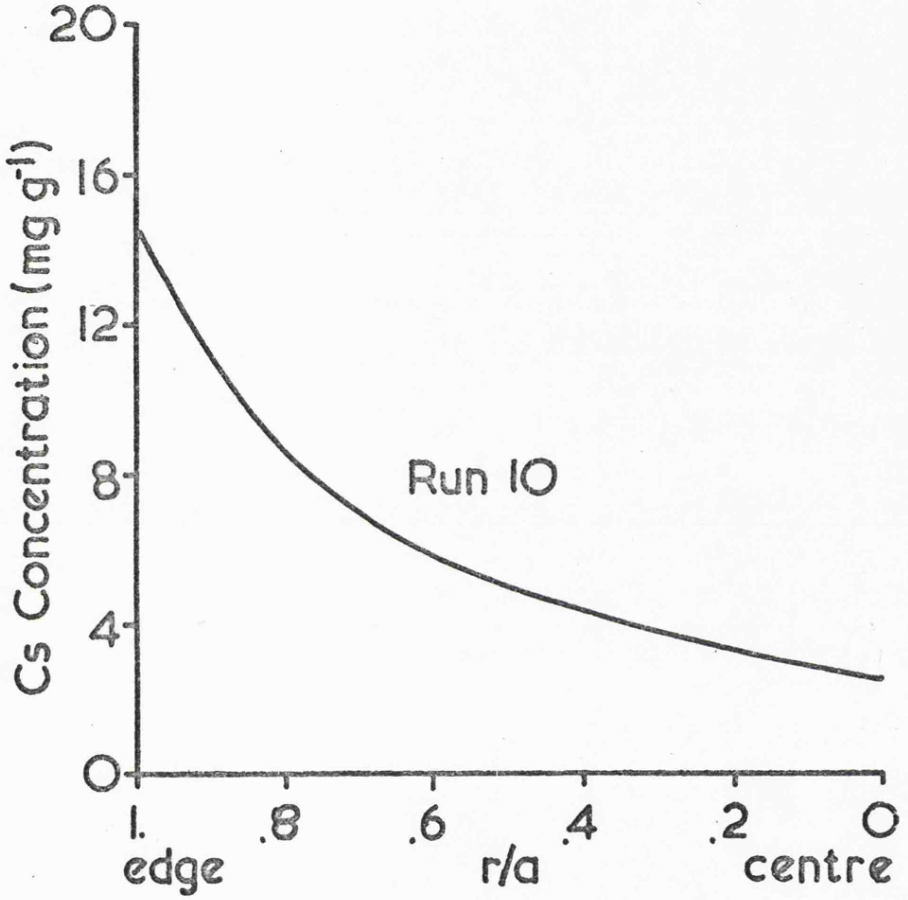


Figure V.3 Caesium Concentration Profile through a Spherical specimen of Gilsonite Graphite after desorption at various temperatures

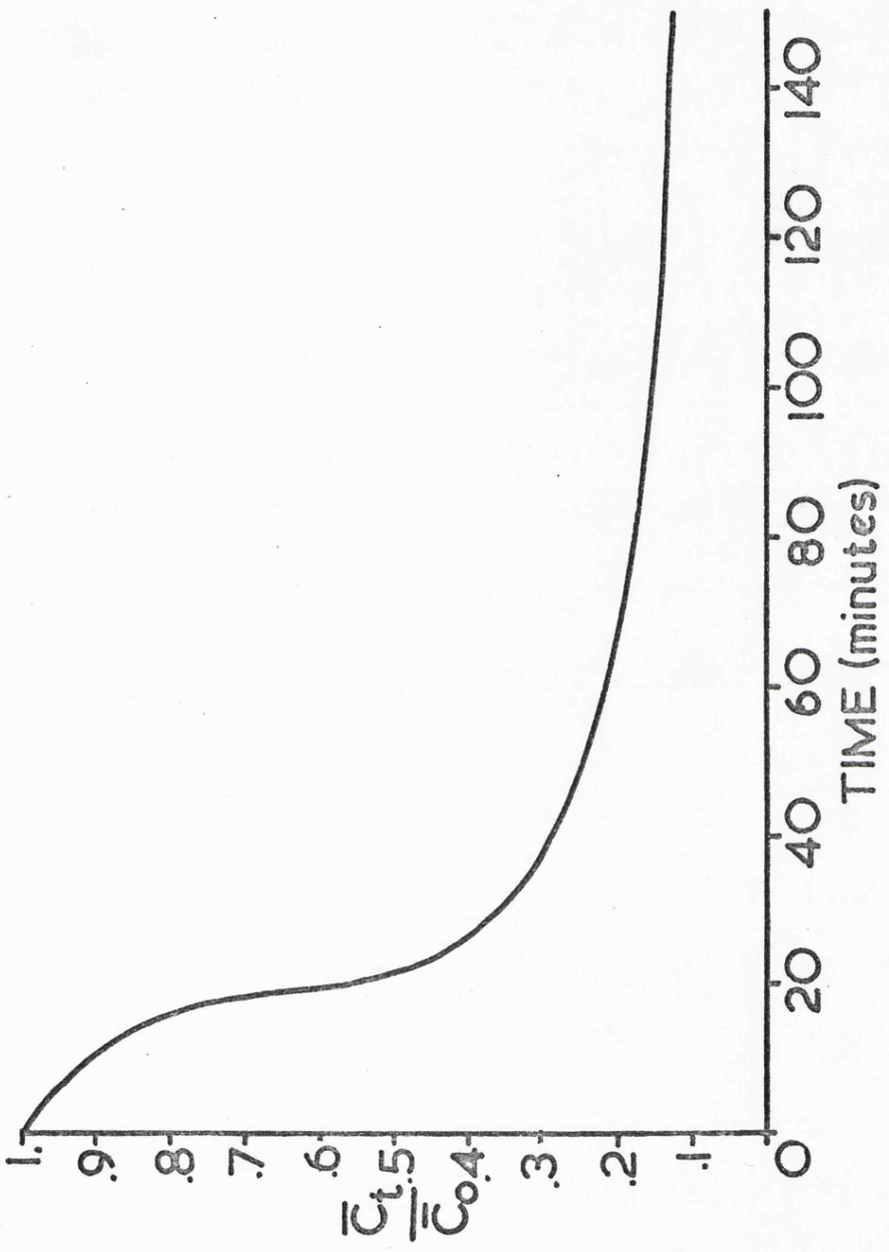


Figure V.4 Desorption of Caesium from Fine Grain Graphite at 1373 K ( Run 11)

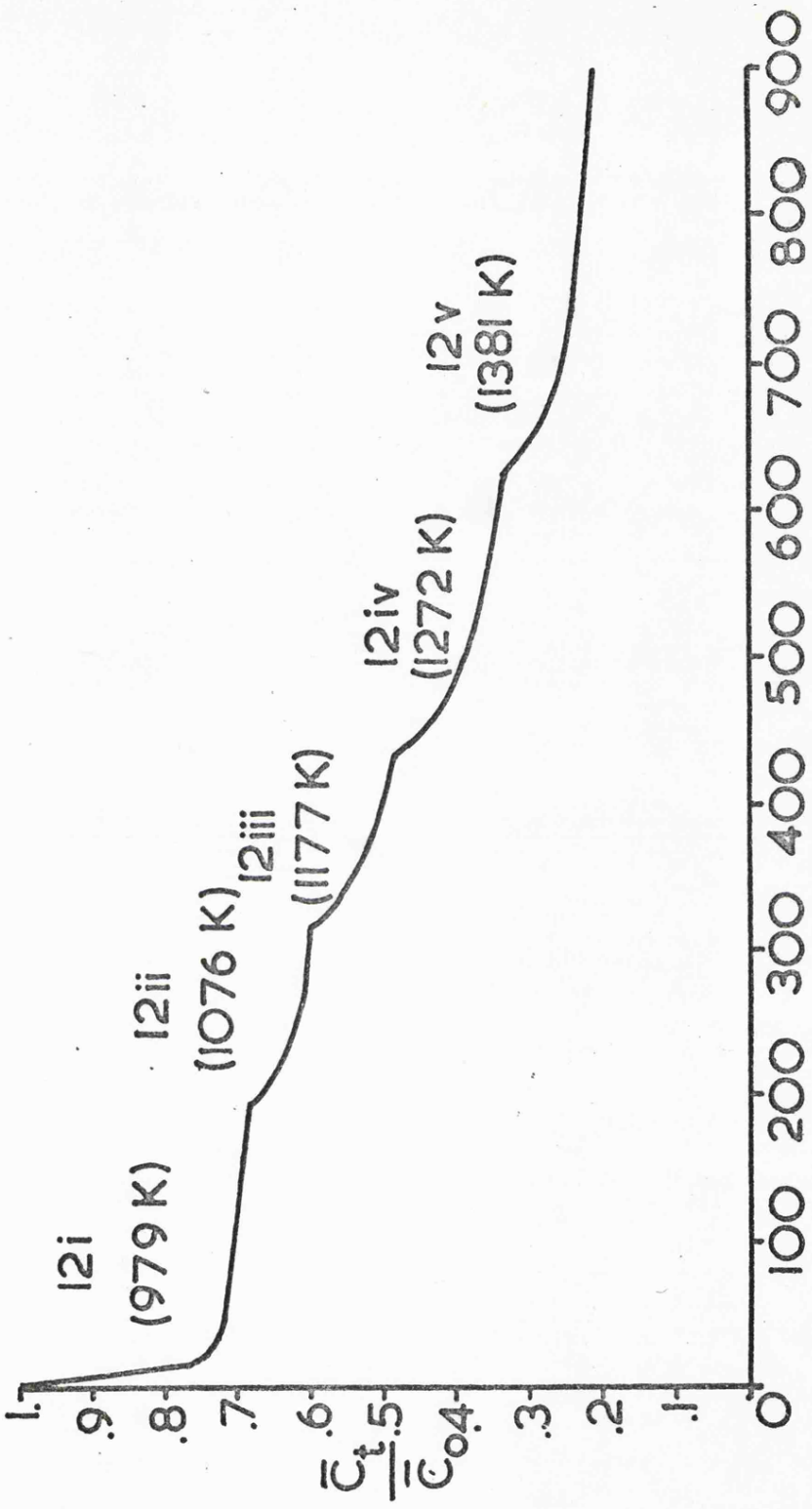


Figure V.5 Desorption of Caesium from Fine Grain Graphite at Various Temperatures ( Run 12)

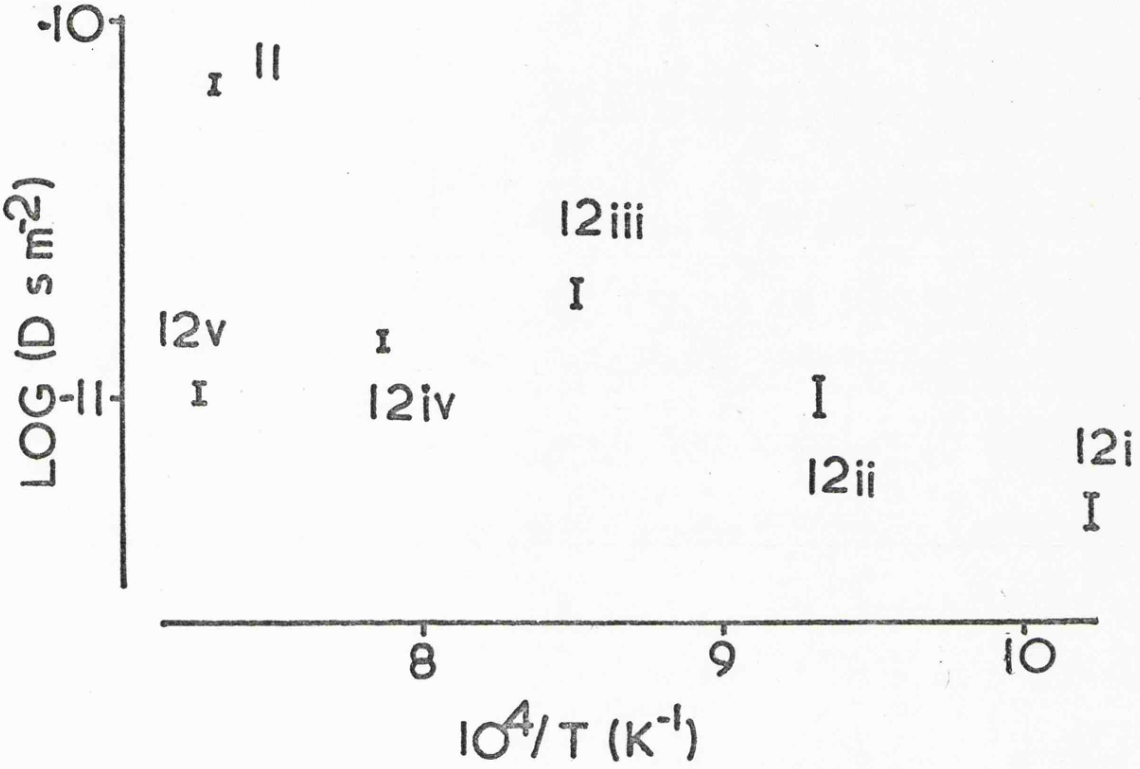


Figure V.6 An Arrhenius plot of Diffusion Coefficients of Caesium in Fine Grain Graphite ( Runs 11 and 12 )

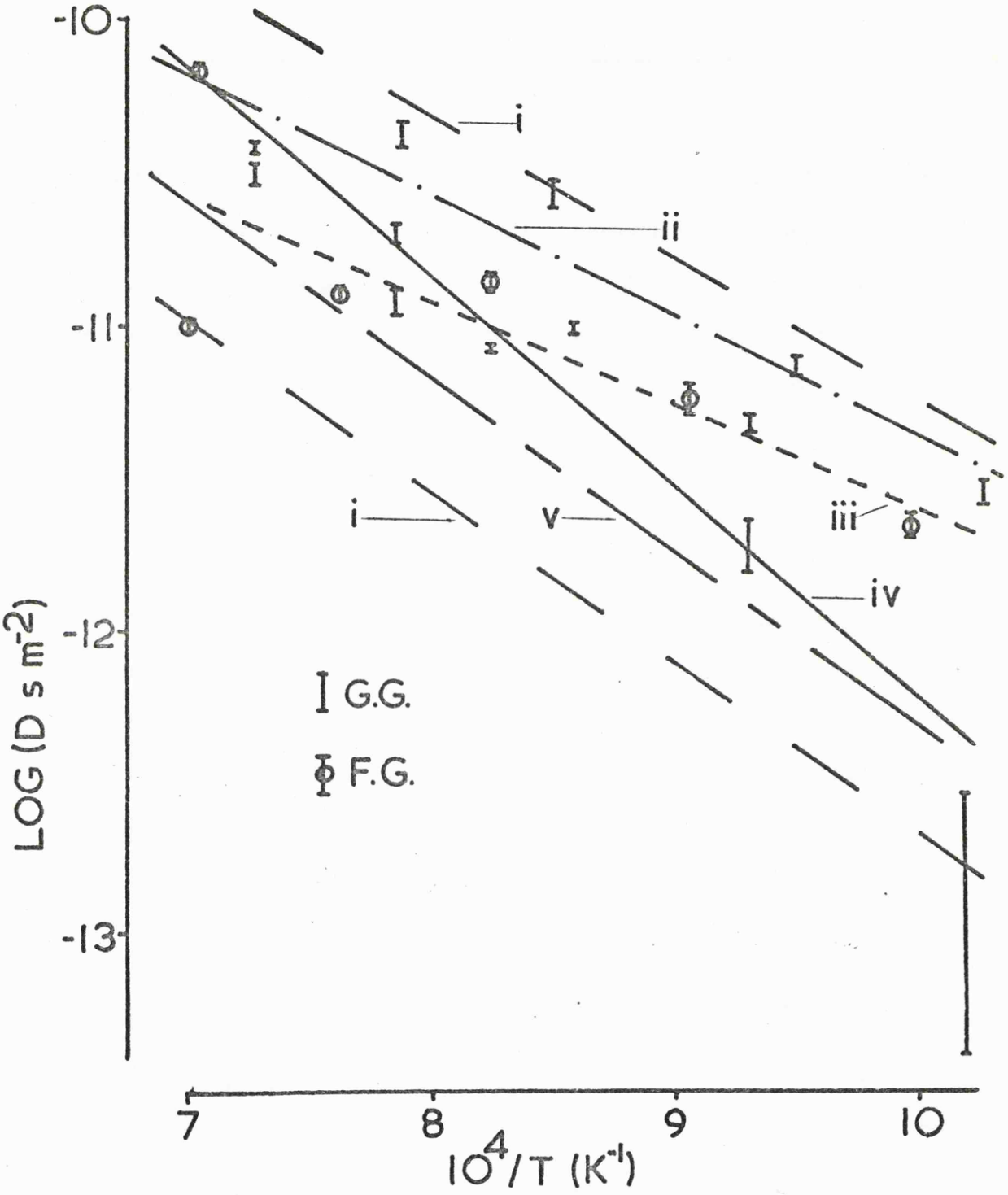


Figure V.7 An Arrhenius plot of Diffusion Coefficients for Caesium in Gilsonite ( G.G.) and Fine Grain ( F.G.) Graphites ( Runs 5 to 12)
i Upper and lower boundaries
ii Runs 5 to 9
iii Runs 11 and 12
iv Run 10
v data of Flowers et al. (1972)

# CHAPTER VI

## THEORETICAL PREDICTIONS OF DIFFUSION EQUATIONS

This chapter is concerned with some variations on the simple diffusion model employed in Chapter V. Consideration of the effect of a non-uniform concentration profile is made, and an analysis of the case of a finite surface resistance condition is presented. The chapter ends with a three part discussion on a two component diffusion model and postulates an explanation for the desorption curves and caesium concentration profiles.

### VI.1 Non-Uniform Concentration Profiles

The concentration profiles of the caesium-gilsonite graphite system observed at various stages in the adsorption, heat treatment and desorption programmes (figures IV.5 and V.3) show that at all stages during the programme a non-uniform concentration profile exists. Since equations V.7 and V.12 are based upon an assumption of an initial uniform concentration profile, their validity is suspect.

For an initial non-uniform concentration profile, given by

$$ {}_rC_o = b + cr + dr^2 + er^3 + fr^4 + gr^5 \qquad \text{VI.1} $$

where ${}_rC_o$ is the concentration at a radial position r within the sphere of radius a at zero time and b,c,d,e,f and g are constants (different from those used in previous chapters) the solution of Equation V.4 is given by Van Orstrand (1940) as

$$ {}_rC_t = 2\sum_{n=1}^{\infty} \sin(n\pi r/a) \exp(-n^2 Dt\pi^2/a^2)\, f(a,n)/ar \qquad \text{VI.2} $$

where ${}_rC_t$ is the concentration at radius r and time t. The function f(a,n) is given by

$$ \begin{aligned} f(a,n) &= ba^2(-n\pi\cos(n\pi))/n^2\pi^2 \\ &+ ca^3(-(n^2\pi^2-2)\cos(n\pi)-2)/n^3\pi^3 \\ &+ da^4(-(n^3\pi^3-6n\pi)\cos(n\pi))/n^4\pi^4 \\ &+ ea^5(-(n^4\pi^4-12n^2\pi^2+24)\cos(n\pi)+24)/n^5\pi^5 \\ &+ fa^6(-(n^5\pi^5-20n^3\pi^3+120n\pi)\cos(n\pi))/n^6\pi^6 \\ &+ ga^7(-(n^6\pi^6-30n^4\pi^4+360n^2\pi^2-720)\cos(n\pi)-720)/n^7\pi^7 \qquad \text{VI.3} \end{aligned} $$

The mean concentration at time t is

$$ \bar{C}_t = 6\sum_{n=1}^{\infty}(-1)^{n+1} \exp(n^2 Dt\pi^2/a^2) f(a,n)/na^2\pi \qquad \text{VI.4} $$

and the initial mean concentration is

$$ \bar{C}_o = 6\sum_{n=1}^{\infty}(-1)^{n+1} f(a,n)/na^2\pi \qquad \text{VI.5} $$

since at zero time the exponential term in equation VI.4 is unity. The solution is subject to the other conditions involved in the solution of equation V.7, i.e. zero surface concentration, no surface exit resistance and a constant diffusion coefficient in an isotropic medium.

The constants of equation VI.1 were found for the concentration profile of the caesium-gilsonite graphite system after heat treatment at 573 K (Run 4), by the use of a multiple regression routine (supplied by I.C.L. Statistical Package) and the resultant fit to the original data is shown in figure VI.1. Concentration profiles for various $Dt/a^2$ values were then computed from equations VI.2 and

VI.5, using the criterion of the (m + 1) term being less than $10^{-6}$ of the sum to m terms, to terminate the summations; the results are shown in figure VI.2. Values of $\bar{C}_t/\bar{C}_o$ were also computed from equations VI.4 and VI.5 for a range of values of $Dt/a^2$, the results being shown in figure VI.3 together with the results of a similar computation based upon equation V.7; in both cases the summations were terminated using the criterion stated above. The resultant profiles of figure VI.3 clearly show the relative insensitivity of equation V.7 to the initial concentration profile, the maximum error in the diffusion coefficient being a factor of two. Thus it may be concluded that the method developed in this work for estimation of diffusion coefficients from measurements of desorption, for an initial uniform concentration of diffusant in an isotropic medium, may be applied more generally to initial non-uniform concentrations with only a small error.

However, comparison of the experimental concentration profiles obtained at various desorption temperatures (figure IV.5) with those calculated from equation VI.2 (figure VI.2) shows that the latter equation does not predict the variation of experimental concentration profiles with increasing desorption temperature (i.e. with increasing $Dt/a^2$). This is seen most clearly in the curve obtained after desorption at 1373 K (Run 9). The value of $Dt/a^2$ calculated from desorption kinetics using the numerical solution of equation V.7 (Chapter V.4) was $3 \times 10^{-2}$ at the end of the run. Interpolation between the curves for $Dt/a^2$ at $10^{-2}$ and $10^{-1}$ calculated from equation VI.2 (figure VI.2) suggests a relatively even concentration profile in the centre of the specimen tending to

zero at the edge. However, the experimental curve for this condition (figure IV.5) is the reverse, with caesium concentration increasing as the surface is approached.

It is concluded, therefore, that the mechanism of isotropic diffusion occurring from an initial non-uniform concentration profile cannot be reconciled with the experimental observations on the caesium-gilsonite graphite system. Indeed, the observations suggest an anisotropic diffusion process occurs which is dependent upon the complex structure of the gilsonite graphite. This aspect will be developed in Chapter VI.3.

## VI.2 Surface Evaporation of Caesium

It has been previously stated (Chapter III.3) that the initial rapid desorption of caesium from the graphites observed in the microgravimetric experiments may be attributed to surface evaporation. It has also been noted (Chapter IV.6) that the finite surface concentration of caesium observed by electron probe microanalysis may be due to rate control by surface evaporation. In this section, the contribution that surface evaporation may make to the desorption of caesium from the graphite will be considered.

For a system where the flux diffusing to the surface is equal to the flux leaving the surface, we have

$$-D\left(\frac{\delta_r C}{\delta r}\right)_{r=a} = \alpha\,({}_sC - S_gC) \qquad \text{VI.6}$$

where $\alpha$ is the surface emissivity per unit area of surface, ${}_sC$ the concentration just within the surface, ${}_gC$ the gas phase concentration

and S the sticking coefficient. Equation VI.6 carries the implicit assumption that the adsorption isotherm of the surface can be described by Henry's Law, i.e.

$$P = K_s C' \qquad \text{VI.7}$$

where K is the Henry's Law constant and $_sC'$ the equilibrium surface concentration. Assuming an initial uniform concentration in an isotropic spherical system of radius a, whose surface is subject to the condition of equation VI.6, with a constant diffusion coefficient, the diffusion equation for radial flow (equation V.4) can be solved, Crank (1967), to give

$$\bar{C}_t/C_o = \sum_{n=1}^{\infty} \frac{6L^2 \exp(-Dt\beta_n^2/a^2)}{\beta_n^2(\beta_n^2 + L(L-1))} \qquad \text{VI.8}$$

where

$$L = a\alpha/D \qquad \text{VI.9}$$

and $\beta_n$ is the $n^{th}$ root of the equation

$$\beta_n \cot(\beta_n) + L - 1 = 0 \qquad \text{VI.10}$$

the other terms having their usual significance. Equation VI.8 describes the flux leaving a sphere under Langmuir free evaporation conditions with an initial uniform concentration profile and a surface concentration described by Henry's Law.

However, Milstead et al.(1966) and others have proposed that the surface concentration of caesium is determined by the Freundlich isotherm. For such a system equation VI.6 transforms to

$$-D\left(\frac{\partial_r C}{\partial r}\right)_{r=a} = \alpha(_sC^u - S\ _gC) \qquad \text{VI.11}$$

where u is the exponent of the Freundlich equation

$$P = K_2 C_s^{u} \qquad \text{VI.12}$$

$K_2$ being the Freundlich equation constant. Unfortunately there is no exact solution of the diffusion equation for a system subject to the condition of equation VI.11. However, the surface concentration varies over a relatively small range (Table IV.1) and thus Henry's Law can be applied to cover this range with small error. Thus the solution of equation VI.8 can be used to give a reasonable indication of the effect of a finite surface resistance upon the desorption rate.

The dimensionless constant L, sometimes known as the Sherwood number, Bromley et al.(1963), depends upon the relative magnitudes of $\alpha$ and D. Figure VI.4 shows the relationship between $\bar{C}_t/\bar{C}_o$ and $\log(Dt/a^2)$ for various values of L, computed from equation VI.8, (the condition that the m + 1 term be less than $10^{-6}$ of the sum to m terms was used to terminate the summation). It is interesting to note that as L tends to infinity, i.e. $\alpha$ becomes large with respect to D, equation VI.10 tends to

$$\cot(\beta_n) = -\infty \qquad \text{VI.13}$$

$$\text{i.e. } \beta_n = n\pi$$

and since $L^2$ is much larger than $\beta_n^2$, equation VI.8 reduces to

$$\bar{C}_t/\bar{C}_o = 6 \sum_{n=1}^{\infty} \exp(-Dt\pi^2 n^2/a^2)/n^2\pi^2 \qquad \text{VI.14}$$

i.e. equation V.7 which describes desorption under conditions of zero surface resistance. The relationship given by equation VI.14 is also

shown in figure VI.4 and it can be seen that for L greater than 100, the effect of the surface condition is negligible. The effect of the surface condition is clearly shown in a linear plot of $\bar{C}_t/\bar{C}_o$ versus $Dt/a^2$ (figure VI.5) where the effect of the variation of L is more clearly seen.

The rate of desorption F, under Langmuir free evaporation conditions, is given by

$$F = EPK_1 (M/2\pi RT)^{\frac{1}{2}} \qquad \text{VI.15}$$

where E is the surface area and $K_1$ is the evaporation coefficient, the insertion of equation VI.7 gives

$$F = EK_1K_sC' (M/2\pi RT)^{\frac{1}{2}} \qquad \text{VI.16}$$

If L is small, i.e. the surface emissivity is small compared with the diffusion coefficient, then to a good approximation (an error of less than 5%) the concentration throughout the sphere is uniform over the whole of the desorption period and thus :-

$$\bar{C}_t = {}_sC'$$

and hence

$$F = \frac{-d(\bar{C}_t)}{dt} = \frac{-d({}_sC')}{dt} \qquad \text{VI.17}$$

Integrating equation VI.16 by the use of equation VI.17 leads to

$$\bar{C}_t/\bar{C}_o = \exp(-K_3t) \qquad \text{VI.18}$$

where $K_3$ is a conglomerate of the constants of equation VI.16. The semilog and linear plots of equation VI.18 are also shown in

figures VI.4 and VI.5 respectively. It can be seen that the condition $\bar{C}_t = {}_sC'$ is effectively met for values of $L \leq 0.1$. Hence, for practical purposes, desorption is controlled by diffusion to the surface for values of $L > 100$, that desorption is controlled by surface evaporation for values of $L < 0.1$ and there is mixed diffusion evaporation control of desorption for $100 > L > 0.1$.

Assuming that the later part of the desorption curves represents a single phase diffusion process, it is of interest to see the effect of a finite surface emissivity upon the surface concentration. The companion equation to equation VI.8 for the concentration at any point within the sphere is given by Crank (1967) as

$$ {}_rC_t/\bar{C}_o = 2La\sum_{n=1}^{\infty} \exp(-Dt\beta_n^2/a^2)\sin(\beta_n r/a)/\{r\sin(\beta_n)(\beta_n^2+L(L-1))\} \qquad \text{VI.19} $$

for an initial uniform concentration. The concentration at a radial distance of $r/a = 0.99$ was calculated for varying $Dt/a^2$ and L values, using the previously mentioned criterion for the termination of the summation. Figure VI.6 shows the variation so calculated, together with the observed values of normalised surface concentration plotted against their respective $Dt/a^2$ values. The values of $\bar{C}_o$ used were the total initial concentrations and the values of the diffusion coefficients were those calculated from equation V.15. Figure VI.6 suggests that the diffusion flux in the latter part of the desorption experiment is controlled by a surface condition with a value of L of approximately 10. However, the effect of two phase diffusion and a non-uniform concentration profile will cause this value of L to be reduced. It is interesting to note that Bromley et al. (1963) reported a value of

L = 4.25 for diffusion of caesium in HX 10 graphite at 1473 K.

## VI.3 The Multi component Diffusion Model: General Considerations

From a knowledge of the manufacturing processes and structures of the nuclear graphites used in this study (Appendix I), one would expect that the diffusion of any component in the graphite would be complex and not amenable to study using simple equations of diffusion through an isotropic medium. Indeed, considerable evidence has been presented in the previous sections for a multi-component diffusion process. It is the aim of this section to show that whilst such a view is strictly correct, useful data can be obtained from simple equations of diffusion since, in certain circumstances, an approximate analysis may be an adequate description of the diffusion process.

Fisher (1951) attempted a solution of the diffusion equations for a system composed of a semi infinite solid of relatively low diffusivity, having a semi infinite, highly permeable slab of thickness $\delta$ imbedded in it, as shown in figure VI.7. Using the boundary conditions of a zero initial concentration in the solid, with the surface maintained at a fixed concentration ${}_sC$ from zero time onwards; assuming the slab to be so thin that the concentration variation across its width is negligible and that no diffusion occurs from the surface into the bulk, then Fisher found that the concentration at any point within the slab could be approximately expressed by

$$x,y{}^{C_t}/_{s}C = \exp\left(-y\left\{\frac{2}{\delta D_1}\right\}^{\frac{1}{2}}\left\{\frac{D_2}{\pi t}\right\}^{\frac{1}{4}}\right)\operatorname{erfc}\left\{x/\left(2(D_2t)^{\frac{1}{2}}\right)\right\} \quad \text{VI.20}$$

where $D_1$ and $D_2$ are the diffusion coefficients in the highly

permeable slab and the low diffusivity material respectively. In a more exact analysis of the system, Whipple (1954) showed that the influence of the slab only became apparent for the condition

$$D_1\delta / 2D_2 (D_2 t)^{\frac{1}{2}} > 1 \qquad \text{VI.21}$$

If the condition of equation VI.21 is not held, then the system reverts to a simple semi infinite homogeneous medium whose concentration profile may be expressed by

$$ {}_yC_t/{}_sC = \operatorname{erfc} (y/2(D_2 t)^{\frac{1}{2}}) \qquad \text{VI.22}$$

It is possible to interpret qualitatively the anomalous concentration profiles observed in this work using equation VI.20. Figure VI.8(a) shows qualitatively the concentration profile in both the x and y co-ordinates after a small period of inward diffusion according to equation VI.20. The profile shows the relatively deep penetration down the slab (the plane of the axes c and y) and the small extent of diffusion into the bulk. This profile is based upon calculations of Fisher (1951) using a value of $D_1/D_2 = 10^6$ and a value for the condition of inequality VI.21 of $5.10^4$. The effect of diffusion from the surface into the bulk is neglected. Figure VI.8(b) shows the effect that heat treatment has upon the concentration profile, causing an effective flattening of the slab concentration profile, coupled with further diffusion into the bulk. The surface is still maintained at a fixed concentration, which is however slightly less than ${}_sC$. Figure VI.8(c) shows the change in the concentration profile produced after a short period of desorption under Langmuir free evaporation conditions, in which the slab concentration profile has fallen near the surface. After a longer period of time for desorption, the

slab concentration drops to effectively zero, since outward diffusion from the slab is rapid and the rate of the diffusion process is now dependent upon diffusion from the bulk into the slab (figure VI.8(d)). It can be seen that the diffusion flux in the slab and the bulk is obeying Fick's first law in all stages of figure VI.8. However, outward diffusion represented by figure VI.8(c) and (d) occurs against an overall caesium concentration profile which is in apparent contradiction to Fick's Law. Thus the behaviour of the caesium-gilsonite graphite system can be interpreted in general terms by means of a two-part diffusion model with a surface condition.

## VI.4 The Multicomponent Diffusion Model: Detailed Considerations

A more detailed interpretation of the effects of adsorption, heat treatment and desorption upon the transport of caesium in graphite according to the multicomponent diffusion model is now presented. During the initial adsorption period at 470 K, caesium diffuses into the specimen along the high diffusivity paths, resulting in a high concentration near the surface. Heat treatment at 573 K allows the continued inward diffusion along the high diffusivity paths and, to a lesser extent, into the low diffusivity material. The flat concentration profile observed in the inner region of the specimen after heat treatment, (Run 4, figure IV.5) indicates that the fast diffusion process has had time to establish a uniform concentration profile in the high diffusivity paths throughout the graphite. Thus the higher caesium concentration in the outer portion of the specimen represents diffusion into the low diffusivity material, which has been enhanced by the high

concentration gradients.

On increasing the temperature of the specimen, desorption of caesium occurs. Initially, the exterior surface of the specimen undergoes a reduction in caesium concentration by direct evaporation. Also, diffusion occurs along the high diffusivity paths to the depleted exterior surfaces where evaporation occurs. The flux associated with the high diffusivity paths is relatively large initially, but decreases because of the decreasing concentration gradient along the high diffusivity path. However, as the concentration in the high diffusivity path drops, diffusion from the low diffusivity material increases because of the increased concentration gradient. After due time, the high diffusivity paths become almost completely depleted of caesium and diffusion now effectively occurs from the low diffusivity material. Thus, in summary, it is proposed that initially desorption is controlled by the rate of evaporation from the surface and the flux of caesium atoms to the surface from the high diffusivity paths. Relatively quickly, the desorption rate becomes controlled by all three mechanisms: - evaporation, diffusion from the high diffusivity paths and also from the low diffusivity material. The desorption rate reduces as the high diffusivity paths become depleted and eventually control of the desorption rate is due to evaporation and diffusion from the low diffusivity material.

It appears that this latter stage of control is only achieved, in the desorption experiments on gilsonite graphite, after desorption has occurred for a long period of time at the highest temperature, i.e. Runs 9 and 10. This is reflected in the concentration profile of the specimen after desorption at 1373 K (Run 9, figure IV.5) where

the caesium concentration in the inner region is not detectable and the caesium in the outer portion is presumed to be associated with the low diffusivity material. The concentration profile of Run 10 (figure V.3) where desorption was carried out for a much longer period of time shows evidence of mobility of caesium within the low diffusivity material, causing the caesium concentration to increase again in the inner region. Thus the diffusion coefficients obtained at the lower desorption temperatures (Runs 5 to 8) reflect mixed control of diffusion. However, the increase in temperature causes an approach to single component control of diffusion and hence the diffusion coefficients found at different temperatures represent varying degrees of mixed control. This effect is shown in figure V.7 where the diffusion coefficient at 1373 K (Run 9) is lower than the diffusion coefficient at 1270 K (Run 8, Table V.3) causing a 'turn over' in the Arrhenius plot. The effect is also shown in Run 1 (figure III.6) for repeated adsorption/desorption of caesium on gilsonite graphite. Each successive cycle of desorptions at various temperatures gives rise to lower diffusion coefficients due to the progressive domination of the slower diffusion process.

The diffusion coefficients for Run 10 represent the slow diffusion from the low diffusivity material, since desorption was initially carried out at 1373 K for 5 hours, by which time rate control had completely transferred to the slow diffusion/evaporation process. Also, since the rate control is by a single diffusion process, the complex mathematical description of two phase diffusion degenerates to a single-phase description and hence the use of the various diffusion equations in the previous chapters is justified. There is still the problem of determining the initial concentration,

$\bar{C}_o$, associated with each phase. It can be shown that provided there is a reasonable distribution of caesium between the two phases, i.e. less than 80% is associated with the high diffusivity paths, then the effect upon the resultant value of the diffusion coefficient is small, i.e. less than a factor of 4. This is due in part to the fact that the diffusion coefficient is in effect calculated from the variation of $\bar{C}_t$ with time and is therefore not very sensitive to the absolute value of $\bar{C}_o$.

It is of interest to note that the equivalent sphere method used by Findlay and Laing (1962) and others is based upon the approximation of a high diffusivity path surrounding each of the hypothetical spheres of graphite. If Findlay and Laing's result for caesium is subjected to analysis using equation III.2, the resultant diffusion coefficient is of the order of $10^{-12}$ $m^2$ $s^{-1}$, which is in good agreement with that observed in this work for the same temperature. It is also worthy of note that the evidence used by Iwamoto and Oishi (1969) to postulate three different trapping sites could also be interpreted in terms of a three part diffusion model.

## VI.5 The Multicomponent Diffusion Model: The Nature of the High and Low Diffusivity components

The terms 'high diffusivity' path and 'low diffusivity' material have been used to describe the two hypothetical phases of the gilsonite graphite. No direct evidence was obtained in this work on the nature of the two phases. However, various minor observations, together with other reported work, allow a reasonable

description of the two phases to be made. Bacon and Sprague (1961) used caesium to decorate grain boundaries, dislocations and other similar features in natural graphite. Electron micrographs show clearly the preferential siting of caesium in the form of caesium hydroxide along such imperfections. They also observed movement of ferric chloride 'bubbles' along grain boundaries, due to the localised heating of the electron microscope beam. Since their technique of experimentation allowed the caesium to oxidise, it is reasonable to conclude that unoxidised caesium would show similar mobility to that of ferric chloride. During electron probe microanalysis, fluorescence from the specimen was observed both on pore edges and also on featureless areas of the graphite. However, no related response was found from X-ray emission. Similar observations have also been recorded for barium on a HX 30 graphite, Faircloth et al. (1966). However, the spikes observed on the electron probe microanalysis trace (figure IV.3) indicate that segregation of caesium must occur in microfeatures less than 50 $\mu$m in size. The high diffusivity paths are probably related to dislocations, grain boundaries, pores and other disordered features. It is however possible to discount micropores since the size of the caesium atom (2.73 nm) is much greater than the micropore size range (up to 2 nm). It is probable that in the macropores, surface diffusion is the dominant transport mechanism which, in turn, would account for a low activation energy found for the diffusion coefficients.

The activation energy for diffusion (137 $\pm$ 31 kJ mol$^{-1}$ for Run 10) compares very closely with the heat of reaction reported (135 kJ mol$^{-1}$) by Salzano and Aronson (1965(a)) for the lower

caesium graphite compounds. It is also interesting to note that the activation energy is approximately one third of the first ionisation potential of caesium. It thus seems reasonable to identify the low diffusivity material with micropores and other such features of similar size, where perhaps a small degree of ionisation has occurred. Although X-ray analysis did not show compound formation, it is also possible that some diffusion into the more disordered of the lamellar planes of the graphite has occurred.

The diffusion coefficients found for the fine grained graphite would seem to confirm the postulated nature of the diffusion paths. The fact that the diffusion coefficients are lower than for gilsonite graphite correlates with the observed slightly higher density and better ordered lamellar planes (Appendix I). Hence, the proportion of micropores in the fine grained graphite is higher than for the gilsonite graphite, thus reflecting a more rapid transition to desorption controlled by diffusion from the low diffusivity material, which is suggested by the more pronounced 'turn over' in the Arrhenius plot observed for the fine grain graphite (figure V.7).

## VI.6 A Summary of Diffusion of Caesium in Gilsonite and Fine Grain graphites

It has been proposed that desorption of caesium from nuclear graphites is controlled by a two phase or multi phase diffusional process with a surface evaporation barrier. The slower diffusion phase is associated with diffusion through micropores and lamellar planes of low graphitic character. The faster diffusion phase is

associated with grain boundaries, macro- and meso-pores and transport probably occurs by surface diffusion along these features. It is argued that the more graphitic nature of the fine grain graphite gives rise to lower diffusion coefficients for the slow caesium diffusion process then found for the gilsonite graphite.

It has been shown that consistent desorption data can be obtained, provided an initial long desorption period is carried out at a high temperature, and that such desorption results can be analysed using equation V.7. Such an analysis showed that for gilsonite graphite the slow diffusion of caesium may be described by

$$\log (D\ sm^{-2}) = -(5.1 \pm 0.3) - (140 \pm 30)10^3/2.303\ RT \quad VI.23$$

A similar result could not be obtained for the fine grained graphite.

Evidence for a surface condition implied by a value of L of approximately 10 was found, in agreement with Bromley et al. (1963). The analysis for the surface condition is subject to an assumption of Henry's Law behaviour. In view of the known Freundlich behaviour of caesium in graphite, Milstead et al. (1966) and others, the use of this value of L over a wide range of concentration is open to a considerable degree of error. Furthermore, the desorption curves used were controlled by mixed diffusion which precludes any detailed analysis of the behaviour of L with temperature or concentration.

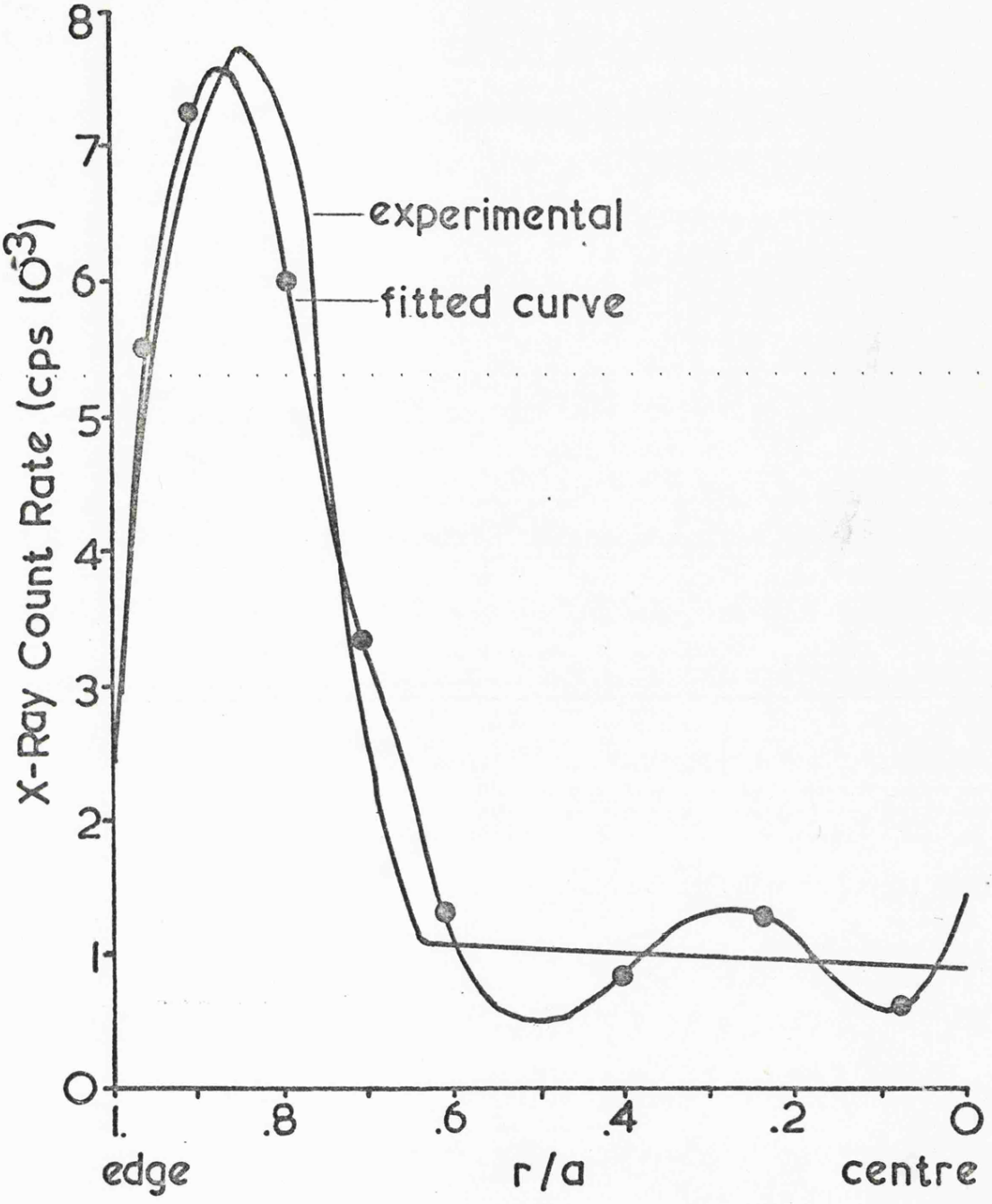


Figure VI.1 Multiple Regresion Fit of a fifth order polynomial to the Caesium Concentration Profile after Run 4

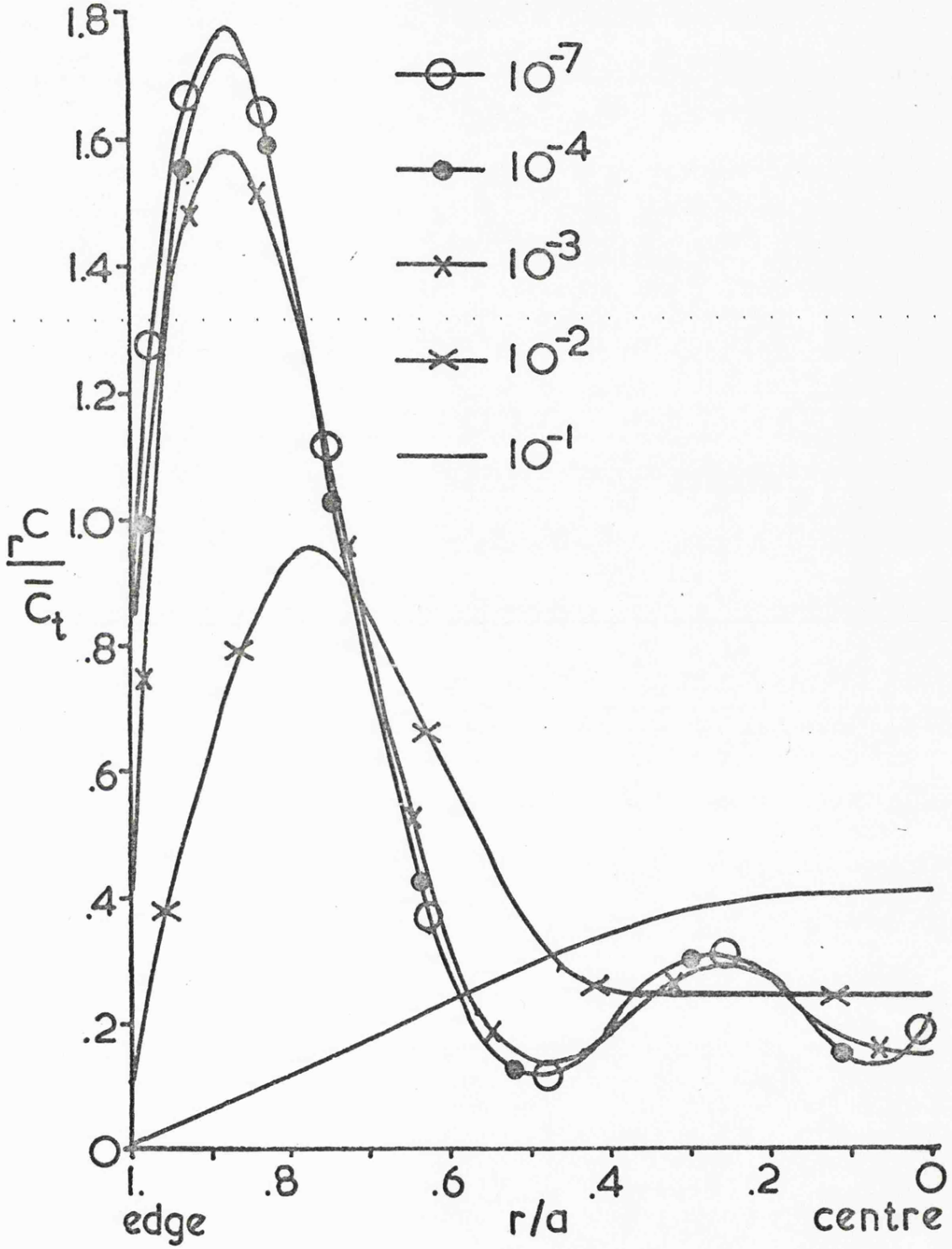


Figure VI.2 Concentration Profiles computed from Equation VI.2 for various $Dt/a^2$ values (denoted on figure) using the Initial Concentration Profile determined by the Regression fit (figure VI.1)

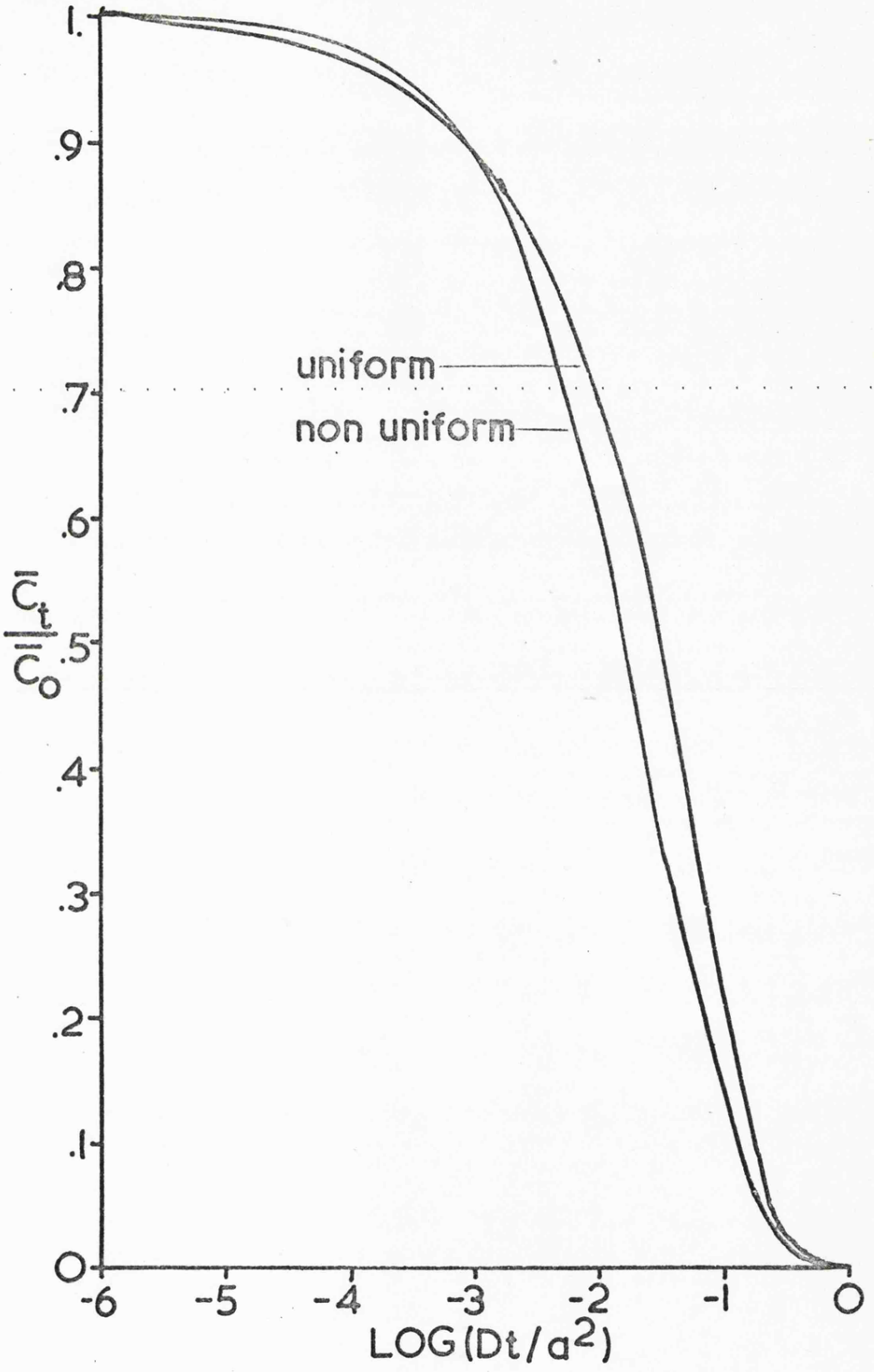


Figure VI.3 Variation of $\bar{C}_t/\bar{C}_o$ with $Dt/a^2$ for Equations V.7 and VI.4 illustrating the effect of uniform and non-uniform concentration profiles

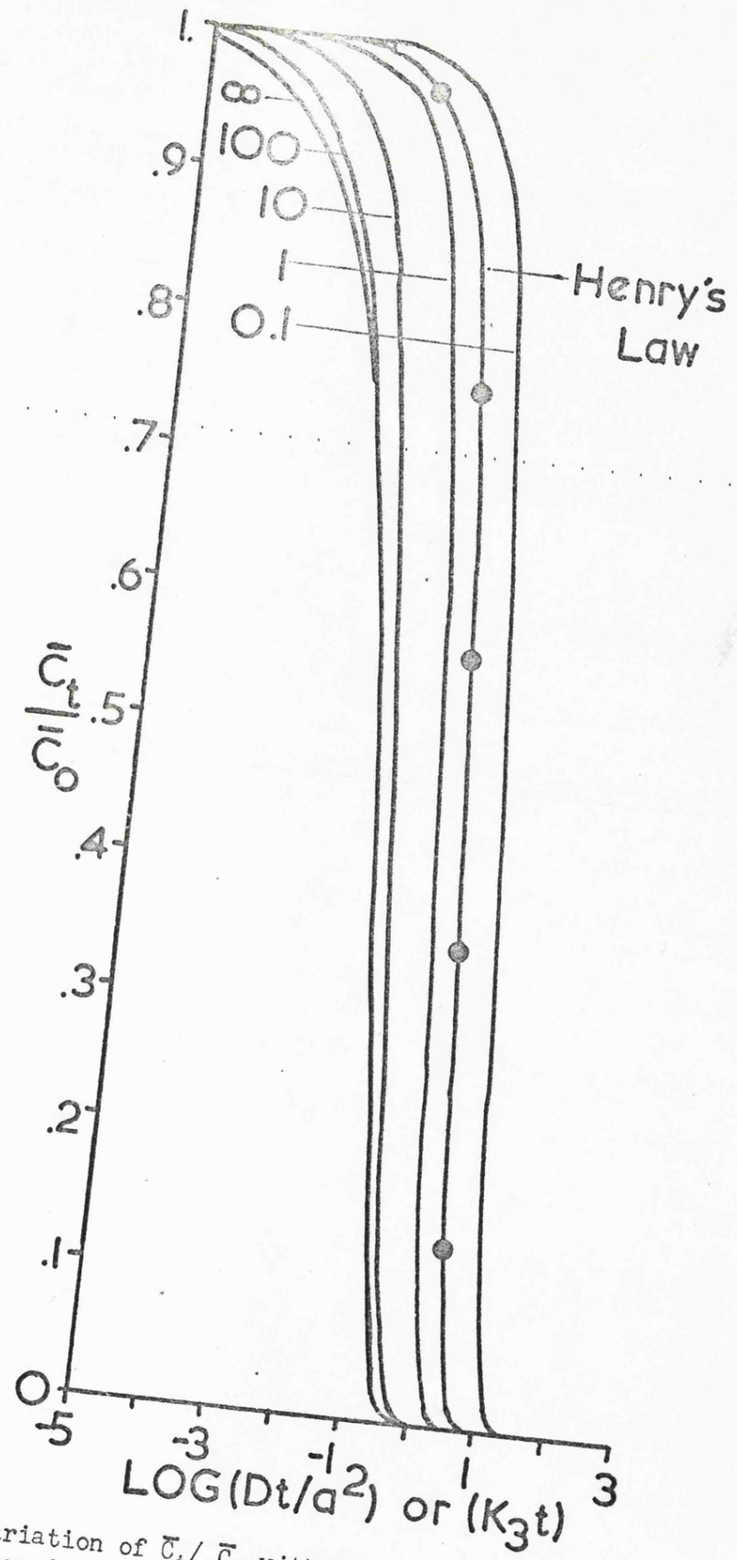


Figure VI.4 Variation of $\bar{C}_t / \bar{C}_0$ with Log ( $Dt/a^2$ ) according to Equation VI.8 illustrating the effect of changing L ( numbers on curves) and the corresponding plot of Henry's Law, Equation VI.18

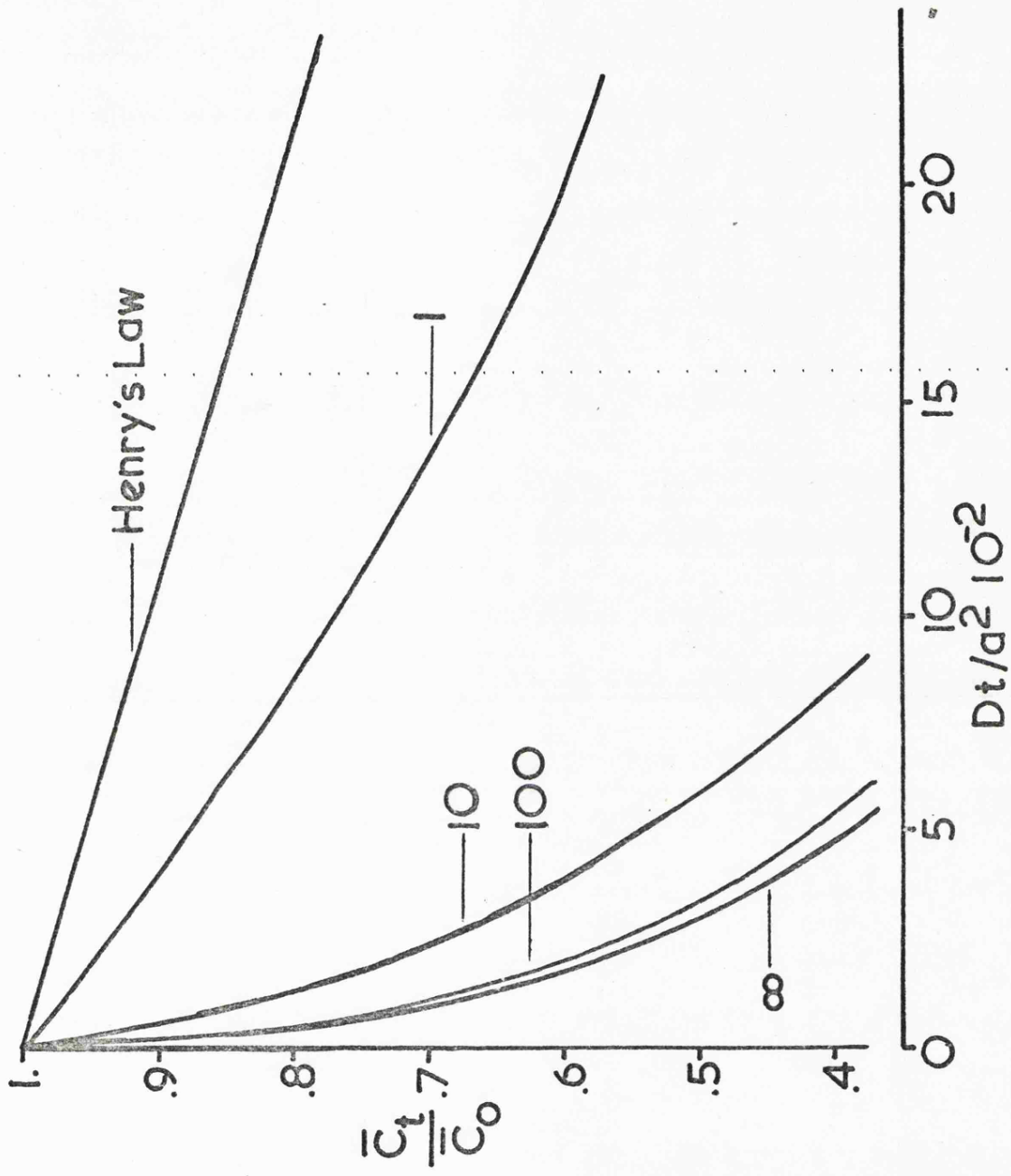


Figure VI.5 Linear variation of $\bar{C}_t / \bar{C}_0$ with $Dt/a^2$ according to Equation VI.8 illustrating the effect of changing L ( numbers on curves) and the corresponding plot of Henry's Law, Equation VI.18

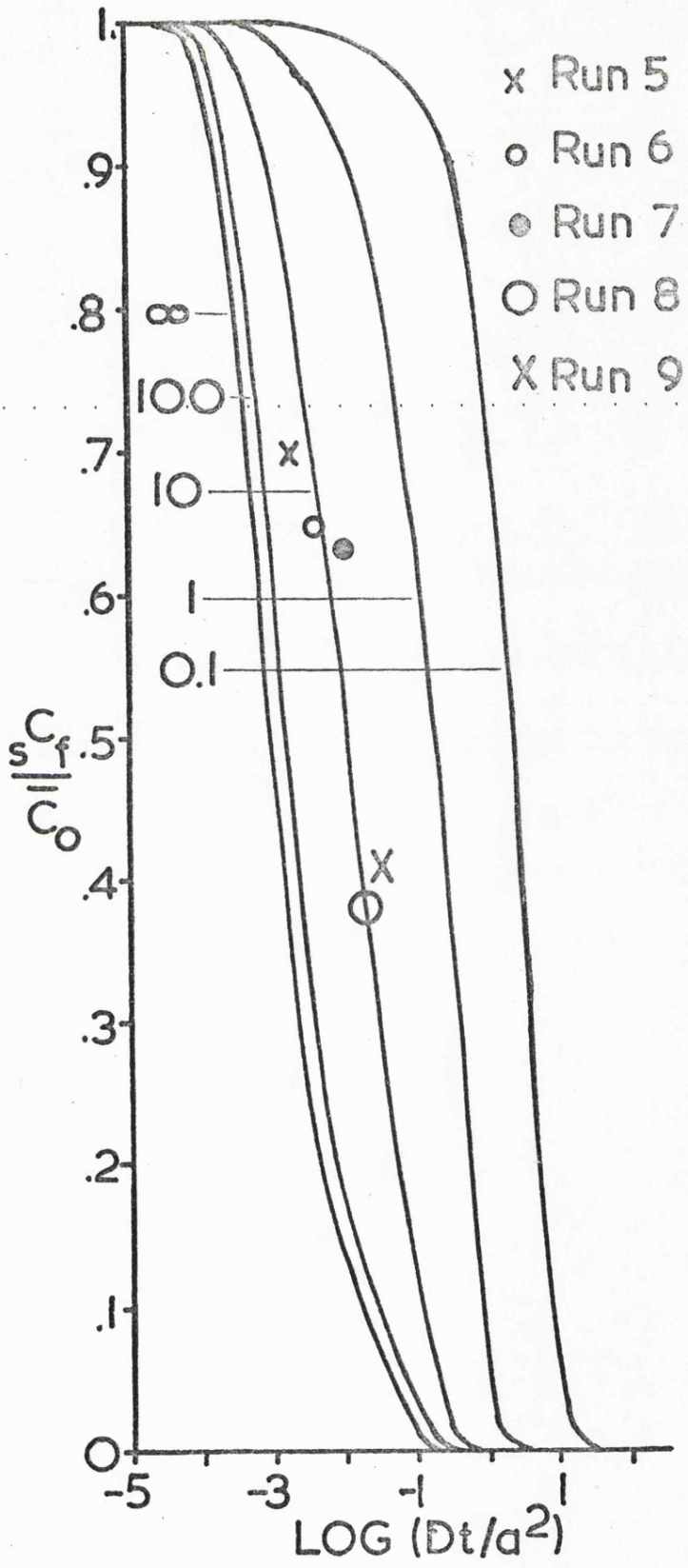


Figure VI.6 Variation of Normalised Near Surface Concentration with $Dt/a^2$ for varying L (numbers on curves) according to Equation VI.19, together with Observed Surface Concentrations (Table IV.1)

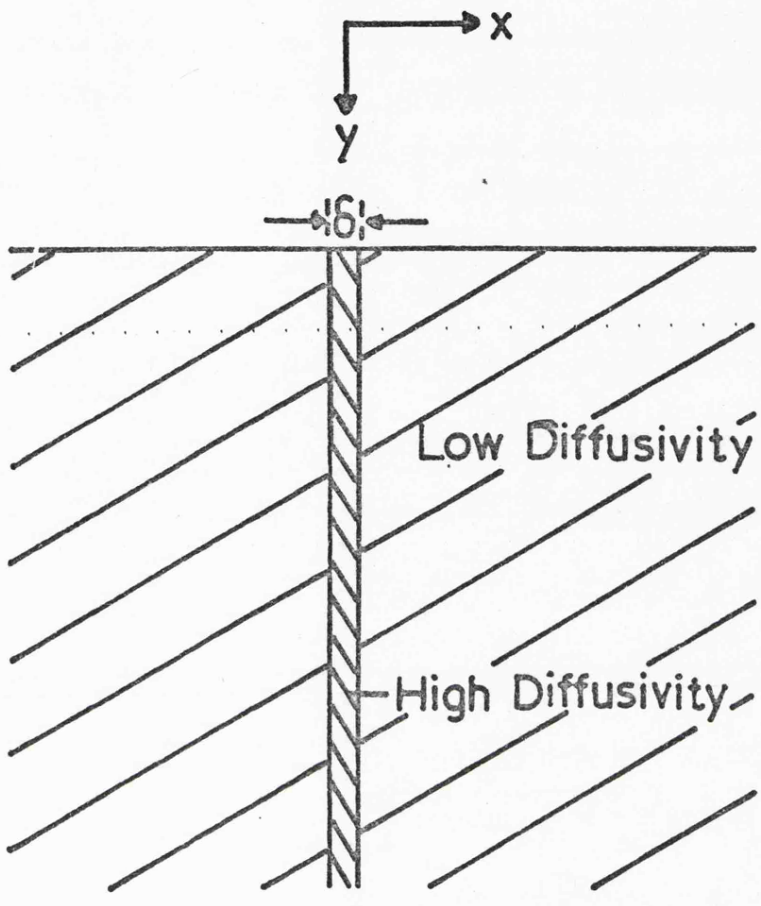


Figure VI.7 Coordinate system for diffusion outside a semi-infinite slab of high diffusivity material imbedded in a semi-infinite solid

Fisher (1951)

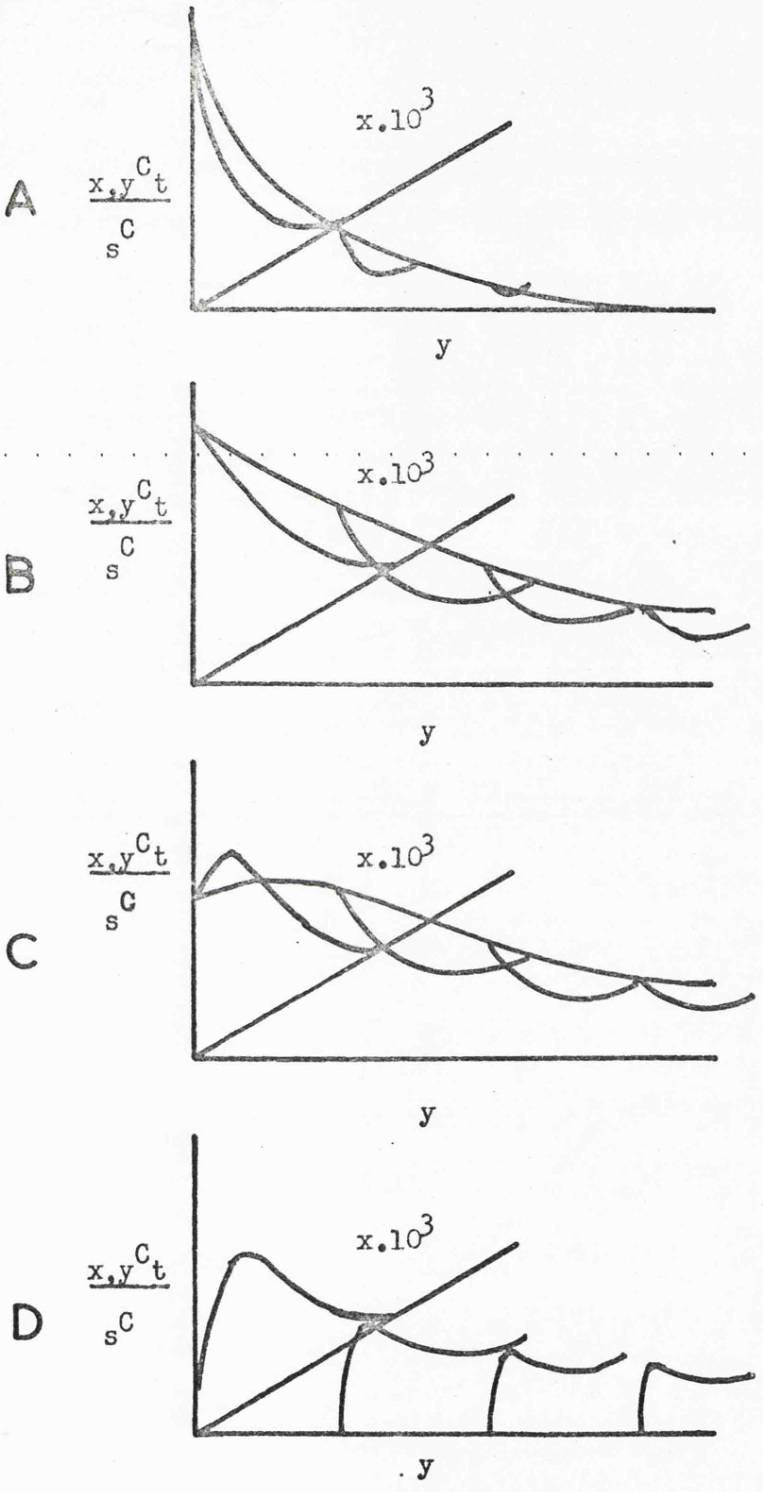


Figure VI.8 Sketches of concentration profiles in a two phase system at various times
A after adsorption
B after adsorption and heat treatment
C after initial period of desorption
D after a long period of desorption

# CHAPTER VII

## A KNUDSEN CELL TECHNIQUE FOR DETERMINING EQUILIBRIUM VAPOUR PRESSURES

This chapter is concerned with the attempt to use a Knudsen effusion cell method to measure equilibrium vapour pressures of caesium-nuclear graphites. The chapter starts with a theoretical outline of the concept of the effusion cell and of the mass spectrometric technique for measuring the effusing flux. The concept of a double Knudsen cell is also described. A detailed discussion of the major source of error in a Knudsen cell mass spectrometry combination is given, with reference to the system of interest. The chapter concludes with a description of the work done in proving the system.

### VII.1 The Theory of the Knudsen cell Mass Spectrometer System

The Knudsen effusion cell method for measuring the vapour pressure of a system relies upon the measurement of the rate of effusion of a vapour, through a small orifice from an enclosure containing the vapour at its saturation pressure. The mass flux F, passing a plane of area E in one direction is given by

$$F_1 = f_1 \bar{c} \; E/4 \qquad \text{VII.1}$$

where $f$ is the mass density of the vapour and $\bar{c}$ the mean velocity of the molecules. The net flux passing through plane E is

$$F_T = E \; \bar{c} \; (f_1 - f_2)/4 \qquad \text{VII.2}$$

where subscripts 1 and 2 refer to the forward and reverse direction respectively. Substituting for $\bar{c}$ and $f$ leads to

$$F_T = E\,(P_1 - P_2)(M/2\pi RT)^{\frac{1}{2}} \qquad \text{VII.3}$$

where $P_1$ and $P_2$ are the pressures on either side of the plane E, or, for the Knudsen cell, the pressures inside and outside the Knudsen cell respectively, M is the molecular weight of the effusing species and the other symbols have their usual significance. For an effusion cell in a high vacuum:

$$P_1 \gg P_2$$

and thus equation VII.3 reduces to

$$F = PE(M/2\pi RT)^{\frac{1}{2}} \qquad \text{VII.4}$$

Thus by measuring the effusing flux it is possible to obtain the pressure within the cell. Equation VII.4 is limited however by the assumption in equation VII.1 of ideal gas behaviour. The condition of no gaseous collisions occurring at the orifice must be obtained for equation VII.4 to be valid, which in practice limits the upper range of measurement to ca. 13 N $m^{-2}$. Another limitation of equation VII.4 is that the orifice is assumed to be infinitely thin. If, however, the orifice has a finite wall thickness, so that effusion occurs through a short pipe rather than a true orifice, it becomes necessary to introduce Clausing's correction factor $K_4$, Clausing (1932), which allows for molecular back-reflections by taking into account the resistance of the orifice to molecular flow, and equation VII.4 is thus modified to

$$F = PK_4E(M/2\pi RT)^{\frac{1}{2}} \qquad \text{VII.5}$$

A wide range of analytical techniques has been used to determine the rate of effusion of species from a Knudsen cell and these have

been reviewed by Nesmeyanov (1963). In the present work the choice of a mass spectrometer was made, since it allows an instantaneous and highly sensitive measurement of the beam flux. It does however suffer from two sources of error, one of which will be discussed in the following section. The other is due to the use of non ideal orifices, which leads to a focusing of the effusing beam and, since the mass spectrometer collects only a small portion of the beam, the relation of the portion collected to the whole is complex. This will be considered in detail further on in the discussion of the double cell.

The number of atoms arriving at the mass spectrometer per second $F_3$, is given by

$$F_3 = K_5 N \bar{c} E K_4/4 \qquad \text{VII.6}$$

where N is the number density of atoms within the cell and $K_5$ is a dimensionless constant determined by the geometrical parameters of the system and the focusing power of the orifice; the other constants taking their previously defined meanings. A part of the flux $F_3$ passes through the ionisation chamber of the mass spectrometer and is capable of undergoing ionisation; this is given by

$$F_4 = K_6 K_5 K_4 N \bar{c} E/4 \qquad \text{VII.7}$$

where $K_6$ is a constant dependent upon the geometrical parameters of the mass spectrometer and the characteristics of collisions between the effusing species and the mass spectrometer surfaces.

Within the ionisation chamber, the flux $F_4$ (atoms $s^{-1}$ $m^{-2}$) is partially ionised by collision with a flux of electrons $N_e$

(electrons $s^{-1}$ $m^{-2}$). Consider a volume b within which all ionisation occurs, then $F_4 b/\bar{c}$ atoms occupy the volume at any particular time. These show a total effective collision area to the electron beam of $QF_4 b/\bar{c}$ $m^2$ where Q is the electron ionisation cross sectional area of the effusing atoms. The number of electrons undergoing ionising collisions, and hence the number of atoms being ionised per second $F_5$ is thus given by

$$F_5 = N_e Q F_4 b/\bar{c} \qquad \text{VII.8}$$

$$\text{i.e.} \quad F_5 = N_e b K_6 K_5 K_4 Q N E/4 \qquad \text{VII.9}$$

The ion current I, indicated by the mass spectrometer is related to $F_5$ by

$$I = K_7 N_e b K_6 K_5 K_4 Q N E/4 \qquad \text{VII.10}$$

where $K_7$ is a constant dependent upon the analysing efficiency and the amplification of the mass spectrometer. Whilst the latter term is determined by the electronics of the mass spectrometer and is therefore constant, the analysing efficiency depends upon the atomic mass to ion charge ratio, the m/e value, of the ionised species. The result is a broadening of the mass peaks at high m/e values and, where this occurs, peak areas instead of peak heights should be used. Hence grouping all the constants together and substituting for N leads to

$$P = IT/K_8 EQ \qquad \text{VII.11}$$

where $K_8$ is a conglomerate constant and E the area of the orifice.

Thus the pressure depends directly upon the ion current and by prior calibration for $K_8$, the pressure within the cell can easily

be obtained. Equation VII.11 does break down at pressures above approximately 13 mN $m^{-2}$ due to the number density of the ions causing a significant space charge which perturbs the electric field due to the ion repeller, and hence reduces the number of ions being ejected into the analyser.

Normally calibration of the system is made by including within the cell a small quantity of an element of known pressure-temperature relationship and electron ionisation cross-sectional area. However, in the present case, the use of another element within the same cell will almost certainly perturb the caesium-graphite system and thus the use of this technique is inadvisable.

In order to overcome the problem of interaction between sample and standard a double Knudsen cell technique was developed for this work. The double cell consists of two separate Knudsen cells fabricated from the same piece of metal, and having near identical orifices in close proximity (figure VII.1). Letting the subscripts E and S refer to the sample and standard systems respectively, then from equation VII.11 it is evident that

$$P_E / P_S = \frac{I_E K_{8S} E_S Q_S}{I_S K_{8E} E_E Q_E} \qquad \text{VII.12}$$

Near identical orifices are achieved by using electron microscope apertures which are produced to high tolerances. Defining the target angle $\omega$ (figure VII.1) Ruth and Hirth (1964) have shown that provided the difference in target angles of the two orifices of the double cell is less than 2 degrees, then the geometric distribution constant of both orifices is effectively the same. Applying this condition to the present work, it can be shown that

effectively identical geometrical distribution constants are obtained for the ratio of the distance between the two orifices to the distance between orifice and target being less than 0.03. Under these conditions equation VII.12 reduces to

$$P_E / P_S = I_E Q_S / I_S Q_E \qquad \text{VII.13}$$

and provided the electron ionisation cross sectional areas are known the pressure of the sample system is easily found. The validity of equation VII.13 can easily be tested and the double cell calibrated by the use of two standard systems, thus obtaining the ratio of the constants of equation VII.12.

The constant $K_8$ may also be evaluated by use of the Clausius-Clapeyron equation

$$\ln (P) = K_9 - \Delta H/RT \qquad \text{VII.14}$$

where $\Delta H$ is the heat of vaporisation and $K_9$ the pre-exponential constant.

Substituting for P in equation VII.11 gives

$$\ln (IT) = K_9 - \ln (K_8 E/Q) - \Delta H/RT \qquad \text{VII.15}$$

and hence $K_8$ may easily be found. Equation VII.15 also offers the simplest technique for proving the Knudsen cell mass spectrometer system by comparing the literature value of the heat of vaporisation of the effusing species with that determined from the plot of log(IT) against I/T.

## VII.2 Electron Ionisation Cross Sections and the choice of a Standard

The major error in the Knudsen cell mass spectrometer system is in the lack of and/or inaccurate knowledge of electron ionisation cross sections. Most measurements of electron ionisation cross sections have been confined to gases and other elements whose vapour pressures at room temperatures are high enough to produce easily measured beam densities. It is this factor alone which precludes the choice of molecular species as standard, since the knowledge of electron ionisation cross sections of molecules is confined to hydrogen and some other simple molecules. Although the advent of quantitative mass spectrometry has revealed major deficiencies in these measurements, surprisingly little experimental work has been done to improve and extend the knowledge of electron ionisation cross sections, particularly for elements of low vapour pressure. Because of the lack of such data, consideration has been given to theoretical estimates of electron ionisation cross section.

Semi-empirical relationships have been proposed by Otvos and Stevenson (1956) and Lampe, Franklin and Field (1957). Both relations give results which are at variance with experimental data by a factor of up to five. Stafford (1966) using a theory due to Gryzinski (1959, 1965) calculated some 47 electron ionisation cross sections. Experimental and calculated data were found to be at variance by a factor of up to three, except for the alkali metal atoms where good agreement was found. This agreement is due to the relatively crude electronic shell hypothesis of Gryzinski, which is similar in concept to the Bohr theory. Lotz (1968, 1969, 1970) proposed an empirical formula for the calculation of electron

ionisation cross section of the elements for which he claimed an accuracy of better than +40% to -30%.

Several attempts have been made to calculate electron ionisation cross sections based upon quantum mechanical considerations. Although the success of these calculations has been encouraging, giving accurate values and also reproducing the irregularities at the threshold region due to auto ionisation, the calculations are extremely complex.

Relatively few absolute determinations of electron ionisation cross section have been made. Quantitative mass spectrometry has been used to obtain relative measurements and thus absolute values can be found by use of known standards. Such values are of doubtful accuracy; in general, the accuracy of electron ionisation cross sections is up to approximately $\pm$30%. However, it is not uncommon to have disagreement between different workers of up to $\pm$ 200%. In view of the complexity of the mechanism of ionisation by electron impact, it is probable that highly sensitive measurements are required in order to obtain reliable and consistent data.

The electron ionisation cross section of caesium has been investigated by several workers but only Tate and Smith (1934), McFarland and Kirney (1965) and Nygaard (1968) have made measurements at the electron energies of interest to this study, i.e. around 70 eV. The agreement of the three sets of data is good in view of the variety of techniques used.

The choice of a standard system for comparison with the caesium graphite system is complex. The major criteria required of a standard are a) that the pressure-temperature relation

must be accurately known and similar to that of caesium-graphite in the temperature range of interest; b) that the ionisation cross section must be known or be capable of calculation; and c) that the standard and cell material must be chemically compatible.

Reference to the vapour pressure of the elements, Nesmeyanov (1963), shows that the elements copper, gold, beryllium, lanthanum, chromium, iron and palladium have suitable ranges of vapour pressures (i.e. below 1.3 mN $m^{-2}$) in the temperature range of interest (up to 1470 K). However, the accuracy of these pressure-temperature relations varies considerably and it appears, Nesmeyanov (1963), that sufficiently accurate pressure-temperature data are available only for chromium, copper, gold and iron.

Experimental measurements have been made on only three of the four elements of interest, chromium being the exception. Iron has been the subject of only one experiment in which Cooper, Pressley and Stafford (1965) found the ratio of the ionisation cross sections of iron and silver at a single electron energy. The ionisation cross section of silver has been measured by Pavlov, Rakhovskii and Fedorova (1967) and Crawford and Wang (1967). However their results differ by a factor of two. Copper has been the subject of investigation by Pavlov, Rakhovskii and Fedorova (1967) and also Crawford (1967). Their results also differ by a factor of up to two. The ionisation cross section of gold has only been measured in the threshold region by Blais and Mann (1960).

It may be concluded from the limited experimental data available that errors in the ionisation cross sections are liable to reach a factor of two. It is this unfortunate lack of accuracy which is the

greatest source of error in quantitative work with mass spectrometers. However, in view of the complete lack of experimental values of ionisation cross sections for chromium, it would seem inadvisable to consider this element as a standard.

The chemical reactivity of the standard towards the cell material (molybdenum) is of obvious importance. The use of molybdenum cells in the determination of the vapour pressure of copper and gold provided no evidence, Nesmeyanov (1963), of reactivity between the sample and the cell. The chemical interaction of iron and molybdenum has been the subject of considerable work for obvious reasons. Although the diffusion of molybdenum in gamma iron has been evaluated, Fridberg et al. (1969), as $10^{-14}$ $m^2$ $s^{-1}$ at 1373 K, the adsorption of iron vapour by molybdenum is unknown and thus the use of iron as a standard seems inadvisable.

It may be concluded that no one element is clearly acceptable as a standard. The final choice must be left to experimental experience with the three elements copper, gold and iron.

## VII.3 The development of the Double Knudsen cell Mass Spectrometer apparatus

The Knudsen cell experiments were carried out in a stainless steel high vacuum chamber, fitted with six radially disposed ports (figure VII.2). Ion pumps were attached to two of these ports, and a two inch diffusion pump, backed by a rotary pump was connected to a third port via liquid nitrogen traps and isolating valves. The mass spectrometer, a $180^{\circ}$ magnetic deflection type (V.G. Micromass I) was attached to a fourth port and the two other ports were fitted with optical viewing ports. The lid to the chamber had three power

lead-throughs placed symmetrically in it, together with a port at the centre, through which the shutter operated and the thermocouple passed, via glass metal seals. The lid was sealed to the chamber by compression of a copper gasket between two knife edges.

A furnace was constructed from molybdenum wire (475 $\mu$m diameter, (18 thou)) straight wound on a Purox former (100 mm long by 15 mm diameter) which had grooves cut into it in order to locate the windings. The furnace was supported from the three power lead-throughs using stainless steel bar and rod so that the furnace's cylindrical axis could be adjusted in both the vertical and horizontal planes. Power was provided by a 4.2 KVA Variac transformer. A preliminary experiment showed that a temperature of at least 1370 K could be achieved with a background pressure of less than 133 $\mu$N $m^{-2}$, without the requirement of radiation shields.

A Double cell was constructed from molybdenum with approximate orifice dimensions of 0.5 mm diameter by 0.5 mm length at a distance of 6 mm apart. A sample of caesium-graphite at an unknown concentration was prepared by prior heating of caesium nitrate and graphite in an evacuated container and was loaded into one of the cells, the other cell being loaded with copper. Copper was chosen for the initial experiments since it had a relatively high vapour pressure at temperatures of interest. The initial experiments used a different arrangement of collimator and shutter and did not have the facility of earthing the Double cell. The results obtained showed that whilst the mass spectrometer resolved the beam components of copper and caesium (figure VII.3) the beam also caused a shift in the base line which almost obliterated the peak due to

caesium (figure VII.3 ). No relationship with temperature was found for either peak, but the base line shift was observed to increase with temperature, and was thus thought to be due to thermionic emission and/or thermal radiation effects from the cell.

An experiment was carried out to investigate this phenomenon, in which the Double cell was replaced by a piece of molybdenum which was connected to an electrical feed-through, so that electrical measurements could be made under operating conditions. Measurement of the potential of the piece of molybdenum with respect to earth using a digital voltmeter and oscilloscope showed a varying A.C. voltage, biased at a negative potential, neither of which was related to the voltage across the furnace windings. The A.C. component was observed to oscillate at 50 Hz indicating a coupling between the piece of molybdenum and the furnace windings. The D.C. current between the piece of molybdenum and earth, measured by an Avometer, increased non-linearly with furnace voltage (figure VII.4) in a manner characteristic of thermionic emission. Calculations based upon the Richardson Dushman equation, Pirani and Yarwood (1963), gave current values in the order of nanoamps. It was also observed that the current between the shutter and earth increased when the shutter was moved into the open position, i.e. a larger surface area of shutter exposed to the furnace windings, thus indicating a possible added contribution to the base line shift of the mass spectrometer. However, this problem was solved by earthing the cell which reduced the base line shift to a negligible level.

In a further experiment using a Double cell loaded with copper and iron, the presence of ions within the effusing beam from the

earthed Double cell was checked by modifying the mass spectrometer to operate without the ionisation source; however no signal was detected. It was observed that the signal due to iron and copper was time dependent (figure VII.5) and increased even before opening the shutter. A long decay of the signal was also observed after the shutter was closed. It was also noted that the background pressure rose during these measurements. It was therefore concluded that these effects were due to re-evaporation of copper and iron from surfaces by radiation from both the furnace and the filament of the mass spectrometer.

Modifications were made to the collimator design to overcome the re-evaporation problem due to radiation from the furnace windings. An oven was also constructed to allow the mass spectrometer to run at elevated temperatures (approximately 420 K) to reduce re-evaporation and outgassing effects due to the filament. A design modification was also made to the mass spectrometer ion repeller plate, since it effectively shielded the ionisation chamber from the effusing beam, by replacing it with a fine mesh. The new ion repeller was constructed from stainless steel mesh (mesh no.120, B.S. 410 (1962)) which had a 35% voidage. A simplified treatment of the electrostatic problem indicated that no significant perturbation to the electrostatic field would be caused by the use of mesh in place of the original plate. Although no ionic species in the effusing beam had been observed, an earthed fine grid was also placed in the effusing beam path in order to filter out any ionic species which might be present.

A further experiment using the Double cell was carried out with one cell loaded with magnesium. Magnesium was selected because its

vapour pressure temperature relationship enabled the apparatus to be tested at a lower temperature range (500 to 800 K) than would be possible with copper or iron, thus reducing problems of re-evaporation and outgassing. The three isotope peaks of magnesium were observed to show time-independent shutter effects, and thus a series of ion current values for the peak m/e value 24 against temperature was obtained. The results of the experiment (figure VII.6) show that a linear relation between log (IT) and I/T was obtained. The experimental heat of vaporisation calculated from the slope by the method of least mean squares is 145.1 kJ $mol^{-1}$ compared with a literature value, Nesmeyanov (1963), of 143.7 kJ $mol^{-1}$ with a standard deviation from the least mean square line of 1.7 and 0.4 respectively.

In the light of the encouraging result obtained with magnesium, a new Double cell was constructed with electron microscope aperture orifices of 200 $\mu$m diameter by 50 $\mu$m long at a distance of 7 mm apart and loaded with copper and silver. Ion current signals from both copper and silver were found to be barely detectable, even at high temperatures, and were also found to be time dependent. No relation between ion current and temperature was found for either copper or silver. It was concluded that the beam flux received by the mass spectrometer was reduced to barely detectable levels either by reduction of the effusing flux due to the small orifice area or misalignment of the cell mass spectrometer system. The time dependent increase in ion current observed was probably due to re-evaporation of copper and silver.

## VII.4 Summary

The Knudsen cell apparatus was shown to work successfully at temperatures up to 720 K using magnesium as a calibrating system, the minimum detectable pressure using a 0.5 mm diameter orifice was 26 $\mu$N $m^{-2}$. Severe difficulties were encountered in developing the equipment to operate at temperatures of interest in this project (900 to 1400 K); in particular problems of re-evaporation of effused species, thermionic emission, and alignment of cell and mass spectrometer were encountered. Added to these problems was the limited sensitivity of the mass spectrometer employed in this work. In view of these difficulties and the limited time available, work on the Knudsen cell experiments was terminated in favour of the microgravimetric- electron probe microanalysis work described in Chapters III to VI.

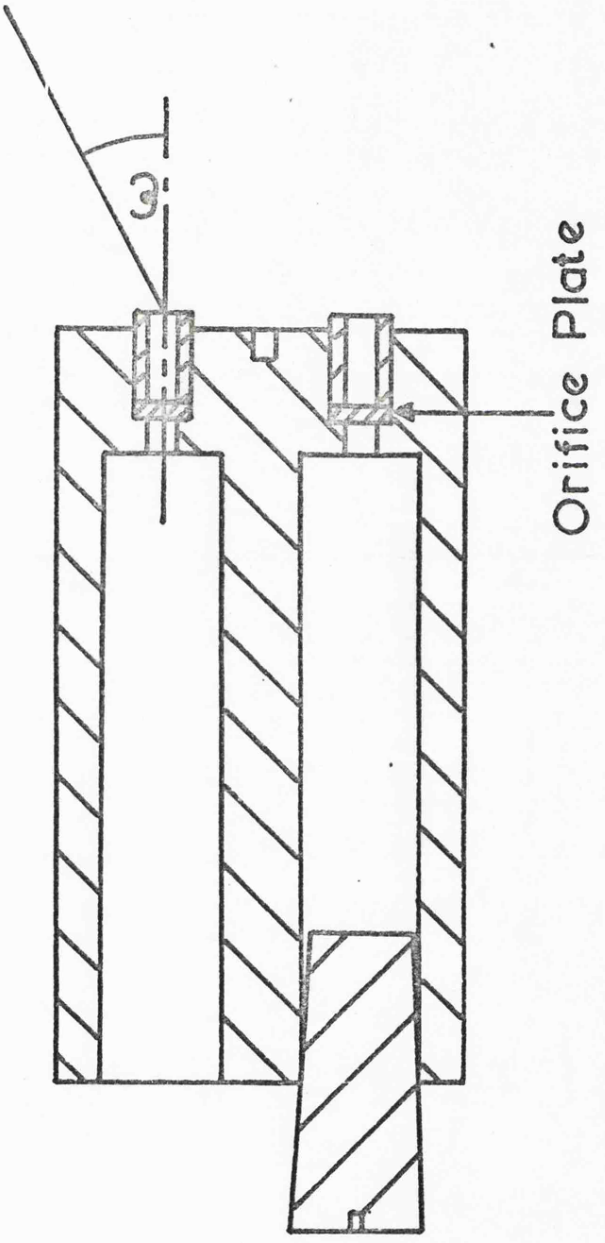


Figure VII.1 A Double Knudsen Cell

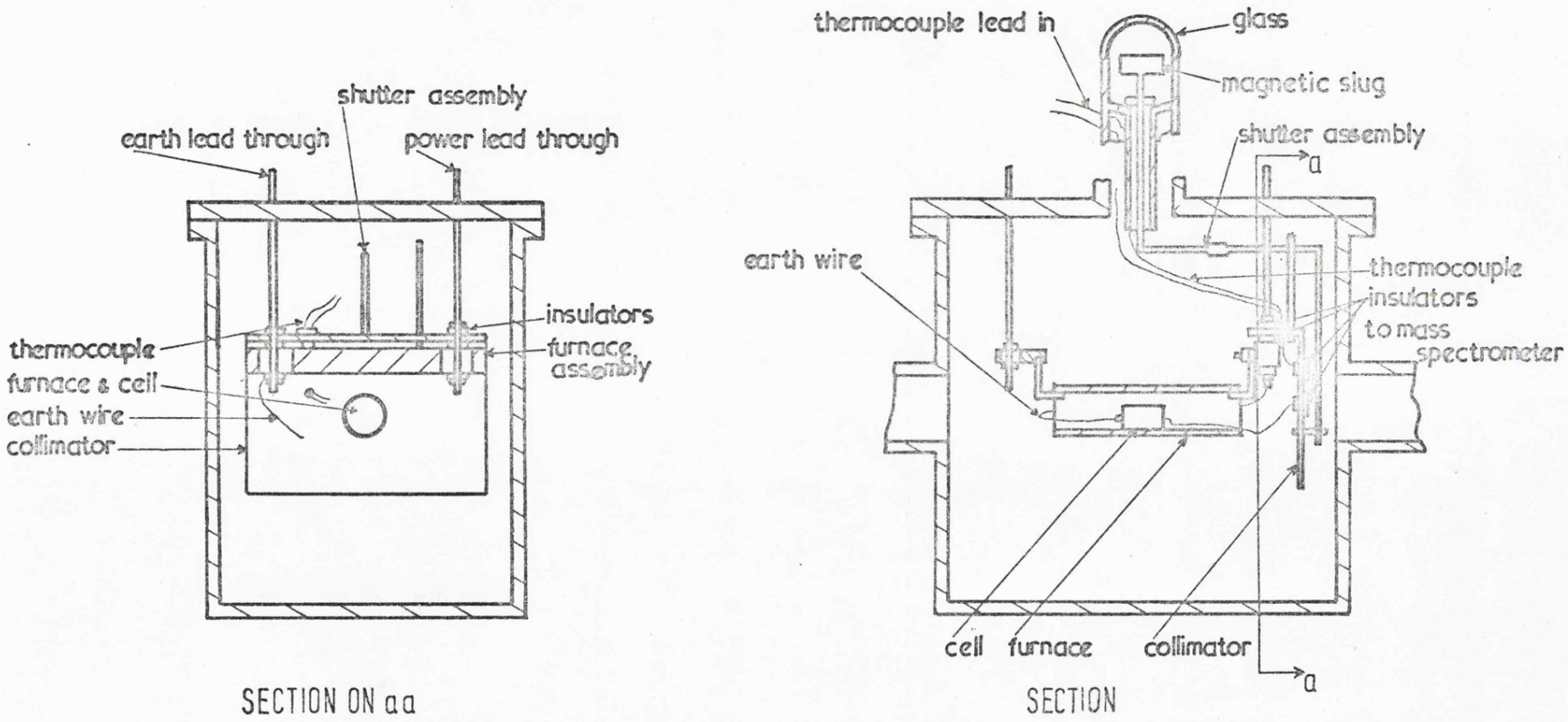


Figure VII.2 Sections through the Knudsen Cell apparatus

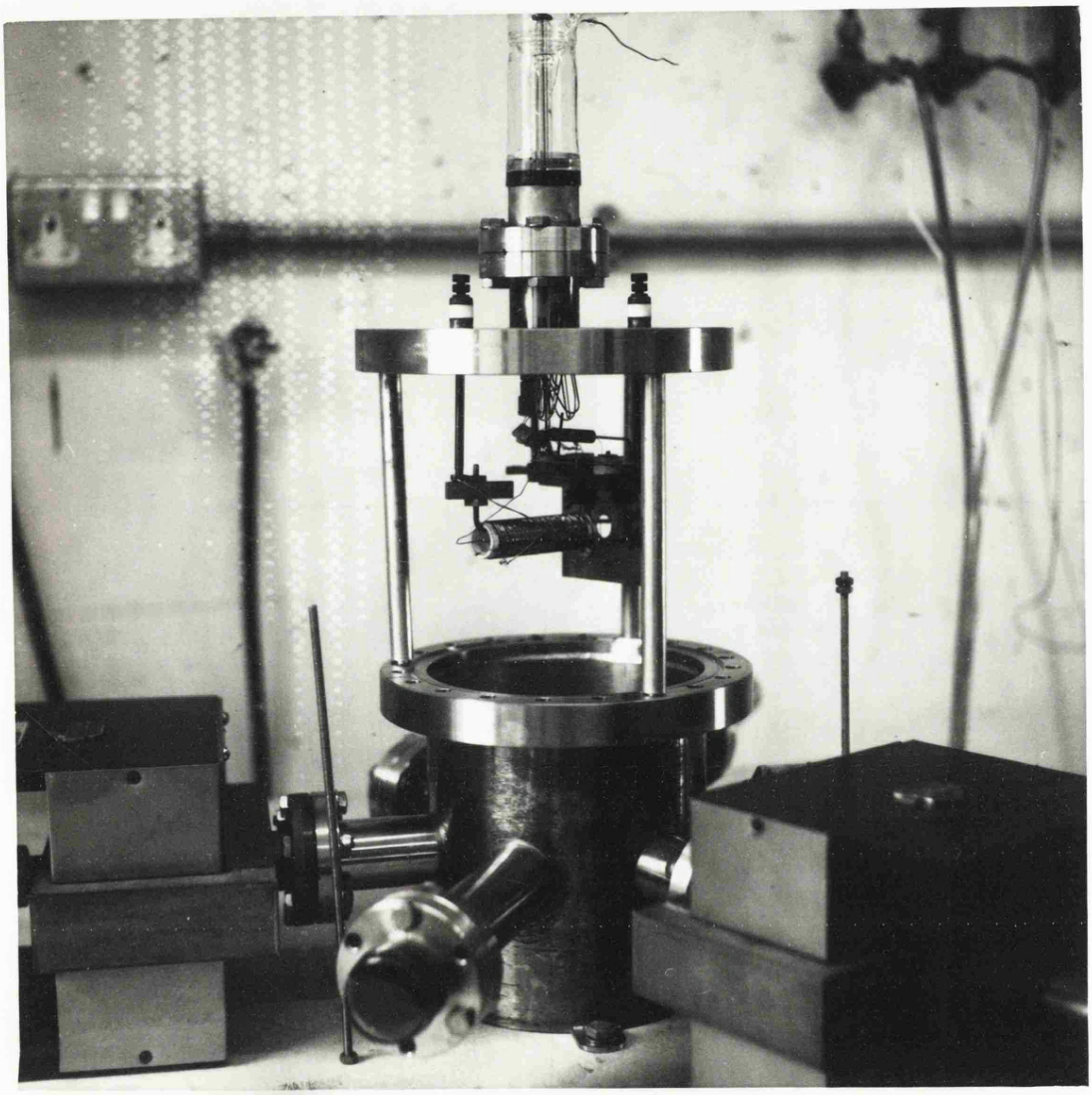

Figure VII.2 The Knudsen Cell Apparatus

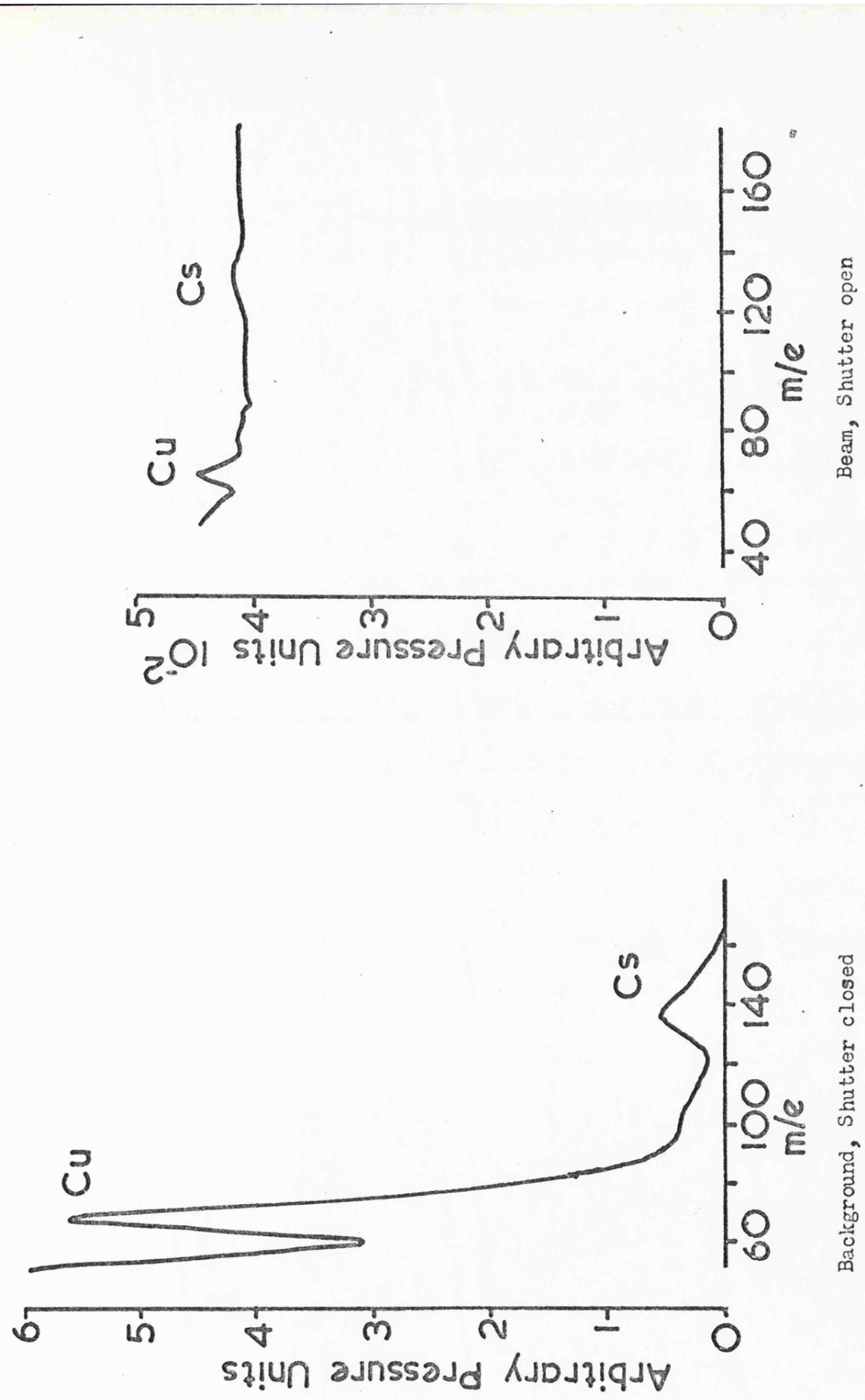


Figure VII.3 Mass Spectra of Copper and Caesium Effused from a cell at 1360 K

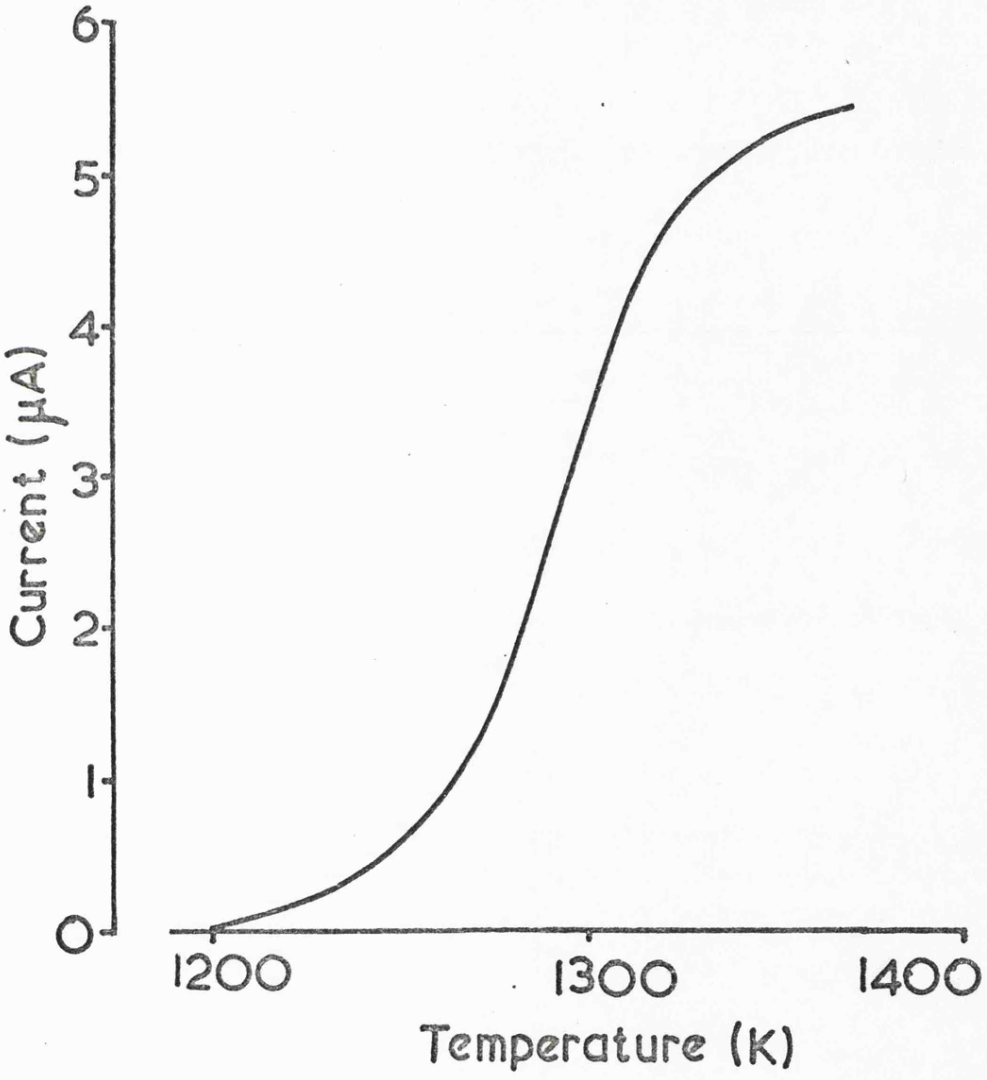


Figure VII.4 Plot of Cell to Earth Current against Temperature

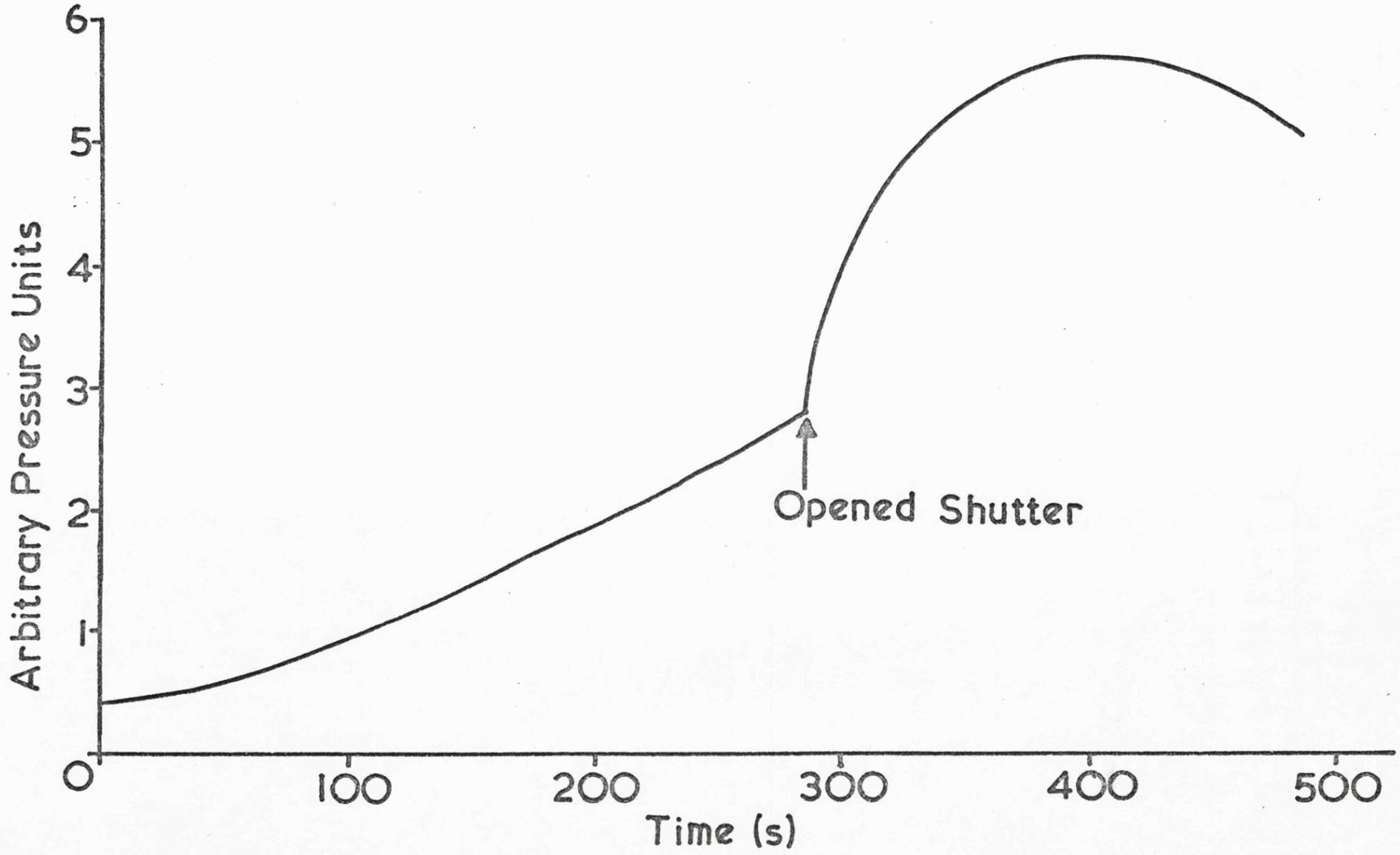


Figure VII.5 Time dependence of Mass Spectrometer signal of Copper

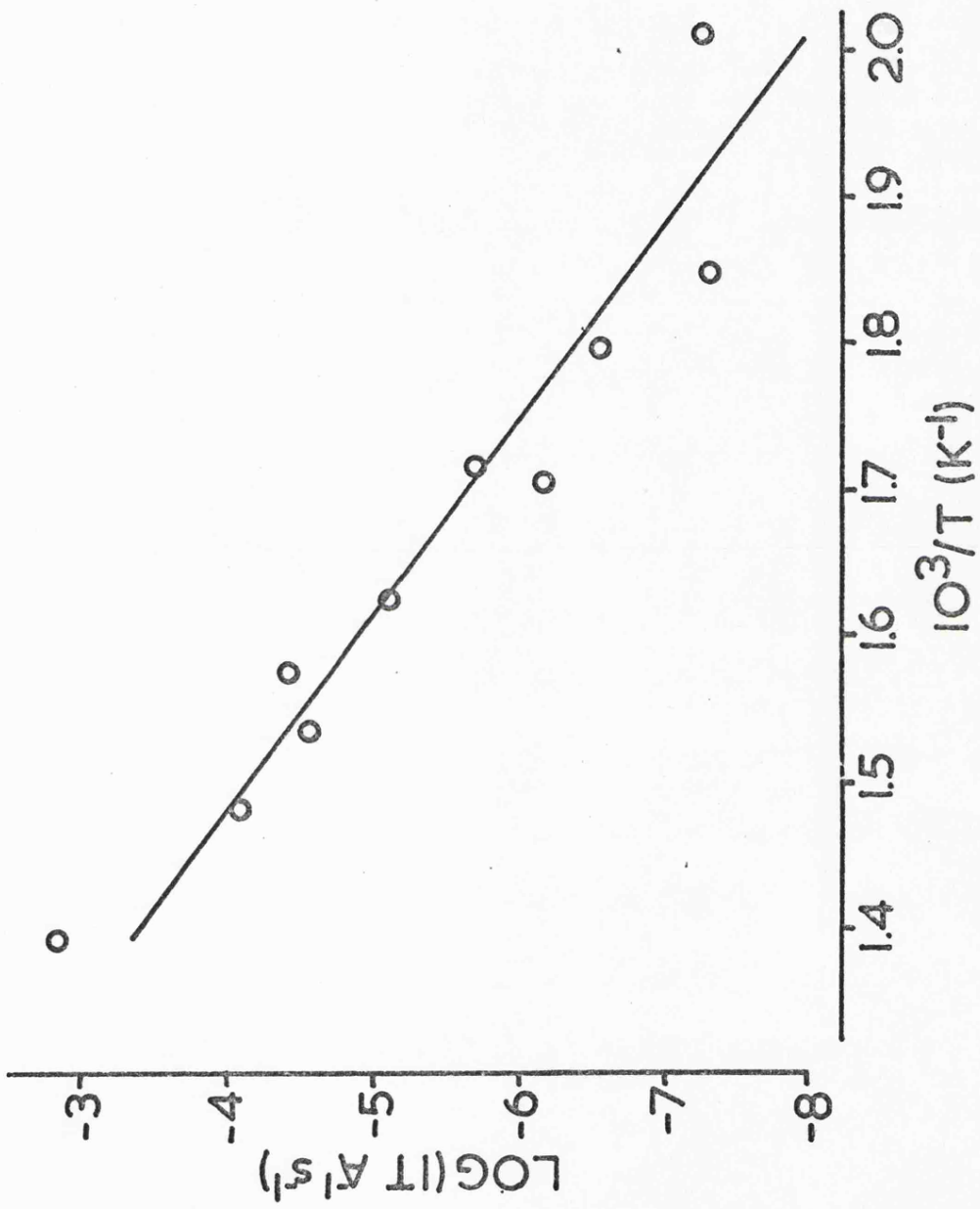


Figure VII.6 An Arrhenius plot according to Equation VII.15, to determine the Heat of Vaporisation of Magnesium

# CHAPTER VIII

## A SUMMARY AND SUGGESTIONS FOR FURTHER WORK

In this chapter a synopsis of the work described in this thesis together with the main conclusions are given. The chapter concludes with some suggestions for further work.

### VIII.1 Microgravimetric Studies

A microgravimetric apparatus was constructed to study sorption of caesium on graphites. Initial experiments revealed serious practical problems associated with the reactivity and transport of caesium. Extensive modifications to the apparatus were made which enabled sorption measurements to be carried out in the range 500 to 1370 K. A considerable amount of evidence was accumulated which showed that in the temperature range 970 to 1370 K desorption of caesium from graphite occurred under conditions of Langmuir free evaporation and thus enabled desorption rates to be analysed to yield diffusion coefficients.

Desorption curves obtained from a cylindrical specimen of caesium-gilsonite graphite at concentration levels between 1 and 9 mg $g^{-1}$ (Run 1) showed an initial fast desorption rate (figure III.4) which decreased relatively rapidly to a slower rate, in agreement with other workers, cf. Doyle (1953). An analysis on the latter part of the desorption curves, assuming that diffusion of caesium in graphite was rate controlling (equation III.2), gave diffusion coefficients (Table III.1) which were in moderate

agreement with other workers (figure III.6). However, the variation of diffusion coefficients from run to run indicated a more complex rate controlling process than had been assumed.

Electron probe microanalysis on a caesium-gilsonite graphite cylindrical specimen (Run 2) showed complete penetration of the caesium (figure III.7) at the heat treatment temperature (570 K) contrary to that expected from extrapolation of the Arrhenius plot for diffusion coefficients in the range 970 to 1370 K.

As a consequence, a series of experiments were performed to obtain caesium concentration profiles by electron probe microanalysis, at various stages in an adsorption, heat treatment and desorption programme on spherical specimens of gilsonite graphite at concentration levels of between 43 and 16 mg $g^{-1}$ (Runs 3 to 9, figure IV.5, Table IV.1). Diffusion coefficients were calculated from the latter part of desorption curves by a similar technique to that used on the cylindrical specimens (equation IV.1, Table IV.1). The results obtained were in poor agreement with other workers (figure IV.2) and the Arrhenius plots for the diffusion coefficients exhibited a curious 'turn over', indicative of a change in the rate controlling mechanism. The concentration profiles obtained by electron probe microanalysis showed an apparent violation of Fick's laws of diffusion, since desorption of caesium from the graphite appeared to occur against a rising caesium concentration profile in some cases. These results suggested that a two part diffusion mechanism occurred, being composed of a fast diffusion mechanism which predominates at low temperatures and a slow diffusion mechanism which predominates at long times and high temperatures.

Evidence for the formation of caesium-graphite intercalation compounds was sought by X-ray analysis. A decrease in peak intensities (figure IV.6) was shown to be due to X-ray adsorption by caesium, and it was concluded that no compound formation occurred.

An experiment (Run 10) was carried out to obtain desorption rates at various temperatures under conditions in which the slow diffusion mechanism controlled the desorption rate (Table V.1).

Two similar experiments were carried out on a fine grain graphite (Runs 11 and 12) and the results showed moderately different characteristics to the gilsonite graphite. The initial fast desorption stage evolved more caesium than had been observed in experiments on the gilsonite graphite (figure V.4 and 1) but the diffusion coefficients obtained from the subsequent slow desorption were of similar magnitude (figure V.7, Table V.3). The 'turn over' in the Arrhenius plot of the diffusion coefficients (figure V.7) was also apparent for the fine grain graphite.

The methods of analysis of the desorption data were critically analysed and the use of equations III.2 and IV.1 was shown to be in error. An alternative (quadratic equation) method for analysis was presented (Chapter V.3) and shown to be reasonably accurate. A third numerical method which was more precise, although more laborious than the quadratic equation method, was also used to calculate the diffusion coefficients (Table V.3). Comparison of the results from all three methods of analysis showed that the relatively simple quadratic equation method was sufficiently accurate.

The effect of non-uniform concentration profiles on the desorption rate was investigated, (Chapter VI.1) and it was shown that diffusion coefficients calculated assuming a non-uniform concentration profile (figure VI.1) differed little from diffusion coefficients calculated assuming a uniform concentration profile (figure VI.3). As further evidence for a two-part diffusion process it was shown that a single diffusion mechanism could not account for the concentration profiles observed during desorption (figure VI.2).

The effect of an evaporation step on the desorption rate was also investigated (Chapter VI.2, figure VI.4). A theoretically derived relationship based upon adsorption obeying Henry's Law, showed that the surface concentrations observed by electron probe microanalysis could be accounted for, by mixed evaporation /diffusion control, and that such a system was in reasonable agreement with previously reported work.

A qualitative analysis of two phase diffusion was presented which offered an explanation for apparent 'non-Fickian' diffusion. The desorption curves and concentration profiles for caesium were explained in terms of a graphite structure comprising a low diffusivity material permeated by high diffusivity paths. It was suggested that the high diffusivity mechanism was associated with surface diffusion along voids and macro- and meso-pores. The low diffusivity mechanism was considered to be diffusion along micro-pores, disordered carbons and poorly orientated lamellae.

It was concluded that the diffusion of caesium in nuclear

graphites is essentially a two phase process leading to mixed control of desorption. The general lack of agreement of the diffusion coefficients obtained in successive experiments and between various workers most probably reflects varying contributions to diffusion by fast and slow transport mechanisms. The degree of mixed control appears to depend upon the thermal history of the specimen and the structure of the graphite. Also, as can be seen from figure V.7, the perturbation of the diffusion coefficients due to these factors is relatively small since all the data for both gilsonite and fine grain graphites can be encompassed with a band which does not exceed an order of magnitude at any given temperature.

## VIII.2 Knudsen cell Studies

A Knudsen cell-mass spectrometer apparatus was developed to attempt to measure equilibrium vapour pressures on caesium-graphite systems. The apparatus included a shutter and collimator to reduce the contamination of the mass spectrometer, and a double Knudsen cell, in order to avoid contamination of the caesium-graphite system by the standard material and to reduce realignment errors. An experiment using copper and iron to test the double cell showed that re-evaporation of these metals occured during measurements causing serious errors.

A major redesign was carried out improving the suspension system for the furnace and Knudsen cell, collimator and shutter, and included the provision of a thermocouple to measure the temperature of the front face of the cell. The mass spectrometer

was also modified to improve the ionisation efficiency. Another experiment using magnesium in the temperature range 500 to 800 K gave a value for the heat of vaporisation in good agreement with published work. Further problems due to re-evaporation were encountered when attempting to extend measurements to the temperature range of interest (up to 1370 K) and no further work was done on the apparatus due to lack of time.

## VIII.3 Suggestions for further work

The microgravimetric technique developed in this work to study rates of desorption from a system, combined with a method for determining diffusant concentration profiles, such as electron probe microanalysis, provides a simple technique for studying mixed multi component diffusion and evaporation systems. Two areas for further work using the apparatus can be readily identified, being the extension of work on the caesium-graphite system and the study of other evaporation/diffusion systems. One major advantage of the microgravimetric technique is that the preparation of and desorption from the system is carried out under a vacuum and hence, problems of reactivity of the system are avoided. Work on the caesium-graphite system may be extended in several directions. The sensitivity of the microgravimetric apparatus could be significantly increased by using a microbalance with a larger capacity. Commercially available microbalances would give up to a fifty fold increase in sensitivity, thus allowing a reduction in concentration levels to sub milligram per gram or, in diffusion coefficients to approximately $10^{-15}$ $m^2$ $s^{-1}$. Higher specimen temperatures could also be achieved, up to at least 1800 K using platinum wire wound

furnaces and 'purox' furnace tubes. However, the use of induction heating is not possible with most commercial microbalances due to interference by the electromagnetic field. The use of lasers or arc image furnaces to achieve temperatures in excess of 1800 K is worthy of investigation. An extension of the method of analysis to include a two phase diffusion model with surface evaporation to predict both desorption curves and concentration profiles would achieve an accurate description of the diffusing system. However, such an analysis would require the postulation of a basic model and extensive computation. Having such facilities and the resources to carry out an investigation over a wide range of graphites, the relationship of structure and diffusion mechanisms may be elucidated. The extension of the microgravimetric technique to lower temperatures, whilst requiring careful assessment of the condition of Langmuir free evaporation, will give further information on the fast diffusion mechanism.

The use of the microgravimetric apparatus with systems other than caesium-graphite is virtually unlimited. The advantages of the apparatus in dealing with reactive systems, coupled with a variety of methods of analysis of desorption data, allow a rapid assessment of the rate controlling mechanism of either evaporation, diffusion or mixed control. The preparation of samples need not however be confined to within the apparatus. For instance, the silver-graphite system, being another fission product of current interest, Nabielek et al. (1973), would be best prepared externally, although it is eminently suitable for study in the microgravimetric apparatus.

The Knudsen cell method is one of the most suitable techniques

for studying caesium-graphite equilibria and has potentialities in exploring the behaviour of highly dilute caesium-graphites under conditions where the mass loss by effusion significantly reduces the residual concentration. Such a study may throw some light on the adsorption/desorption phenomenon and upon diffusion of caesium in graphite. It is however considered that further work on the present design of the Knudsen cell-mass spectrometer system for work on caesium-graphites in the temperature range 970 to 1370 K is inadvisable. This is due to the problems of re-evaporation and the limited sensitivity of the spectrometer. If the mass spectrometer technique were to be retained as the analytical method, then better results may be obtained using a suitable quadrupole mass spectrometer; such spectrometers have become readily available since the inception of this work. However, if the Knudsen cell method is to be used for further work, an alternative analytical technique should be considered due to the inherent limitations imposed on mass spectrometry by an inadequate knowledge of electron ionisation cross sections (Chapter VII.2). A significant increase in sensitivity over the mass spectrometric technique can be achieved using a radioactive tracer/target condensation method, Nesmeyanov (1963).

In conclusion, although the work reported in this thesis is of technological origin, a number of problems of an academic nature have been identified in the course of the work. In particular, the complex nature of diffusion of caesium in graphite has been clearly revealed. It is certain that there are many solid state diffusion systems which exhibit similar properties and therefore there is a need for a general analysis of multicomponent diffusion.

A start has been made on such an analysis in this thesis but a great deal more work needs to be done before a complete understanding is achieved.

## REFERENCES


Anderson, E.E. Wessmann, G.L. and Zumwalt, L.R. , Nucl. Sci. Eng. , 12, 106 - 10, 1962.

Asher, R.C. and Wilson, S.A. , Nature , 181, 409 - 10, 1958.

Bacon, G.E. , Acta Cryst. , 4, 558 - 61, 1951.

Bacon, R. and Sprague, R. , Conf. "Direct Observations of Imperfections in Crystals" , St. Louis, Missouri , Ed. Newkirk, J.B. and Wernick, J.H. , Interscience, New York , p 357 - 74, 1961.

Blais, N.C. and Mann, J.B. , J. Chem. Phys. , 33, 100 - 15, 1960.

Br. Stand. , B.S. 410, Fine Mesh Series , 1962.

Bromley, J. , Prog. nucl. Energy , Series 4, 5, 173 - 220 , Pergamon Press, Oxford , 1962.

Bromley, J. and Large, N.R. , "Proc. 5th Conf. on Carbon" , Pennsylvania , p 365 - 76, 1962.

Bromley, J. , AERE Harwell Internal Report R. Chem. R.C./P.111 , "Caesium-graphite compatibility" , 1963.

Bromley, J. Moul, A.N. and Paddon, A.R. , AERE Harwell R4337 , 1963

Bromley, J. , J. Brit. Nucl. Energy Soc. , 3, 99 - 105, 1964.

Bromley, J. and Moul, A.N. , AERE Harwell Internal Report M1295 , 1964.

Bromley, J. , Private communication , 1973.

Bryant, E.A. Cowan, G.A. Sattizahn, J.E. and Wolfsberg, K. , Nucl. Sci. Eng. , 15, 288 - 95, 1963.

Carslaw, H.S. and Jaegar, J.C. , "Conduction of heat in solids" , Oxford University Press, London , 1973.

Clausing, P. , Ann. Physik , 12, 961 - 89, 1932.

Cooper Jr., J.L. Pressley Jr., G.A. and Stafford, F.E. , J. Chem. Phys. , 44, 3946 - 49, 1965.

Cowan, G.A. and Orth, C.J. , "Proc. 2nd Int. Conf. Peaceful Uses Atomic Energy" , Geneva , 7, Paper 613, p 328 - 34, 1958.

Crank, J. , "The Mathematics of Diffusion" , Oxford University Press, London , 1967.

Crawford, C.K. , U.S. Air Force Materials Laboratory Report AFML - TR - 67 - 376 , Wright-Patterson A.F.B., Ohio , 1967.

Crawford, C.K. and Wang, K.I. , J. Chem. Phys. , 47, 4667 - 69, 1967.

Croft, R.C. , Quart. Revs. (London) , 14, 1 - 15, 1960.

De Beni, G.F. Gautsch, O. and Wahl, H. , Euratom Report EUR-4549e , Ispra, Italy , 1970.

Doyle, C.B. , North American Aviation Inc. Report NAA - SR - 255 , 1953.

Everett, D.H. , Proc. Chem. Soc. , 38 - 53, 1957.

Faircloth, R.L. Pummery, F.C.W. and Rolls, B.A. , symposium on Thermodynamics , Vienna , IAEA , 1966.

Faircloth, R.L. and Flowers, R.H. , Private communication , 1970.

Findlay, J.R. and Laing, T.F. , J. Nucl. Mater. , 7, 182 - 91, 1962.

Fisher, J.C. , J. App. Phys. , 22, 74 - 77, 1951.

Flowers, R.H. Sayers, J.B. and Price, M.S.T. , "Colloquium on Safety aspects of High Temperature Reactor Systems" , OECD, Paris , Paper 16, Dragon Project Report D.P. 789 , 1972.

Frankenburg, W.G. , J. Am. Chem. Soc. , 66, 1827 - 38 ; 66, 1838 - 47, 1944.

Fredenhagen, K. and Cadenback, G. , Z. anorg. allgem. Chem. , 158, 249 - 63, 1926.

Fredenhagen, K. and Suck, H. , ibid. , 178, 353 - 65, 1929.

Fridberg, J. Torndahl, L.E. and Hillert, M. , Jernkontorets Ann. , 153, 263 - 76, 1969.

Gethard, P.F. and Zumwalt, L.R. , U.S. At. Energy Comm. Report GA - 7478 , 1966.

Glueckauf, E. , Trans. Faraday Soc. , 49, 1066 - 79, 1953.

Graham, L.W. , Dragon Project Report D.P. 719, part 4 , 1970.

Gryzinski, M. , Phys. Rev. , 115, 374 - 83, 1959 ; ibid. , 138 A, 305 - 58, 1965.

Haire, M.J. and Zumwalt, L.R. , Nucl. Sci. Eng. , 50, 91 - 97, 1973.

Hérold, A. , Compt. rend. , 232, 838 - 39, 1951.

Hérold, A. , Bull. soc. chim. France , 187, 999 - 1012, 1955.

Hérold, A. Collin, M. Daumas, N. Diebold, R. and Saehr, D. , Chem. Soc. (London) Spec. Pub. No. 22 , p 309 - 16 , 1967.

Hennig, G.R. , Prog. inorg. Chem. , I, 125 - 205 , Interscience Publishers Inc., New York , 1959.

Hick, H. , Private Communication , 1973.

Iwamoto, K. and Oishi, J. , J. Nucl. Mater. , 29, 285 - 301, 1969.

Jost, W. , "Diffusion in solids, liquids, gases" , Academic Press Inc., New York , 1960.

Lampe, F.W. Franklin, J.L. and Field, F.H. , J. Am. Chem. Soc. , 79, 6129 - 32, 1957.

Lotz, W. , Z. Phys. , 216, 241 - 47, 1968 ; ibid. , 220, 466 - 72, 1969 ; ibid. , 232, 161 - 67, 1970.

McFarland, R.H. and Kinney, J.D. , Phys. Rev. , 137 A, 1058 - 61, 1965.

Marton, L. , "Electron Probe Microanalysis" , Ed. Tousimis, A.J. and Marton, L. , Academic Press Inc., New York , 1969.

Merz, E. , Nukleonik , 11, 38 - 44, 1968.

Merz, E. and Scharf, H. , Atomkernenergie , 17, 287 - 92, 1971.

Milstead, C.E. , Carbon , 7, 199 - 200, 1969.

Milstead, C.E. Riedinger, A.B. and Zumwalt, L.R. , Carbon , 4, 99 - 106, 1966.

Nabielek, H. Hick, H. Wagner-Löffler, M. and Voice, E.H. , Dragon Project Report D.P. 828 , 1973.

Nesmeyanov, An. N. , "Vapour Pressure of the Elements" , Infosearch Ltd., London , 1963.

Novikov, Yu. N. and Vol'pin, M.E. , Russ. chem. Revs. , 40, 733 - 46, 1971.

Nygaard, K.J. , J. Chem. Phys. , 49, 1995 - 2002, 1968.

Otvos, J.W. and Stevenson, D.P. , J. Am. Chem. Soc. , 78, 546 - 51, 1956.

Parry, G.S. , "3rd. Conf. on Ind. Carbons Graphites" , London , p 58 - 61 , 1971.

Pavlov, S.I. Rakhovskii, V.I. and Fedorova, G.M. , Zh. Eksp. Teor. Fiz. , 52, 21 - 28, 1967.

Pirani, M. and Yarwood, J. , "Principles of Vacuum Engineering" , Chapman and Hall, London , 1963.

Riedinger, A.B. Milstead, C.E. and Zumwalt, L.R. , "Proc. 5th Conf. on Carbon" , Pennsylvania , p 405 - 10, 1962.

Rowland, P.R. , Private communication , 1972.

Rüdorff, W. , Adv. inorg. Chem. Radiochem , 1, 223 - 66 , Academic Press Inc., New York , 1959.

Rüdorff, W. and Schulze, E. , Z. anorg. allgem. Chem. , 277, 156 - 71, 1954.

Ruth, V. and Hirth, J.P. , "Int. Symp. Condensation Evaporation of Solids" , Ohio , p 99 - 126 , Gorden and Breach, New York , 1964.

Salzano, F.J. and Aronson, S. , J. Inorg. Nucl. Chem. , 26, 1456 -

58, 1964.

Salzano, F.J. and Aronson, S. , J. Chem. Phys. , 42, 1323 - 30, 1965 (a).

Salzano, F.J. and Aronson, S. , ibid. , 43, 149 - 54, 1965 (b).

Salzano, F.J. and Aronson, S. , ibid. , 45, 4551 - 55, 1966 (a).

Salzano, F.J. and Aronson, S. , ibid. , 45, 2221 - 27, 1966 (b).

Salzano, F.J. and Aronson, S. , ibid. , 44, 4320 - 26, 1966 (c).

Salzano, F.J. and Aronson, S. , ibid. , 47, 2978 - 81, 1967 (a).

Salzano, F.J. and Aronson, S. , Nucl. Sci. Eng. , 28, 51 - 54, 1967 (b).

Salzano, F.j. and Eshaya, A.E. , Brookhaven National Laboratory Report BNL 633 , 1960.

Schleede, A. and Wellmann, M. , Z. physik. Chem. , B 18, 1 - 28, 1932.

Smith, C.A. and Young, C.T. , North American Aviation Inc. Report NAA - SR - 232 , 1953.

Smith, C.A. and Young, C.T. , ibid. NAA - SR - 72 , 1957.

Stafford, F.E. , J. Chem. Phys. , 45, 859 - 62, 1966.

Tate, J.T. and Smith, P.T. , Phys. Rev. , 46, 773 - 76, 1934.

Trofiniov, A.M. Smirnov, V.A. and Tetervin, G.K. , Radiokhimiya , 15, 241 - 44, 1973.

Van Orstrand, C.E. , Geophysics , 5, 57 - 59, 1940.

Whipple, R.T.P. , Phil. Mag. , 45, 1225 - 36, 1954.

Yates, M.K. and Fitzpatrick, G.O. , Gulf General Atomic Inc. Report No. GA - 8574 , 1968.

Young, C.T. , North American Aviation Inc. Report NAA - SR - 247 , 1953.

Zumwalt, L.R. , Trans. Am. nucl. Soc. , 13, 566 - 68, 1970.

# APPENDIX I

## THE CHARACTER OF THE GRAPHITES

The two graphites used in this study exhibit contrasting properties which arise from their different origins. The gilsonite graphite is based upon the naturally occurring gilsonite carbon particles which are made up of spherically orientated graphitic crystallites. The fine grain graphite, however, is manufactured from crushed petroleum coke. Both forms of graphite have been subjected to a bonding process using pitch and carbonisation and further pitch impregnation, graphitisation and purification.

The petroleum graphitic coke is crushed to produce particles of the order of 40 μm size, which are then subjected to a resin bonding process and carbonisation at approximately 1900 K to produce the fine grain graphite. The crushing/bonding process is necessary in the manufacture of the fuel tubes of the Dragon reactor, which are produced by resin bonding a mixture of fuel microspheres and petroleum coke particles, followed by carbonisation. Hence the purity of the fine grain graphite is less than that of the gilsonite graphite with respect to hydrogen and oxygen, because of the difference in final heat treatment temperatures. Spectrographic analysis of the gilsonite graphite reveals a total impurity level of 33 p.p.m. of which silicon is the most abundant at 25 p.p.m., a similar impurity level for the fine grain graphite is expected, although it has not been measured. The hydrogen oxygen impurity level is reflected in the more extreme pre heat treatment required for the fine grain graphite in order to achieve stability within

the microgravimetric apparatus.

The microfeatures of the two graphites reflect their different origins; the fine grain graphite exhibits a smaller grain size than the gilsonite graphite (figure A.1). The spherical nature of the gilsonite particles is reflected in the circular nature of the massive pores visible in the polished specimen. The high magnification scanning electron micrographs of the fractured surfaces reveal the dramatic differences in the grist employed in the two graphites, that of the fine grain graphite being composed of flat layers whilst that of the gilsonite graphite is comparatively massive. The scanning electron micrographs of the polished specimens reveal differences in pore structure, the gilsonite graphite containing relatively large pores, or more correctly voids, which are not found in the fine grain graphite. A difference in porosity is also revealed by the measured densities of the two graphites (Table A.1). The closed porosity of gilsonite graphite is approximately twice that of the fine grain graphite, whilst the open porosity of the gilsonite graphite is only half that of the fine grain graphite. Thus one may conclude that the pore size of the gilsonite graphite is large compared to the fine grain graphite, but the surface pores in the fine grain graphite penetrate further into the specimen.

X-ray analysis of the two graphites gives apparent interlayer distances of 341.1 pm and 335.8 pm for the gilsonite and fine grain graphites respectively. Using Bacon's (1951) relationship between apparent interlayer distance and the degree of disorder, the proportion of disoriented layers in gilsonite and fine grain graphites is 0.8 and 0.17 respectively, that is, the fine grain

graphite is better ordered. This is also suggested by the high magnification scanning electron micrograph of the fracture surface of the fine grain graphite.

Table A.1

Some physical properties of the Two Graphites

| | Gilsonite Graphite | Fine Grain Graphite |
|---|---|---|
| Bulk Density ($mg\ mm^{-3}$) | 1.76 ± 0.02 | 1.51 ± 0.01 |
| Apparent Solid Density ($mg\ mm^{-3}$) | 2.03 ± 0.02 | 2.09 ± 0.01 |
| Apparent Open Porosity (%) | 13.4 ± 0.3 | 27.7 ± 0.3 |
| Closed Porosity* (%) | 9.1 ± 0.5 | 5.4 ± 0.5 |

Determined using methanol as the immersion fluid

* Using true density value 2.265 $mg\ mm^{-3}$

Polished
Gilsonite
x 87

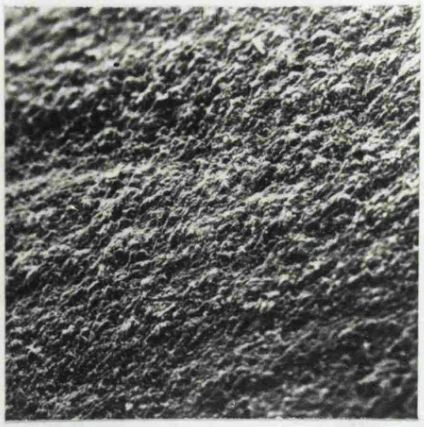

Polished
Fine Grain
x 910

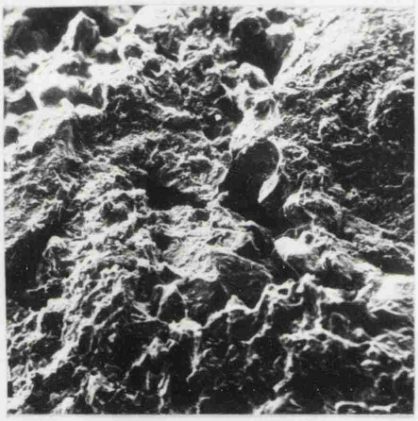

Fractured Surface
Gilsonite
x 51

Fractured Surface
Fine Grain
x 47

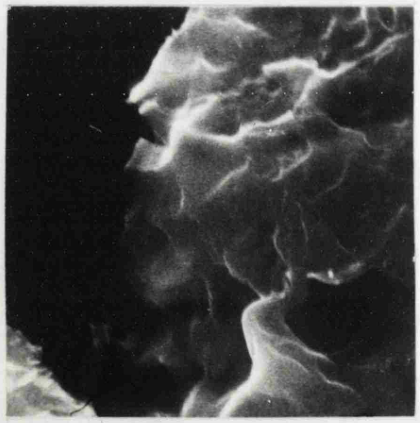

Fractured Surface
Gilsonite
x 5100

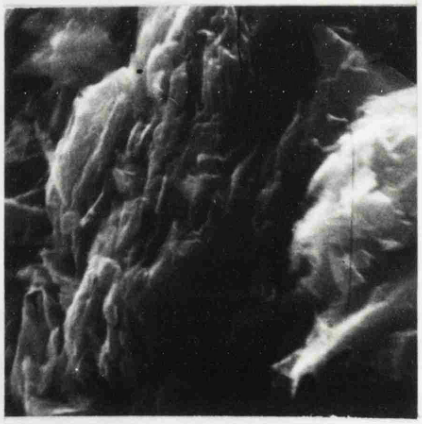

Fractured Surface
Fine Grain
x 4700

Figure A.I Microsurface Features of Polished and Fractured Surfaces of Gilsonite and Fine Grain Graphites by Scanning Electron Microscopy

## APPENDIX II

### THE EFFECT OF SPECULAR AND DIFFUSE REFLECTION UPON DESORPTION RATES

A perfect sphere representing the graphite sample, centred on the cylindrical axis of a cylinder which represents the fused silica walls of the furnace tube (figure A II(i)) is assumed for this treatment. It is further assumed that the temperature and hence the wall characteristics of the furnace tube are uniform over the length of interest, y′. The effect of gas phase collisions is neglected (cf. Chapter III.3) as is the effect of diffusely reflected atoms which undergo two or more wall collisions before returning to the sphere. Specularly reflected atoms which collide with the sphere can only have undergone one wall collision.

I. Diffuse Reflection

A flux F atoms $s^{-1}$ of even hemispherical distribution is assumed to be emitted from an elemental area $dS_1$ associated with a point D on the surface of the sphere (figure A II(i)). The fraction of F leaving point D and passing through the elemental area $dS_2$ associated with point C on the surface of the cylinder is therefore

$$\frac{F\, dS_2}{2\pi [DC]^2} \qquad \text{A II.1}$$

However

$$[DC]^2 = [OC]^2 + [OD]^2 - 2[OC][OD]\cos\theta \qquad \text{A II.2}$$

Thus the total fraction of flux that passes through $dS_2$ from

the arc $\overline{[BADE]}$ is

$$2FdS_2 \int_0^{\phi} \frac{d\theta}{2\pi\{x^2 + y^2 + r^2 - 2r(x^2 + y^2)^{\frac{1}{2}} \cos\theta\}} \qquad \text{A II.3}$$

where

$$\cos\phi = r/(x^2 + y^2)^{\frac{1}{2}} \qquad \text{A II.4}$$

Let the integral A II.3 be denoted by $2FdS_2 f(\theta)$. Hence the total fraction of flux emitted from the sphere which passes through $dS_2$ is

$$\pi(f(\theta))^2 FdS_2 \qquad \text{A II.5}$$

If the flux that passes through $dS_2$ is diffusely reflected at point C, the fraction which recollides with the sphere is given by

$$2\pi\left(1 - \cos(B\hat{C}O)\right)/2 \qquad \text{A II.6}$$

where

$$\cos(B\hat{C}O) = \{(x^2 + y^2 - r^2)/(x^2 + y^2)\}^{\frac{1}{2}} \qquad \text{A II.7}$$

i.e. the solid angle prescribed by the angle $B\hat{C}E$. Thus the fraction of flux desorbing from the sphere, diffusely reflecting at C and recolliding with the sphere is

$$\left(1 - \{(x^2 + y^2 - r^2)/(x^2 + y^2)\}^{\frac{1}{2}}\right)\pi F\left(f(\theta)\right)^2 dS_2 \qquad \text{A II.8}$$

and hence the total fraction of flux which returns to the sphere is

$$\frac{2}{4\pi r^2 F} \int_0^{2\pi xy'} \left(1 - \{(x^2 + y^2 - r^2)/(x^2 + y^2)\}^{\frac{1}{2}}\right)\pi F\left(f(\theta)\right)^2 dS_2 \qquad \text{A II.9}$$

i.e. the surface integral over a cylinder of length $2y'$ and radius x.

Since

$$dS_2 = 2\pi x dy \qquad \text{A II.10}$$

the term A II.9 transforms to

$$\frac{\pi x}{r^2} \int_0^{y'} \left(1 - \{(x^2 + y^2 - r^2)/(x^2 + y^2)\}^{\frac{1}{2}}\right)\left(f(\theta)\right)^2 dy \qquad \text{A II.11}$$

The integral $f(\theta)$ is soluble, but the resultant integral A II.11 is not. However, using Simpson's integration formula with a value of $y'$ of 190 mm and increasing y in 1 mm steps, the integral was computed to give the percentage flux returning after only one wall collision as 0.31%.

II. Specular Reflection

Consider the effect of approximating the sphere to a cylinder of length 2r and radius r. The volume occupied, and hence the flux intercepted by the cylinder wall, will be greater than that for the sphere. The approximation produces two cylinders whose surfaces are parallel, and thus the system may be considered as two parallel planes (figure A II (ii)). Furthermore the reflected flux intercepted by the inner cylinder may be represented by a mirror system and hence the imaginary image of the inner cylinder may be used to facilitate the calculation (figure A II (ii)).

The inner cylinder surface represents a plane of length 2r and width $2\pi r$, whereas the image is only of width $\pi r$, since only half the cylinder is seen on reflection. The distance z is the difference between the the radii of the inner and outer cylinder, i.e. x - r. The fraction of flux emitted from [N] which returns, is therefore the ratio of the solid angle represented by the pyramid

[N J K L M] to a hemisphere of radius [N J]. To simplify the calculation, the point N is taken as the mid-point H ; as H will receive the highest fraction of specularly reflected atoms the simplification is conservative. Simple trigonometric calculation, assuming r is 4 mm and x is 15 mm, gives the ratio as 3.1%. Since the approximations are conservative, the true percentage of atoms returning to a sphere after specular reflection from a cylinder will be far less than 3.1%.

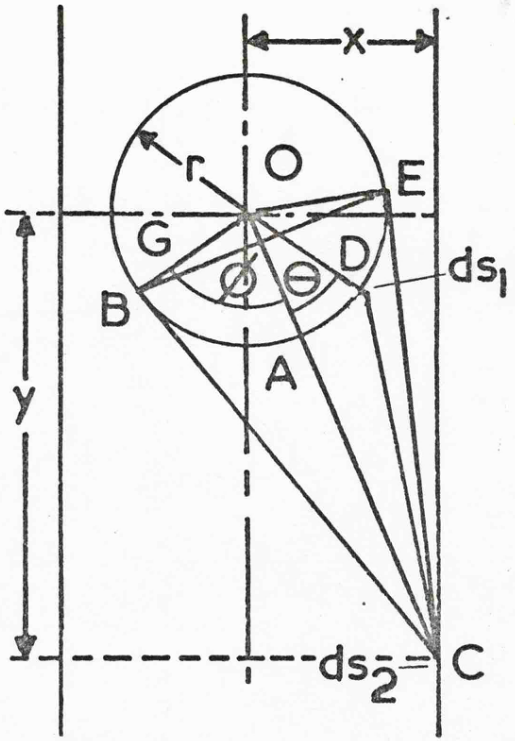


Figure A2 (i) Model for atoms which leaving a Spherical Specimen are Diffusely Reflected from a Cylindrical Furnace Tube

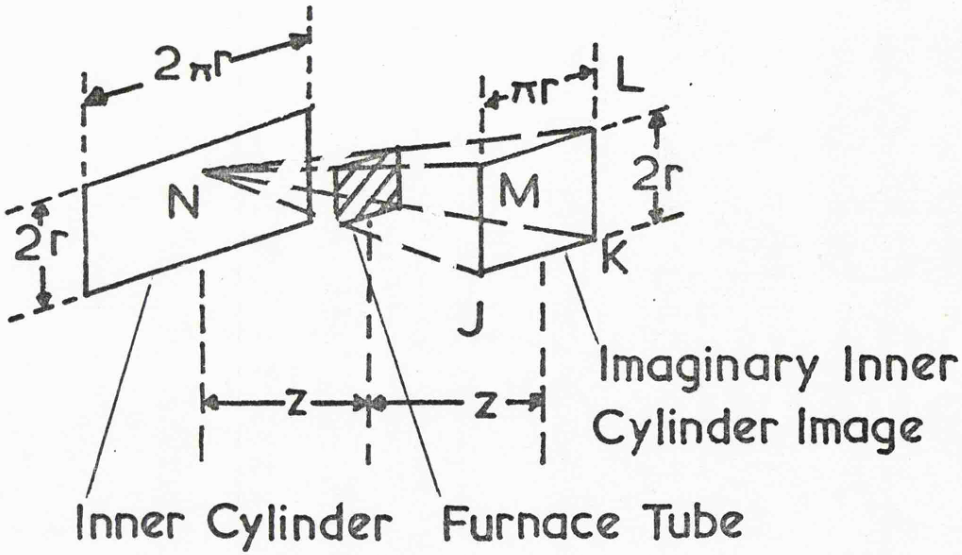


Figure A2 (ii) Model for atoms which leaving an Inner Cylindrical specimen are Specularly Reflected from an Outer Cylindrical Furnace Tube